

https://dspace.org/

Evaluation of the impact of excess sulphide on manganese metal quality

Phahle, Magaboke Themba

2022

https://hdl.handle.net/10539/34102

Downloaded from a DSpace repository. https://dspace.org/



EVALUATION OF THE IMPACT OF EXCESS SULPHIDE ON MANGANESE METAL QUALITY

MSc RESEARCH DISSERTATION

Prepared by

Magaboke Themba Phahle

1343010

Submitted to

School of Chemical and Metallurgical Engineering, Faculty of Engineering and the Built Environment, University of the Witwatersrand, Johannesburg, South Africa

Supervisor: Prof. Geoffrey S. Simate

Co-Supervisor: Dr. Walter Fourie

December, 2021

DECLARATION

I declare that this report is my own, unaided work. It is being submitted for the degree of Master of Science in Engineering to the University of Witwatersrand, Johannesburg. It has not been submitted before for any other degree or examination in any other University.



Magaboke Themba Phahle

13 December 2021

ABSTRACT

This work evaluates the challenges of unacceptable high levels of sulphur in the deposited manganese and production losses through uncontrollable cracking at a South African Electrolytic-Manganese (El-Mn) producing company called Manganese Metal Company (MMC). In order to have insight on the high levels of sulphur and the cracking, it was important to first understand the role and effects of sulphide on the manganese metal. Several experiments were conducted in laboratory scale electrowinning cells using the manganese sulphate solution prepared at the MMC plant.

The experiments involved varying concentrations of sodium sulphide reagent and aerating the solution to determine the effect. The factorial design tool was used to structure and determine the number of experiments required. The experimental data were collected using equipment such as X-ray fluorescence (XRF), eH/pH probe, LECO CS744 sulphur analyser, Bruker energy dispersive spectrometry (EDS), Scanning electron microscope (SEM) image and airflow meter. Other analytical methods such as titration and qualitative lead acetate test were also adopted to collect the data in the experimental phase. The results were presented in the form of graphs (i.e. line, bar, boxplot and scatterplot), visual pictures, tables and SEM-EDS images.

The results show that when sulphide exists in excess in the standard feed solution of an electroplating process, a manganese sulphide (MnS) film was formed on the surface of the metal deposit. The flaking of the metal deposit occurred instantaneously when the solution consisting of excess sulphide was aerated, resulting in a low current efficiency (% C.E) at 13%. The results also indicated that the MnS film was observed at a high level on both run 15 and run 16, where the sulphur (denoted as inherent or intergranular) was measured at 19.2 % and 22.0 % respectively. The low % C.E and increased sulphur was ascribed to the increased presence of thiosulphate and sulphide in the feed solution. It was also confirmed that for every 1 mmol of NaHS concentration consumed, about 0.0095 mmol of thiosulphate is produced. Using a statically based analysis called two-sample t-test, it was indicated that the oxidation of the solution at MMC was significant at the steep transfer launder.

This work has shown that when sulphide is present at increased concentrations in the feed solution of a manganese metal electrolytic process, the quality of metal and current efficiency will be drastically reduced.

DEDICATION

I dedicate this work to my Grandmother, Ziphora Magodave Nchabeleng, and my Mother, Makoloane Rachel Phahle, for the love and support.

Ke a leboga

ACKNOWLEDGEMENTS

The travel towards completing this dissertation has been a journey that provided great enlightenment. This journey wouldn't have been possible without support from various people who committed their time and effort to ensure completion of this document. First of all, I would like to thank the Almighty for being with me in my life and keeping me stronger throughout the toughest moments. Indeed, 'he who goes out weeping, carrying seed to sow, will return with songs of joy, carrying sheaves with him' (Psalms 126:6). My family has provided a great warmth and support when the feeling of loneliness and giving up was trying to sneak in and steal this opportunity away from me. My heart melts when a slight thought of them crosses my mind.

Many thanks to the MMC – EXCO team (under the leadership of Mr Louis Nel), first for giving me an opportunity to join the best manganese – non-selenium – beneficiation company in the World. In addition, for funding this dissertation and providing necessary facilities to ensure full experimentation. I am very much humbled by the amount of resources and professionals that were put together to make sure that everything is smooth regardless of the challenges I was facing at the time. Dr. Walter Fourie, for the time taken to provide guidance in my work and academic environment, which was needed in ensuring that there is direction. Dr Fourie has played a role in ensuring that the distance between WITS and MMC – 350 km – is shortened with the objective of maintaining an academic standard in my research. I would like to thank Professor (Prof.) Geoffrey Simate for agreeing to supervise me. Prof. Simate's patience and firm approach towards maintaining core research principles has been necessary in ensuring that I become a better researcher.

Finally, to Team-MMC, thank you for believing in me from the first day at the company, for providing support where I felt short and imparting necessary knowledge in relation to the complex process. This includes all the operators, controllers, samplers – team leaders, plate treaters, cell strippers, knock-off controllers, engineering, interns, IT, procurement, and day team. This report will sound familiar when going through it, as it was made possible by some of their great suggestions – hopefully your voice has been clearly recorded. Indeed, each day presents us with the opportunity to better ourselves and become greater people. As Mark Twain would say: "Continuous improvement is better than delayed perfection".

TABLE OF CONTENTS

1. CHAPTER ONE: INTRODUCTION 1

1.1. Introduction 1
1.2. Problem statement 3
1.3. Research Objectives 5
1.4. Hypothesis 5
1.5. Research Methodology 5
1.6. Dissertation Layout 5

2. CHAPTER TWO: LITERATURE REVIEW 6

2.1. General Introduction 6
2.2. Mineralogy and Characteristics of Manganese Ore 6
2.2.1. Mineralogical properties of manganese ore 7
2.2.2. Chemical properties of the manganese Ore 8
2.3. The Reduction of Ore 11
2.4. Manganese Leaching 12
2.4.1. Manganese Leaching and Impurity Co-Precipitation 12
2.5. Manganese Sulphate Purification Process 13
2.5.1. The presence and impact of impurities 13
2.5.2. Impurity removal and solution purification 15
2.5.3. Mechanisms for co-precipitation for impurity removal 16
2.5.4. The impact of the presence of fines in a solution 17
2.5.5. Impact of the addition of excess sulphide 18
2.5.6. Chemical oxidation of polysulphide 20
2.6. Electroplating of Manganese Metal 21
2.7. Sulphur Speciation and Deposition 23
2.7.1. Presence of sulphur dioxide in the electrolyte 24
2.7.2. Thiosulphate in aqueous solutions 25
2.8. Impact of Hydrogen Embrittlement on Metal Characteristics 26
2.9. Summary 28

3. CHAPTER THREE: MATERIAL, EQUIPMENT AND METHODS 30

3.1. Introduction 30
3.2. Materials: Solution Preparation 30

3.2.1. Feed solution 30
3.2.2. Reagents 31
3.2.3. Reagent dosing setup 32
3.2.4. Solution aeration 33
3.2.5. Filtration equipment description 33
3.3. Equipment: Laboratory Electrolytic Cells 34
3.3.1. Electrical current connection and flow 35
3.3.2. Temperature control 36
3.3.3. Solution supply and control 36
3.4. Analytical Techniques 37
3.4.1. pH measurements 37
3.4.2. Sulphur analysis in metal content 38
3.4.3. Scanning electron microscope analysis 38
3.4.4. Determination of the SO_2 content using titration 39
3.4.5. Determination of the thiosulphate content using titration 39
3.4.6. Determination of excess sulphide using lead acetate test 39
3.4.7. Analysis of manganese concentration in the solution 39
3.5. Design of Experiments 40
3.6. Data Analysis Method 42
3.7. Method: Solution Preparation 42
3.7.1. The feed solution quality 43
3.7.2. Volume of NaHS required for dosing 44
3.7.3. Tests performed 45
0 NaHS and 0 Aeration 45
0 NaHS and 1 Aeration 46
0.5 NaHS and 0 Aeration 46
0.5 NaHS and 1 Aeration 46
1 NaHS and 0 Aeration 47
1 NaHS and 1 Aeration 47
3.7.4. Solution filtration procedure 47
3.7.5. Oxidation of the solution in the plant 48

3.8. Method: Laboratory Electrolytic Cells....49
3.8.1. Preparation of the labcells material....50
Laboratory electrolytic cells preparation....50
Preparation of anodes....50
Anode box diaphragm preparation....51
Cathode Preparation....51
Preparation for start-up of the cells....51
3.8.2. Operation of the labcells....51
3.8.3. Metal harvesting....53
3.9. Calculations....54
3.9.1. Yield of reactions....54
3.9.2. Determination of the deposition time....54
3.9.3. Determination of the current density....54
3.9.4. Determination of current efficiency and energy consumption....55
3.10. Summary....55
4. CHAPTER FOUR: RESULTS AND DISCUSSION....57
4.1. Introduction....57
4.2. Determination of the degree of oxidation and behaviour of sulphur species....57
4.2.1. Solution oxidation in the process launder....57
4.2.2. The oxidation of T102 solution in various hydrogen sulphide concentration....59
4.2.3. The presence of polysulphides during excess sulphide oxidation....60
4.2.4. The impact of the presence of SO_2 on the excess sulphide oxidation....61
4.3. Performance of the Labcells....65
4.3.1. Overall performance of the labcells....65
4.3.2. Performance of the labcells at standard and aerated solution....67
Catholyte concentration....67
Characteristics of the manganese deposit....69
Sulphur content and current efficiency....69
4.3.3. NaHS dosing at 0.5 setting and aeration....70

Catholyte concentration 70
Characteristics of the manganese deposit 72
Sulphur content and current efficiency 72
4.3.4. NaHS dosing at 1.0 and aeration 74
Catholyte concentration 74
Characteristics of the manganese deposit 75
Sulphur content and current efficiency 76
4.3.5. The overall comparison of the labcells performance 77
4.4. Surface morphology and EDS analysis 78
4.4.1. Sample characteristics and examination 79
4.4.2. Morphology of the metal at 0 NaHS setting and 0 aeration 79
4.4.3. The Morphology of the metal at 0.5 NaHS setting and 1 aeration 81
Run 9 84
Run 10 85
Run 15 87
Run 16 88
4.4.4. The Morphology of the metal at 1.0 setting and aeration 90
4.5. Summary 92
5. CONCLUSIONS AND RECOMMENDATIONS 96
5.1. Conclusions 96
5.2. Recommendations 97
Excess sulphide using the lead acetate test 97
Analysis campaign on the white solids formed in feed solution 97
Impact of impurities on the quality and cell efficiency 97
The presence of impurities on the metal grain boundaries 98
Buffing of cathode plates 98
Oxidation of solution at the supertube launder 98
REFERENCES 99
APPENDIX A 105

A. BRIEF DESCRIPTION OF THE MMC CELLHOUSE 105

B. APPENDIX B: COMMISSIONING OF THE LABCELLS AND CHALLENGES 107

B.1 Dry Commissioning 107

B.2 Cold Commissioning 108

B.3 Hot Commissioning 109

APPENDIX C 113

C. OPTIMISATION OF THE LABCELS 113

C.1 Optimisation of the current and voltage 113

C.2 Optimisation of the manganese concentration 114

C.3 Measurement of variation between equipment 117

APPENDIX D 118

D. EXPERIMENTAL RESULTS 118

APPENDIX E 127

E. KEY OPERATION EVENTS AT MMC 127

E.1 Recovery in the Nelspruit operations during the last quarter of FY1997 following a sustained period of low out and poor sulphur quality. 127

E.2 Study on the sulphur in metal deportment and control prepared by Gluck et al. (1997) 127

Table E.1 The details on the location and forms of sulphur species in the metal and mechanism of incorporation Gluck et al. (1997) 128

E.3 Petroleum and natural gas industries-Materials for use in H2S-containing environments in oil and gas production by ANSI Webstore (2020) 129

LIST OF FIGURES

Figure 1.1 Typical flow diagram of manganese production at Manganese Metal Company 2

Figure 2.1 Standard electrode potential chart diagram for the 3d-block elements (Brown, 2020: Appendix, para.2) 14

Figure 2.2 Seeded and unseeded test comparison for cobalt in a reaction vessel (Bijsterveld, 1984) 17

Figure 2.3 Nickel and cobalt concentrations in the batch experiments using an aqueous sulphide source (Lewis and van Hille, 2005) 19

Figure 2.4 The concentration of sulphite vs sulphur in metal (Saunders and Ribane, 1986) .. 25

Figure 2.5 The concentration of thiosulphate vs sulphur in metal (Saunders and Ribane, 1986) 26

Figure 2.6 Schematic Showing the Generation of Hydrogen Producing SSC (NACE, 2002) 27

Figure 3.1 Solution collection point a) Valve at F-bank rotameter. b) Installed valve for solution collection 31

Figure 3.2 Test setup for solution preparation 32

Figure 3.3 Materials used to control the aeration of solution a) High-pressure airline for oxidation. b) Airflow meter 33

Figure 3.4 Macsalab filter press for solid separation 34

Figure 3.5 Laboratory electrowinning cells A and D 34

Figure 3.6 Types of electrodes used in the labcells a) Stainless Cathode Plate b) Anode Plate 35

Figure 3.7 Direct Current Power Supply 35

Figure 3.8 Equipment to control the temperature of the cells a) Elemental water bath b) Glass condenser for heat exchange 36

Figure 3.9 The top-view of the lab-cells section 37

Figure 3.10 LECO CS744 sulphur content analysis 38

Figure 3.11 Manganese analysis equipment a) Innovex setup for manganese in solution b) Olympus test stand compartment 40

Figure 3.12 Flow diagram for the solution preparation experiments.....43

Figure 3.13 Supertube launder.....48

Figure 3.14 (a) T171 launder with no eH/pH probe (b) T171 launder eH/ pH probe installed 49

Figure 3.15 Flow diagram for the labcells operations 50

Figure 4.1 Observation of the solution at the inlet and exit of the supertube (a) Solution at supertube inlet (b) Solution at supertube exit 58

Figure 4.2 Thiosulphate and NaHS concentration for T102 solution.....60

Figure 4.3 Percent yield for T102 solution and stain test 61

Figure 4.4 The relation of the thiosulphate with change in aeration and sulphide 63

Figure 4.5 Solution appearance for preparation run 11 and run 12 64

Figure 4.6 Mass of Manganese precipitated in each run 65

Figure 4.7 The average manganese catholyte of the test programme.....66

Figure 4.8 The average catholyte pH of the test runs 67

Figure 4.9 The catholyte concentration for runs at fresh feed and aeration 68

Figure 4.10 Physical characteristics of metal run 1 and run 2 before stripping.....68

Figure 4.11 Physical characteristics of metal run 1 and run 2 after stripping 69

Figure 4.12 The catholyte concentration for runs at 0.5 NaHS and aeration.....71

Figure 4.13 a) Characteristics of deposit from run 3 and run 4 b) Characteristics of deposit from run 15 and run 16 72

Figure 4.14 The catholyte concentration for runs at 1.0 NaHS and aeration.....74

Figure 4.15 Physical characteristics of metal run 5B and run 6B.....75

Figure 4.16 Digital images of manganese metal produced in run 11 and run 12 76

Figure 4.17 Sample photographs for SEM analysis.....79

Figure 4.18 BSE images and EDS spectrum of manganese metal flakes and manganese oxide in run 7 80

Figure 4.19 BSE images of fine discrete manganese metal sheets, manganese oxide prisms and manganese sulphide agglomerates in Run 9 85

Figure 4.20 EDS spectrum of manganese sulphur agglomerates in Run 9 85

Figure 4.21 BSE images of developing Mn metal prisms with surface coated by manganese sulphide and fine discrete manganese metal sheets in Run 10 86

Figure 4.22 EDS spectrum of manganese sulphur agglomerates in Run 10 86

Figure 4.23 Detailed BSE images of well-developed manganese oxide spheres with the surface coated by manganese sulphide in material in Run 15. 87

Figure 4.24 EDS spectrum of manganese sulphur agglomerates in Run 15 87

Figure 4.25 Detailed BSE images of well-developed manganese metal prisms with the surface and ridges coated by fibrous manganese sulphide particles in Run 16 89

Figure 4.26 EDS spectrum of manganese sulphur agglomerates in Run 16 89

Figure 4.27 Detailed BSE images of well-developed manganese oxide spheres, and the cementing material manganese sulphide, in Run 12 91

Figure 4.28 EDS spectrum of manganese sulphur agglomerates in Run 12 91

Figure A.1 Cell Design and Current Flow 105

Figure B.1 Ammeter for voltage and current measurement 107

Figure B.2 a) Level of water in the glass condenser b) Level of water in glass condenser restored 108

Figure B.3 a) Visible residue present in the lines b) Equipment after cleaning solution 109

Figure B.4 a) Smooth plating on Cell A b) Brown surface of Cell D 110

Figure B.5 a) Catholyte colour on Cell A and D b) Presence of MnO_2 in Cell D 110

Figure B.6 a) Corrosion characteristics on cell A b) Cracking of deposit on the cathode plate 112

Figure C.1 Current measurement on cathode for trial 1 and trial 2 113

Figure C.2 The current readings on the cathode for trial 3 and 4 114

Figure C.3 Catholyte Mn concentration and flow rate 114

Figure C.4 Deposit flaking from the second cathode of trial 2 115

Figure C.5 Impact of buffed and unbuffed plated on the plating of trial 3 and trial 4 116

Figure D.1 Minitab summary report for T102 exit and T171 comparison 118

Figure D.2 The Sample t-test conducted to compare the behaviour of the sulphide dosing rates at the two lines (T102A and T120B) of the solution purification 119

Figure D.3 The two Sample t-test conducted to compare the behaviour of the flow of solution at the two lines of the solution purification 120

Figure D.4 Sulphide thickeners number 102-A (T102A) and 102-B (T102B) used for the purification of the solution by removal of the precipitate or solid particles 120

Figure D.5 The two-sample t-test conducted to compare the difference between the catholyte pH of the aerated and not aerated solution 121

Figure D.6 The tracking of HKOs in the cellhouse plant during the test programme 121

Figure D.7 Anolyte blockage at the overflow weir due to the presence of $Mn(OH)_2$ in the pipeline. Mn metal flakes used to unblock the weir by metal dissolution with the anolyte 122

Figure D.8 Observation of cracking at the of top part of cathode plate during run 4 122

Figure D.9 Burning on the metal surface from the cathode plate (Run 9 – 10) due to the starting up of the cells at concentration below 9 mg/L 122

Figure D.10 Hydrogen fire occurring in the cellhouse mostly when there is water leak in the cellhouse or during the cracking and flaking condition of the cellhouse 125

Figure D.11 BSE images of manganese metal flakes and manganese oxide in Run 7 at a resolution of 100 and 10 µm 125

Figure D.12 BSE images of manganese oxide prisms and manganese sulphate agglomerates in Run 9 at a resolution of 100 and 10 µm 125

Figure D.13 Overview BSE images of well-developed manganese oxide spheres, and the cementing material in Run 12 at a resolution of 100 and 30 µm 126

Figure D.14 Overview BSE images of well-developed manganese metal prisms with the surface coated by fibrous manganese sulphate particles in Run 16 at a resolution of 20 and 10 µm. 126

LIST OF TABLES

Table 1.1 Classification of the manganese quality based on metal sulphur content.....4

Table 2.1 Minerals present in raw ore (Scholtz, 2020).....8

Table 2.2 MMC Laboratory chemical analysis of ore samples (Scholtz, 2020).....9

Table 2.3 Typical values of trace elements in raw ore (Scholtz, 2020).....10

Table 2.4 Maximum level of impurities in cell feed (Bijsterveld, 1984; Harris *et al.*, 1977) .14

Table 2.5 Concentration of sulphide required for metal precipitation (Murray *et al.*,1994) ...16

Table 2.6 Total sulphide mass balance at different pH values (Kleinjan *et al.*, 2005).....20

Table 2.7 Some of the Sulphur Species and Oxidation States (Murray *et. al*, 1994) 23

Table 2.8 The composition of sulphur content in the metal (Jacobs *et al.*, 1946) 24

Table 3.1 Definition of factors and levels.....41

Table 3.2 Factorial design and design matrix for test program 41

Table 3.3 Specification of fresh plant solution 44

Table 3.4 Descriptive Statistics.....45

Table 3.5 Standard experimental parameters.....52

Table 4.1 Oxidation of sulphide in manganese sulphate solution 59

Table 4.2 The behaviour of the sulphur species with the change in the solution type 62

Table 4.3 Performance of the labcells at 0 NaHS – Aeration and No aeration 70

Table 4.4 Performance of the labcells at 0.5 NaHS – Aeration and No aeration 73

Table 4.5 Performance of the labcells at 1.0 NaHS - Aeration and No aeration.....77

Table 4.6 Comparison of the labcells performance at different solution types using power consumption and sulphur content 78

Table 4.7 Chemical composition and speciation of the Mn Metal produced at run 7 81

Table 4.8 Chemical composition and speciation of the Mn Metal produced 82

Table 4.9 The percent yield of thiosulphate and excess sulphide using the stain test at various feed solution type 84

Table 4.10 Chemical composition and speciation of the Mn Metal produced at run 12 90

Table C.1 Sulphur content in metal from Trial run 117

Table C.2 Comparison between the Sol. Prep and Cellhouse Innovex 117

Table D.1 Determination of the total volume of feed solution added in the labcells for solutions consisting of 7.33 mmol/L NaHS reagent 123

Table D.2 Overall performance of the laboratory cells 123

Table E.1 The details on the location and forms of sulphur species in the metal and mechanism of incorporation Gluck et al. (1997) 128

1. CHAPTER ONE: INTRODUCTION

1.1. Introduction

The manganese plating process produces the purest form of electrolytic manganese metal (El-Mn or metal) used in various industries such as batteries, aluminium, steel alloying, copper, chemical and other electronic industries. The manganese metal can be obtained from both sulphate and chloride electrolytes. However, the corrosive nature of the chloride media makes it difficult to handle the solution since it requires expensive materials of construction. In addition, the evolution of harmful fumes at the anodes makes the process disadvantageous for manganese electrodeposition (Padhy *et al.*, 2015). Consequently, the commercial implementation of the chloride media process has proven challenging.

In the sulphate media, ore as the raw material – consisting of hematite (Fe_2O_3), hausmannite ($Mn^{2+}Mn_2^{3+}O_4$), braunite ($Mn^{2+}Mn^{3+}6(SiO_4)O_8$) or pyrolusite ($MnO_2$) – is first calcined to reduce higher oxidation manganese of +4, to the more leachable +2 oxidation state (calcine). Thereafter, the calcine passes through a leach section in which sulphuric acid generated from the electrowinning stage (cell house) is used to dissolve manganese into solution. However, the impurities that dissolve with the soluble manganese are required to be removed from the solution. For example, Iron is removed by oxidation to ferric hydroxide and settled in the thickeners. Sulphides in the form of hydrogen sulphide (H_2S), ammonium sulphide $(NH_4)_2S$ or sodium sulphide Na_2S (or sodium hydrogen sulphide – NaHS) are used to precipitate other heavy metal impurities into insoluble metal-sulphide form.

After thickening and filtration, the solution is then pumped into a holding tank where the addition of sulphur dioxide (SO_2) takes place. The SO_2 is primarily added to prevent the electroplating of γ-Mn and allowing the formation of α-Mn on the cathode. The γ-Mn is less thermodynamically stable, has a low current efficiency of 42.1% and is ductile (Jacobs *et al.*, 1946). Therefore, continual addition of SO_2 is necessary to increase the rate of formation of α-Mn compared to that of γ-Mn (Murray *et al.*, 1994). Figure 1.1 provides an illustration of a typical process flow diagram for manganese metal production.

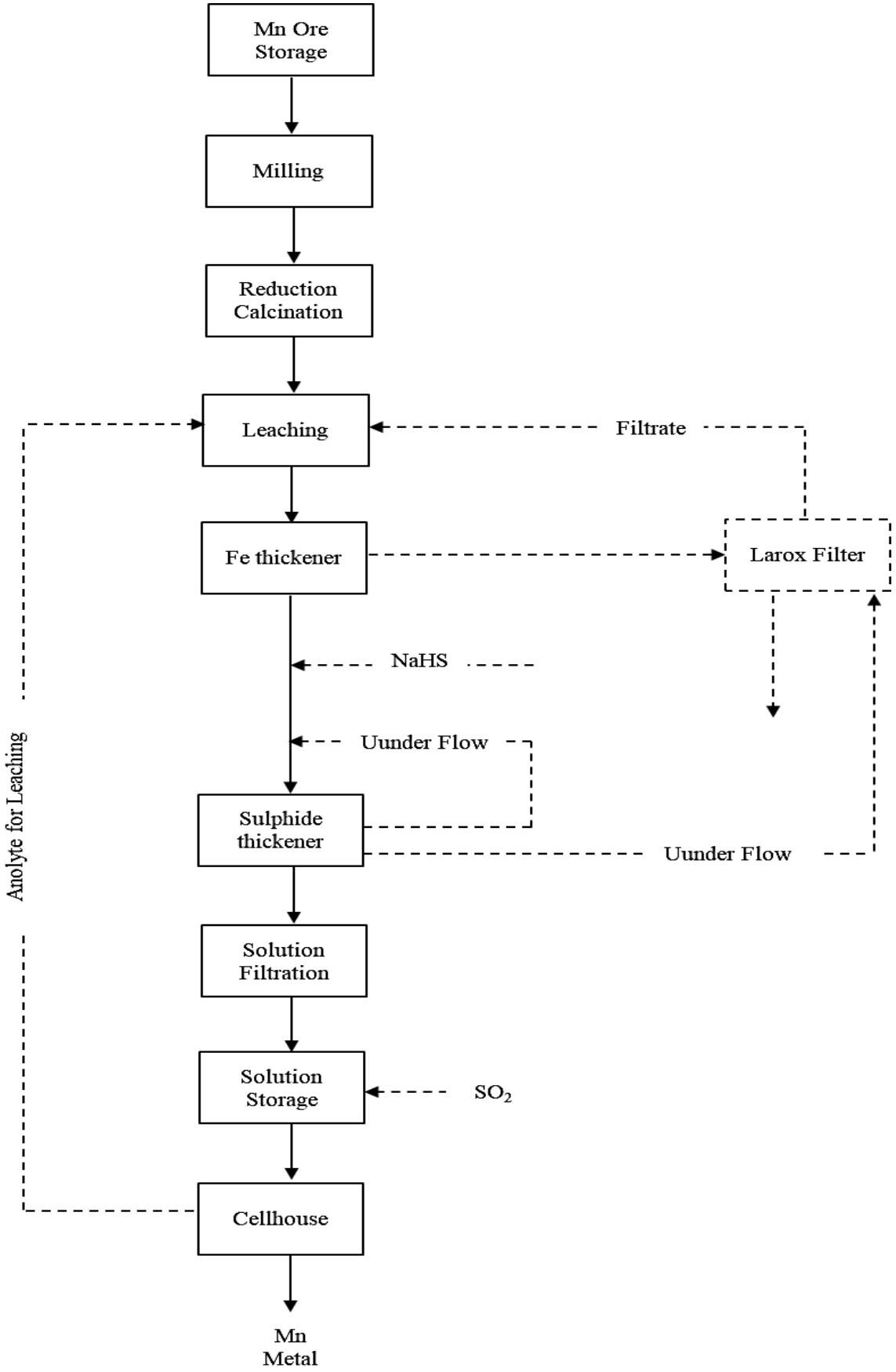


Figure 1.1 Typical flow diagram of manganese production at Manganese Metal Company

It must be noted, however, that all metals that are more positive on the standard electrode potential than manganese, if present in quantities above critical limits, will decrease the cathodic current efficiency (% C.E.) at which manganese can be plated (Harris *et al.*, 1977). This is due to the low electro-reduction potential (E^0 (Mn^{2+}/Mn) = – 1.18 volts at standard hydrogen electrode – |Vs| SHE) of manganese, which makes it difficult to plate El-Mn at higher % C.E (Padhy *et al.*, 2015). Therefore, the failure to remove impurities in the purification step will result in a deleterious effect on the manganese plating. For example, the impact of impurities is practically evidenced by the re-dissolution of deposited manganese product and formation of black borders around the deposition area (Harris *et al.*, 1977). Other cases that exhibit the influence of impurities involve the formation of a ductile, pin-holed and nodular deposit, which is difficult to remove from the cathode (Harris *et al.*, 1977) – a term known as hard knock offs (HKOs). The inverse is also possible, where the deposited metal is flaking off the cathode and making it difficult to handle. Therefore, the presence of impurities in the feed solution affects the production of pure manganese, increases the ore to metal ratio, increases operational costs and affects the efficiency of the downstream processes.

Manganese Metal Company (Pty) Ltd (MMC) in Nelspruit, Mpumalanga Province of South Africa, is an El-Mn producing plant with a production capacity of over 28 000 tons per annum. The primary drive of MMC's core-values is to attain high production volume at a premium quality. However, the production of manganese at MMC has in the past shown challenges that have resulted in inconsistent production and quality, which thus far have no qualitative root cause. As a result, MMC has on several occasions consulted various professional organisational bodies to understand the complexity of the process and its challenges. Some of the processes at the MMC plant is operated without a sound understanding of the underlying chemistry (Murray *et al.*, 1994; Lewis, 2018). This reason may be the case for the challenges concerning unacceptable high levels of sulphur in the deposited manganese and production losses through uncontrollable cracking and HKOs. This work will focus on the evaluation of the impact of excess sulphide on the manganese metal quality produced from MMC.

1.2. **Problem statement**

During the electroplating process, metal cracking in the cell house is vital for the process to ease knock off and recovery of the manganese metal from the cathode plates. However, when the metal cracking phenomenon becomes uncontrollable, metal tends to flake off on the cathode compartment and re-dissolves in the catholyte. The metal that re-dissolves causes

instabilities in the cells due to the undesired increase in the manganese concentration of the catholyte. Therefore, to prevent the increase in the concentration of the manganese in the catholyte, MMC procedures are carried out in such a way that the flaking cathode must be removed as soon as possible. Unfortunately, such action affects the yield and throughput for which manganese was supposed to have been produced during that period. For example, from January to December 2019, a total of 1074 tons has been lost in the MMC process, out of that, 457 tons were lost due to uncontrollable metal cracking in the cell house.

Similarly, the quality of the metal produced was found to be below specification, for example, the material produced in March 2019 consisted of 16.7% of premium manganese metal quality. Thus, the large proportion of the material produced within that period resulted in a negative impact on the company sales revenue. Table 1.1 indicates the classification of the quality of the metal produced.

Table 1.1 Classification of the manganese quality based on metal sulphur content

Manganese metal specification	Sulphur content specification (ppm)
Off specification	> 0.04
Medium specification	0.034
In-specification	0.024 – 0.034
Ultra-low specification	< 0.024

Although the purification of metal ions and the electroplating of manganese metal from a manganese sulphate media has been widely studied there is, however, very little information on the effects of excess sulphide on the plated metal after the purification step. Yet, it is theorised that the sulphur species play a role in the hydrogen absorption in steel materials resulting in material cracking. According to Murray *et al.* (1994), it seemed likely that oxidation of sulphide may occur in the steep launder at MMC. However, there was no point at the time to solve the impact of the oxidation as the variation in the sulphur quality seemed to be the symptom of the fact that the thickeners may not be removing the precipitated solids efficiently. Therefore, this is the conceptual theory upon which this research is based upon.

1.3. Research Objectives

The objective of this study is to:

1. Ascertain the degree of oxidation in the steep launder at Manganese Metal Company.
2. Determine the presence of thiosulphate when a solution comprising of excess sulphide is under oxidation.
3. Establish how the presence of excess sulphide results in an increased level of sulphur impurities in the metal.
4. Identify the relationship between the presence of excess sulphide in the process solution and the metal cracking or flaking during the electrodeposition of manganese metal

1.4. Hypothesis

The presence of excess sulphide in solution after the purification process will result in high levels of sulphur in the metal and cracking of the manganese metal during electrowinning.

1.5. Research Methodology

The research methodology for this study involved the following major tasks: literature review, experimental design, laboratory electrowinning cells setup, testing, test data analysis, main plant data analysis, results and discussions, conclusions, and recommendations.

1.6. Dissertation Layout

This dissertation consists of five chapters. Chapter one is an introductory chapter that provides the motivation for the research and the overall objectives of this study. Chapter two is the literature review which includes Mn ore characterisation, leaching, presence of impurities, purification using sulphur species and the impact of sulphur on the Mn metal. Chapter three describes the materials and methods used in the study. The subsequent chapter (chapter four) is comprised of the laboratory test results and discussion. The dissertation is finalized in chapter five with a conclusion and recommendations. Appendices of some of the findings relating to the subject matter is included.

2. CHAPTER TWO: LITERATURE REVIEW

2.1. General Introduction

Manganese metal has many important uses in the steel and aluminium industries. Manganese is added to all grades of steel and acts as a deoxidiser and a desulphiser. The metal stabilizes the austenitic phase at high temperatures and can replace part of the nickel content of stainless steel. It also decreases the carbon content of the stainless steel, giving it a greater toughness and fluidity (Rodrigues, 1983). Furthermore, when manganese metal is added in the aluminium alloys, it improves the mechanical, thermal and corrosion resistance properties of aluminium alloys (Rodrigues, 1983; Pereira et al., 2014).

In the battery industries, manganese (Mn) is used in a cathode for electronic vehicle (EV) batteries. The cathode of the EV batteries is generated when nickel sulphate ($NiSO_4$), manganese sulphate ($MnSO_4$) and cobalt sulphate ($CoSO_4$) are mixed at controlled ratios to form a black paste, known as a precursor (Todd, 2021). Other smaller industrial uses of manganese metal are in the production of alloys of various non-ferrous metal such as manganese-magnesium and manganese-bronze, which display some important electric and magnetic properties. Copper-manganese alloys are also produced industrially due to extremely high strength qualities, with applications in ship propellers, valves, bolts and nuts. Special ferrous (Fe) super-alloys are used in jet engines, marine turbines and in nuclear energy industry. Some non-metallurgical applications of manganese are in dry cell batteries in the form of manganese dioxide, in paint and varnish driers, ceramic products, plant fertilizers, animal feed, colourant for bricks and pharmaceuticals (Rodrigues, 1983; Pereira et al., 2014).

2.2. Mineralogy and Characteristics of Manganese Ore

Manganese Metal Company (MMC), Nelspruit, receives a Wessels fines (W4F) and Wessels concentrate (WC) raw ore from Wessels Mine. The raw ore is dried and milled, at a production rate of 13 tons per hour, to a particle size ±80% passing 75 µm in an air swept vertical spindle mill (MMC, 2009). The raw ore is analysed to determine the characteristics and the information is used to design and specify the downstream processes. This is because any change in the material constituent of the manganese ore will have a negative impact on the performance of the process. The physical, chemical and mineralogical characteristics of the ore vary as different sections of the ore body is excavated; however, raw ore is blended to maintain desired

specification. The manganese ore classification is determined using the chemical and mineralogical analysis.

2.2.1. *Mineralogical properties of manganese ore*

The classification of the manganese ores is done according to the Mn content as high grade (Mn > 44%), medium grade (Mn 40 – 44%), low grade (Mn 35 – 40%) and steel mill grade (Mn 28 – 35%) (Pereira et al., 2014). The manganiferous ore body has a dark grey colour, with an intermediate density of 3.55 g/cm^3 and a Mn/Fe weight ratio of 4.85 (Ma and Ek, 1991; Sorensen, 2010). The mineralogical composition of the manganese ore is determined using X-Ray Diffraction (XRD). To obtain an estimation of the mineralogical composition of the ore, chemical analysis, qualitative XRD mineralogy and Differential Thermal Gravimetry (DTG) information are reconciled. DTG is performed in a thermo-analyser and provides an indication of the mass losses associated with thermal decomposition reactions of minerals (MMC, 2009).

Minerals such as bixbyte (Mn_2O_3), hausmannite (Mn_3O_4), braunite I (Mn_7SiO_{12}), braunite II ($CaMn_{14}SiO_{24}$) and hematite (Fe_2O_3) are major constituents comprising above 85% of the ore, as illustrated in Table 2.1 (Sorensen et al., 2010; Scholtz, 2020). Sorensen et al. (2010), found that Braunite exist in two modifications of high and low silica, where the high silica braunite comprised of a relatively small Mn content.

Table 2.1 Minerals present in raw ore (Scholtz, 2020)

Mineral name	Mineral formula	Average value (%)
Bixbyite	Mn_2O_3	14.70
Hausmannite	Mn_3O_4	19.60
Manganite	MnOOH	2.40
Braunite I	Mn_7SiO_{12}	11.20
Braunite II	$CaMn_{14}SiO_{24}$	28.00
Jacobsite	$MnFe_2O_4$	-
Hematite	Fe_2O_3	13.00
Calcite	CaO_3	2.90
Portlandite	$Ca(OH)_2$	-
Marokite	$CaMn_2O_4$	-
Andradite (garnet)	$Ca_3Fe_3(SiO_4)_3$	10.20

2.2.2. *Chemical properties of the manganese Ore*

The chemical analysis is conducted to determine the elemental composition of manganese ore body. The analysis is normally done by means of titration for Mn and Fe, and Atomic Absorption Spectrometry (AAS) for major impurities. Table 2.2 provides a typical chemical content of the raw ore analysed by the MMC ore supplier (Scholtz, 2020).

Table 2.2 MMC Laboratory chemical analysis of ore samples (Scholtz, 2020)

Chemical name	Chemical content (%)
Mn	42.60
Fe	10.80
CaO	6.30
MgO	0.34
SiO_2	9.20
Al_2O_3	0.34
P	0.024
H_2O	5.80

However, elements such as cobalt (Co), copper (Cu), zinc (Zn) and nickel (Ni) are found in the solution after leaching, indicating their presence in the raw ore. Such elements present in the ore in trace quantities can be detected by means of an Inductively Coupled Plasma Atomic Emission Spectroscopy (ICP-AES) or Inductively Coupled Plasma Mass Spectrometry (ICP-MS) analysis (MMC, 2009). Table 2.3 lists elements and the typical concentrations as conducted by the MMC Laboratory on an ICP-MS analysis (Scholtz, 2020).

Table 2.3 Typical values of trace elements in raw ore (Scholtz, 2020)

Element	Concentration in raw ore (mg/kg)
Al	1400 - 1600
As	20 - 40
Ag	<10
B	500 - 700
Ba	3000 - 4000
Be	<1
Cd	<1
Co	50 - 70
Cu	80 - 100
Li	<10
Mo	<10
Ni	20 - 40
P	400 - 600
Pb	100 - 200
S	1000 - 1200
Sb	<10
Se	<5
Te	<5
Zn	100 - 200
CO_2	0.90 - 1.20%

2.3. **The Reduction of Ore**

The ore body from the Wessels Mine consists of manganese containing minerals, at higher oxidation states i.e., Mn_2O_3 and Mn_3O_4. These minerals are not soluble in dilute sulphuric acid. The reduction of the manganese bearing minerals at elevated temperatures (occurring in rotary kilns) result in the formation of manganous oxide (MnO), a process known as calcination. The calcination of manganese oxides is accomplished by roasting with a carbon containing material such as coal, coke, produced gas, butane, or oil which is widely used in the industrial scale (MMC, 2009). The carbon containing material undergo a phase change when heated, to produce vapours such as carbon monoxide (CO), hydrogen (H_2) and methane (CH_4), suitable for calcination (MMC, 2009). Sorensen et al. (2010) and Cheraghi et al. (2018), conducted the isothermal reduction in a mixture of an inert gas and reducing vapour (CO, H_2 and CH_4).

At MMC, the calcination process occurs in a cylindrical tube calciner, rotated by a drive situated at the feed end of the tube. The middle section of the tube is heated externally by electrical elements, fitted above and below the tube. The milled ore is transferred to the calciner at throughputs between 3 – 4 tons per hour using feed screws through an inlet seal. The oil enters the calciner at the feed screws. In the first section of the calciner tube, the feed section, the ore and oil are mixed and displaced into the heated section by internal flights. In the heated section, the ore and oil react to produce a reduced ore. Since no MnO_2 is present in the Wessels ore body and no Mn metal is formed in the rotary kilns at temperatures lower than 800 °C, only two steps occur in the calciners i.e. $Mn_2O_3 \rightarrow Mn_3O_4 \rightarrow MnO$ as indicated in Equation 2.1 (MMC, 2009; Sorensen et al., 2010; Cheraghi et al., 2018):

$$\left.\begin{aligned} 3\,Mn_2O_{3(s)} + C_{(s)} &\rightarrow 2Mn_3O_{4(s)} + CO_{(g)} \\ 2Mn_3O_{4(s)} + C_{(s)} &\rightarrow 3MnO_{(s)} + CO_{(g)} \end{aligned}\right\} \quad (2.1)$$

The above process lowers the oxidation state of the manganese from Mn^{4+} to Mn^{3+} to Mn^{2+}, to a more soluble MnO and iron oxides to metallic iron (Sorensen et al., 2010). Cheraghi et al. (2018), has shown that the metallic iron and FeO is normally produced from the reduction of the hematite in the ore. At MMC, the ferrous ion (Fe^{2+}) is monitored at an hourly basis, where the ore feed rate and reductant are controlled as input variables to control Fe^{2+} into

specification. The prominent phase of MnO in the ore results into a greenish colour for the ore particles and is mostly produced from the braunite phase (Cheraghi et al., 2018).

2.4. **Manganese Leaching**

2.4.1. *Manganese Leaching and Impurity Co-Precipitation*

The solution of manganese sulphate ($MnSO_4$) and ammonium sulphate ($(NH_4)_2SO_4$) is required to produce El-Mn. The dissolution of the of manganese oxides (Mn_2O_3 and Mn_3O_4) in sulphuric acid proceeds to partial completion, where the process is terminated at $\alpha = 0.66$ (i.e. α is the ratio of the concentration of Mn^{2+} ions in the solution to the total manganese in the oxide sample (Artamonova et al., 2013). The lower recovery of manganese (i.e. 1.2% at an ore:reductant ratio of 1.0) from the manganese oxide shows that a reducing agent is required when leaching with sulphuric acid (Moro et al., 2021). Alternatively, the higher manganese oxidation state (Mn^{4+}) is reduced in the calcination processes to attain a lower oxidation state manganese (Mn^{2+}) (Sorensen et al., 2010; Cheraghi et al., 2018; MMC, 2009). The $MnSO_4$ is obtained by dissolving MnO with sulphuric acid as indicated in Equation 2.2 (Jacobs *et al.*, 1946).

$$MnO_{(s)} + H_2SO_{4(aq)} \rightarrow MnSO_{4(aq)} + H_2O_{(l)} \qquad (2.2)$$

The reaction proceeds rapidly and almost completely at a pH less than 3.0 and the leach efficiency is high when the pH is as low as possible. Unfortunately, the lower the pH drops, the higher the level of impurities produced (Jacobs *et al.*, 1946). Therefore, upstream control of the solution is necessary to minimize the excessive consumption of the sulphide reagent and impurity generation. Thus, optimum leaching is necessary to get as much desirable materials into solution as possible whilst keeping other components at a minimum concentration. A complete Fe (II) oxidation or precipitation is attained in the manganese leaching circuit when the pH is maintained at 6.5 under adequate agitation and aeration (Schaekers, 1995).

The pH in the leaching circuit is adjusted or controlled using calcine to neutralize the excess acid and raise the pH to 6.5 (Jacobs *et al.*, 1946). At pH 5.25 the precipitation reaction is slower, approximately 80% of the ferrous could be removed, while at pH 4.00 the precipitation is incomplete (Schaekers, 1995). The high pH causes the iron to precipitate out as ferric hydroxide and with other small amounts of impurities (Foxcroft *et al.*, 1985; Schaekers, 1995). The ferric hydroxide formation is described in Equation 2.3.

$$4Fe^{2+}{}_{(aq)} + O_{2\,(g)} + 6H_2O_{(l)} \rightarrow 4FeO(OH)_{(s)} + 8H^{+}{}_{(aq)} \quad (2.3)$$

Otherwise, when iron is added as ferrous sulphate, with consequent oxidation and precipitation of ferric hydroxide, the process was effective in removing impurities such as arsenic (As), molybdenum (Mo), colloidal sulphur (S) and organic matter (Jacobs *et al.*, 1946).

2.5. **Manganese Sulphate Purification Process**

Ionic precipitation is based on the fact that when a reagent is added to a solution containing metal ions, a compound is formed whose solubility is very low under these conditions that precipitation takes place (Habashi, 1999). The principal process in a precipitation reaction is the formation of a new solid phase from a solution (Bijsterveld, 1984). For example, when Na_2S is added to a solution of $CuSO_4$, immediate precipitation of CuS takes place because Cu^{2+} ions and S^{2-} ions react to form a compound of very low solubility as indicated in Equation 2.4 (Habashi, 1999).

$$Cu^{2+}{}_{(aq)} + S^{2-}{}_{(aq)} \rightarrow CuS_{(s)} \quad (2.4)$$

2.5.1. *The presence and impact of impurities*

The current efficiency (% C.E) is the measurement of the efficient use of the total supplied current in the production of the required metal. However, the co-deposition of impurities and production of hydrogen gas results in current inefficiencies (Lenthall and Bryson, 1997). Due to the low electrode-reduction potential of manganese, Mn^{2+}/ Mn of -1.18 V as indicated in Figure 2.1 (Docbrown, 2020: Appendix, para.2), the electrodeposition of the metal at high % C.E is affected (Padhy *et al.*, 2015). Therefore, to obtain increased % C.E and better deposit quality, the electrolyte must be free from the metal ion impurities. As indicated in Figure 2.1, metals such as copper (Cu), cobalt (Co), chromium (Cr), nickel (Ni) and iron (Fe) will be reduced first when present in a cell to which a potential more negative than that of Mn were applied (de Wet, 1995).

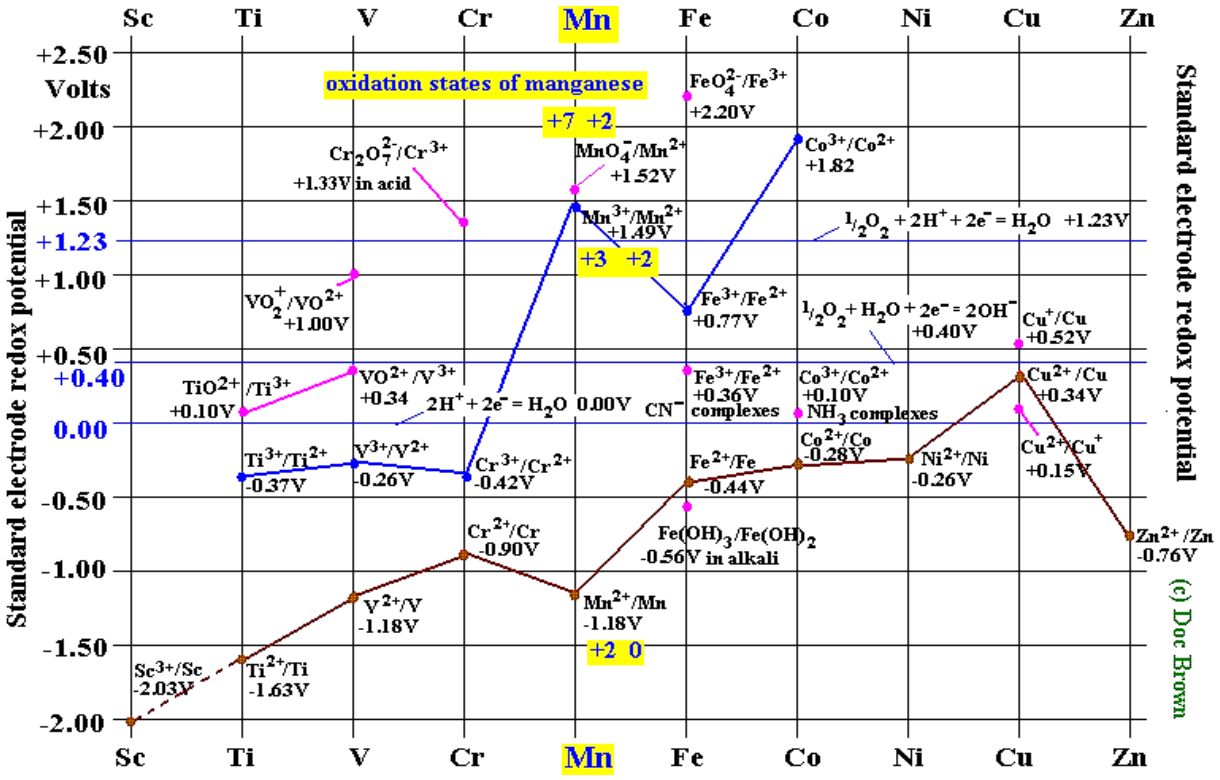


Figure 2.1 Standard electrode potential chart diagram for the 3d-block elements (Brown, 2020: Appendix, para.2)

Nevertheless, the maximum level of some impurities that can be tolerated in the cell feed without affecting the % C.E is illustrated in Table 2.4 (Bijsterveld, 1984; Harris *et al.*, 1977).

Table 2.4 Maximum level of impurities in cell feed (Bijsterveld, 1984; Harris *et al.*, 1977)

Component	Maximum concentration (ppm)
Nickel	1.0
Cobalt	0.3
Iron (ferrous)	15.0
Silicon	10.0
Copper	5.0
Zinc	10.0

Bijsterveld (1984), expressed that a combination of these impurities often has a greater negative effect than any one impurity alone, although, cobalt has illustrated the greatest negative impact of all impurities in Table 2.4 (Agladze and Gofman, 1957).

2.5.2. *Impurity removal and solution purification*

The consequence of the nature of Mn is that all other metal ions must be removed from a Mn-rich solution before electroplating can be performed. The removal of metal ions or impurities which affects the process efficiency is done by the purification or ionic precipitation (Rodrigues, 1983). In hydrometallurgical processes, metal sulphide are preferred instead of hydroxide precipitation due to high degree of metal removal at relatively low pH values (Lewis and van Hille, 2006). Other advantages are the limited nature of sulphide precipitates, favourable dewatering characteristics and stability of the metal sulphides formed (Lewis and van Hille, 2006). The commercially accepted reagent for the purification of the impurities in the manganese solutions is ammonium sulphide $(NH_4)_2S$ (Bijsterveld, 1984). Other commercially used precipitation reagents are sodium sulphide (Na_2S), sodium hydrogen sulphide (NaHS) and hydrogen sulphide (H_2S).

The purpose of adding the sulphide reagent is to precipitate the heavy metal impurities as their sulphides. The interaction of metal impurities with the $(NH_4)_2S$ is well described by Dube *et al.* (2015) (see Equation 2.5). It is possible to utilize other sulphide reagents in describing the step reaction. This is because sulphide precipitation involves the reaction of hydrosulphide ions to give first the hydrosulphide of the metal which, by secondary loss of hydrogen sulphide results in the formation of the metal sulphide (Kolthoff and Moltzau, 1935).

$$\left.\begin{aligned} &(NH_4)_2S_{(aq)} \rightarrow 2\,NH_{3(aq)} + H_2S_{(g)} \\ &2NH_{3(aq)} + H_2S_{(g)} \rightarrow 2NH_{3(aq)} + HS^-{}_{(aq)} + H^+{}_{(aq)} \\ &2Mn^{2+}{}_{(aq)} + HS^-{}_{(g)} \rightarrow 2\,Mn(HS)_{2(s)} \\ &Mn(HS)_{2(s)} + 2(Metal)^{2+}{}_{(aq)} \rightarrow 2(Metal)S_{(s)} + Mn^{2+}{}_{(aq)} + 2H^+{}_{(aq)} \end{aligned}\right\} \quad (2.5)$$

When the step reaction 2.5 takes place at a reasonably fast rate, it is important to ensure that a suitable excess of manganese is present in the precipitated sulphide sludge (Harris *et al.*, 1977). According to Murray *et al.* (1994), low quality manganese produced in the cellhouse has raised questions concerning the efficiency of the sulphide precipitation. Lebakeng (2002), established

that when the second dosing stage of $(NH_4)_2S$ was introduced, the current efficiency improved at greater than 62% average as compared to the standard solution. However, the second stage dosing of $(NH_4)_2S$ resulted in the precipitation of manganese, i.e. Mn losses. Therefore, the presence of excess manganese in the form of manganese sulphide ($MnS_{(s)}$) during the purification step serves to flag an "endpoint". Murray *et al.* (1994), determined the endpoint using the solubility of the metals for simulation (see Table 2.5).

Table 2.5 Concentration of sulphide required for metal precipitation (Murray *et al.*,1994)

Metals	Sulphide (mol/L)
Hg, Cu, Zn, Co	$< 10^{-8}$
Fe, Ni	$10^{-7} – 10^{-6}$
Mn	3×10^{-3}

In this case, metal requiring lower sulphide concentration will precipitate first and remain in the solid phase because of thermodynamic stability (insoluble). Furthermore, Murray *et al.* (1994), stipulates that when $MnS_{(s)}$ has precipitated and measured in the solid phase, this indicated that sufficient sulphide is added to precipitate other heavy metals since $MnS_{(s)}$ is most soluble. To control the dosing of sulphide reagents the ratio of metals (i.e. known as the bed ratio) in the sludge is monitored (see Equation 2.6), on a mass-by-mass basis in dry sludge.

$$\text{Bed ratio} = \frac{[\text{Mn}]}{[\text{Fe}]+[\text{Zn}]+[\text{Co}]+[\text{Ni}]} \qquad (2.6)$$

2.5.3. *Mechanisms for co-precipitation for impurity removal*

During the separation of metals in the second and third groups of the qualitative analysis scheme, the metal sulphides of group II may cause the appearance of the sulphides of group III in the precipitate, under conditions which would not allow the precipitation of the latter if present alone (Kolthoff and Moltzau, 1935). Such phenomenon is referred to as 'induced precipitation' and various workers have discussed and proven the case. For example, Bijsterveld (1984), established that introducing particle seeds on the precipitation of the cobalt and manganese, an induced catalysis effect resulted. This is illustrated in Figure 2.2 whereby;

cobalt is immediately precipitated (identified as seeded test 7) from solution as compared to the unseeded test (identified as test 3.1 and test 3.2).

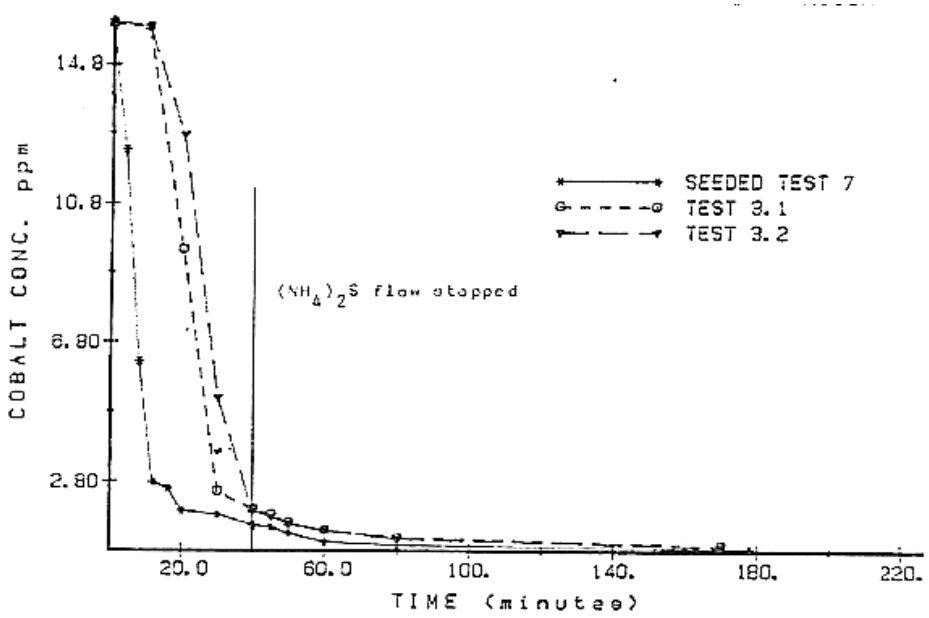


Figure 2.2 Seeded and unseeded test comparison for cobalt in a reaction vessel (Bijsterveld, 1984)

Kolthoff and Moltzau (1935), indicated that the rate of the precipitation of the more soluble component is much greater at the interface of the component than in the bulk of the solution. For example, hydrogen sulphide adsorbed on the surface of the metal has a much stronger tendency to ionize than which is present in the bulk solution. Thus, the precipitation rate on the surface of the metal sulphide increases due to the domination of crystal growth over primary nucleation. To achieve the induced precipitation, the MMC process reuses some of the precipitate or solids settled in the sulphide thickeners for purification.

2.5.4. *The impact of the presence of fines in a solution*

It is essential that a clear filtrate is maintained as the presence of solid particles affects the deposition of the metals by (Harris *et al.*, 1977):

1. Causing occlusion in the deposit which contaminates the purity of the metal, thus increase the sulphur content to unacceptable limits
2. Lowering the hydrogen overpotential when absorbed onto the surface of the deposit, resulting in the evolution of hydrogen and the re-dissolution of the deposited manganese metal

The solid particles are removed by filtration using the stellar or funda filters and a clear filtrate is ensured when the filter is precoated with a diatomaceous earth filter aid (Harris et al., 1977). However, fine particles have the possibility of passing through the filters – 0.45 µm filter size – (or are unable to settle out in the thickeners), thus co-travel with the aqueous fraction (Lewis, 2010). The rate of fines formation is related to supersaturation, whereby for nickel and cobalt sulphide, the formation of fines occurred after 10 minutes in a fluidised bed reactor and immediate with copper sulphide (Lewis, 2010). In addition, the fines are also formed by highly turbulent conditions due to attrition of the fragile layer deposited on the seeds.

According to Bijsterveld (1984), the MnS precipitate had no particles larger than 20 µm. Most of particles were between 0.2 – 1.0 µm and about 10% of the particles were found to be lower than 0.1 µm. Therefore, when the unfiltered solution remained in contact with the solid particles for an increased period, redissolution of the solids into solution occurred within 10 minutes (Jacobs *et al.*,1946). This was proven when a positive test for impurities was established resulting to the cellhouse experiencing challenges relating to an impure solution.

2.5.5. *Impact of the addition of excess sulphide*

Addition of excess sulphide with a resulting loss of manganese as $MnS_{(s)}$ has shown to increase the particle size by being retained on a 0.45 µm filter (Lewis and van Hille, 2005). Moreover, the addition of excess sulphide or immediately filtering the "gassed" solution has both shown an improvement in the cellhouse (Jacobs et. al, 1946). Furthermore, a two-stage dosing of $(NH_4)_2S$ resulted into a reduced fluctuation of the % C.E in the cellhouse (Lebakeng *et al.*, 2002). Nonetheless, for industrial practice, the addition of sulphide should be carefully controlled to avoid areas of high local sulphide concentration, as it causes redissolution of the formed precipitate (Lewis, 2010). According to Lewis and van Hille (2005), when excess sulphide was used the remaining sulphide in solution was less than expected from the stoichiometry. Whereas, the metal concentration remained unchanged. Furthermore, the free sulphide in solution continued to decrease, indicating that both the nickel and cobalt re-dissolved as aqueous polysulphide complexes as indicated in Equation 2.7.

$$MS_{(s)} + HS^-_{(aq)} \rightarrow MS(HS)^-_{(aq)} \qquad (2.7)$$

Shea and Helz (1988), illustrated that polysulphide speciation is more complex because it depends not only on protonation equilibra, but also on the aqueous concentration of zerovalent sulphur as indicated in Equation 2.8.

$$xS^{0}_{(s)} + HS^{-}_{(aq)} \rightarrow S_xS^{2-}_{(aq)} + H^{+}_{(aq)} \quad (2.8)$$

In addition, these can react further and rearrange (see Equation 2.9) thus polysulphide ions of different chain length can coexist in aqueous solution.

$$(x-1)S_xS^{2-}_{(aq)} + HS^{-}_{(aq)} \rightarrow nS_{x-1}S^{2-}_{(aq)} + H^{+}_{(aq)} \quad (2.9)$$

Similarly, Luther *et al.* (1996), used the redissolution phenomena of metal sulphide precipitate by adding excess sulphide to determine the stoichiometry, structure, and stability constant of sulphide complexes. This is a titration method using seawater or sodium chloride (NaCl) solutions at pH 8 with +2 cations of Cu and Zn. In the early phase of the titration method, Luther et al. (1996), established that the added sulphide reacted immediately with the Cu^{2+} and Zn^{2+}, forming a complex of 1:1 stoichiometry to the sulphide concentration. Lewis and van Hille (2005), have also shown that at ratios of 1:1 and 1:1.2, nickel and cobalt precipitated immediately. In addition, over a period of time, the nickel concentration increased drastically as compared to the cobalt concentration (see Figure 2.3).

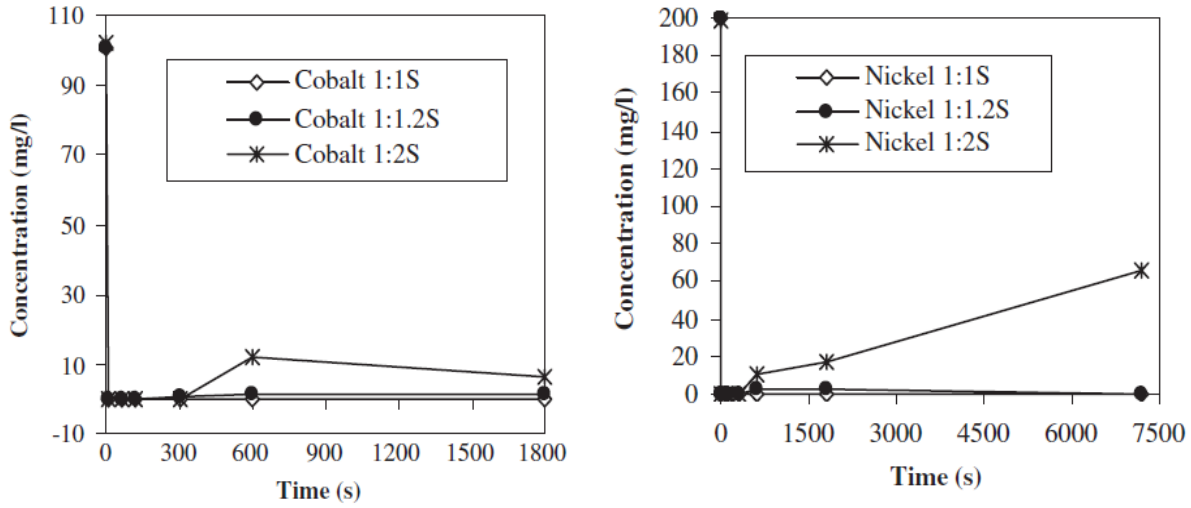


Figure 2.3 Nickel and cobalt concentrations in the batch experiments using an aqueous sulphide source (Lewis and van Hille, 2005)

However, when the sulphide is added at increased concentration of the metal, the Cu^{2+} and Zn^{2+}, are released into solution, forming a complex with a stoichiometric molar ratio of 3 sulphur to 2 metal ions (Luther *et al.*, 1996). Therefore, the presence of excess sulphide compromises the metal removal efficiency.

2.5.6. *Chemical oxidation of polysulphide*

When oxygen is continuously bubbled through a concentrated solution of polysulphide, the physical characteristic (a yellow-to-orange colour) of the polysulphide solution disappears (Steudel *et al.*, 1986). The stoichiometry of the oxidation of polysulphide is well described in Equation 2.10, were the formation of thiosulphate and sulphur are resultant. In addition, components such as sulphate, sulphite or polythionate ($S_xO_6{}^{2-}$) could not be detected (Steudel *et al.*, 1986).

$$S^{2-}{}_{x(aq)} + \frac{3}{2}O_{2(g)} \rightarrow S_2O_3{}^{2-}{}_{(aq)} + (x-2)S^0{}_{(s)} \qquad (2.10)$$

Kleinjan *et al.* (2005), indicated that the rate of thiosulphate formation was also pH dependant as shown in Table 2.6.

Table 2.6 Total sulphide mass balance at different pH values (Kleinjan *et al.*, 2005)

pH	$\Delta[S^{2-}]_{total}$ (mmol/L) (consumption)	$\Delta[O_2]$ (mmol/L) (consumption)	$\Delta[S_2O_3{}^{2-}]$ (mmol/L) (consumption)	$\Delta[O_2]/[S^{2-}]_{total}$ (mmol/L) (consumption)	$\Delta[S_2O_3{}^{2-}]/[S^{2-}]_{total}$ (mmol/L) (consumption)
7	0.08	0.09	0.06	1.16	0.82
8	0.15	0.17	0.14	1.21	0.97
9	0.17	0.24	0.18	1.40	1.03
10	0.07	0.24	0.31	3.26	4.34
11	-0.02	0.23	0.36	-1.04	-16.00
12	-0.12	0.24	0.45	-1.91	-3.62

Kleinjan *et al.* (2005), stated that the stoichiometric relationship of the polysulphide oxidation was established when the pH values were between 7 and 9. Mainly, because at lower pH values, the equilibrium between HS^- and $S^{2-}{}_x$ is shifted towards HS^- and therefore sulphide oxidation interferes with polysulphide oxidation at low pH. However, the total sulphide consumption at pH between 10 and 12 is increased steadily and formation of additional thiosulphate was

observed. Kleinjan *et al.* (2005), attributed this formation to the hydrolysis of elemental sulphur as described in Equation 2.11.

$$4S^{0}{}_{(s)} + 4OH^{-}{}_{(aq)} \rightarrow S_2O_3{}^{2-}{}_{(aq)} \quad (2.11)$$

Therefore, the presence of air in the system has an impact on the MMC process. Murray *et al.* (1994), suspected that oxidation transpires excessively in the delivery launders.

2.6. **Electroplating of Manganese Metal**

The electrodeposition of $Mn_{(s)}$ involves three stages i.e. the transfer of aqueous Mn species from the bulk electrolyte to the surface of the cathode, reduction of Mn^{2+} to Mn^{0} and deposition of the reduced Mn on the cathode plate (Murray *et al.*, 1994). When manganese is reduced from aqueous solutions, the following major reactions occur at the electrodes (Benetis *et al.*, 1996; de Wet, 1995; Jacobs *et al.*, 1946).

		Potential	
Cathodic reactions	$Mn^{2+}{}_{(aq)} + 2e^{-} \rightarrow Mn_{(s)}$	-1.18 V	(2.12)
	$2H_2O_{(l)} + 2e^{-} \rightarrow H_{2\,(g)} + 2OH^{-}{}_{(aq)}$	-0.83 V	(2.13)
	$Mn^{2+}{}_{(aq)} + 2H_2O_{(l)} \rightarrow Mn(OH)_2 + 2H^{+}{}_{(aq)}$		(2.14)
	$2H^{+}{}_{(aq)} + 2e^{-} \rightarrow H_{2(g)}$	0.00 V	(2.15)
Anodic reactions	$2H_2O_{(l)} \rightarrow O_{2(g)} + 4H^{+}{}_{(aq)} + 4e^{-}$	+1.23 V	(2.16)
	$Mn^{2+}{}_{(aq)} + 2H_2O_{(l)} \rightarrow MnO_{2(s)} + 4H^{+}{}_{(aq)} + 2e^{-}$	+1.21 V	(2.17)

The amount of manganese plated from the solution is replaced by an equivalent amount of sulphuric acid, which is used to dissolve manganese from the reduced ore in the leach section. Manganese electroplating cannot be carried out in acidic conditions because a high

concentration of H^+ ions would make Equation 2.15 thermodynamically preferable, resulting into high rate of H_2 generation on the cathode (Benetis *et al.*, 1996).

The generation of hydrogen gas results in the reduction of the soluble manganese thus affecting the cell efficiency. Equation 2.16 and 2.17 illustrates that H^+ ions are also formed in the anode compartment, thus making the anolyte acidic. The electrolysis of water (as the potential is greater than that of manganese in Equation 2.13) will lead to the excessive formation of $Mn(OH)_2$ in the catholyte following Equation 2.14.

The presence of excessive $Mn(OH)_2$ is detrimental to the electroplating process as the following problems begin to develop (Benetis *et al.*, 1996; de Wet, 1995; Jacobs *et al.*, 1946).

1. Blinding of diaphragms which leads to the obstruction of solution flow and ion migration in the cell

2. Deposited manganese becomes increasingly stressed causing peeling by cracking and flaking off the cathode

3. Formation of nodules and trees which lower the current efficiency

4. Changing of the deposit from light to dark grey with a bronze lustre, where the current efficiency is lowered and peeling results within a few hours

5. The deposition of Manganese stops due to the presence of high Mn concentration in the cell

Therefore, to avoid the challenges resulting from the formation of both the hydroxide and hydronium ions in the cells, a diaphragm is used. The diaphragm regulates the movement of ions between the catholyte and the anolyte and allows these two solutions to have such different compositions. The solution flow in the cells is from the catholyte to anolyte, although there is considerable back-diffusion of the H^+ ions (Jacobs *et al.*, 1946). In addition, the presence of $(NH_4)_2SO_4$ in the feed solution is necessary to prevent the hydrolysis of manganese (Jacobs *et al.*, 1946). This is achieved by increasing the solution conductivity and buffering the catholyte between pH 7 and 8, to avoid the precipitation of $Mn(OH)_2$.

The buffering effect results because $(NH_4)_2SO_4$ forms a manganese-ammonia complex, which lowers the concentration of the manganese cation (Mn^{2+}) in the solution. This increases the

solubility of manganese in the solution as the element is now distributed between Mn^{2+} and the manganese-ammonia complex, allowing a higher pH to be reached without precipitation of the manganese hydroxide (Rodrigues and Bell, 1996). However, the metal becomes pitted and the current efficiency lowered as the concentration of $(NH_4)_2SO_4$ is increased further (Jacobs *et al.*, 1946).

2.7. **Sulphur Speciation and Deposition**

Sulphur speciation is largely dominated by kinetics because many of the reactions are irreversible while others proceed very slowly or do not take place at all. Table 2.7 provides a summary of the sulphur species and the effective oxidation state (Murray *et. al*, 1994). This section is limited to reactions and behaviour of thiosulphate, sulphite, polysulphide, and sulphur dioxide in aqueous solutions known to have been critical in the MMC process.

Table 2.7 Some of the Sulphur Species and Oxidation States (Murray *et. al*, 1994)

Formula	Chemical Name	Effective Oxidation State
SO_3	Sulphur trioxide	6
SO_4^{2-}	Sulphate	
SO_2	Sulphur dioxide	4
SO_3^{2-}	Sulphite	
$S_2O_4^{2-}$	Dithonite	3
$S_2O_3^{2-}$	Thiosulphate	
S_2O	Disulphur oxide	1
S	Elemental sulphur	0
S_3^{2-}, S_4^{2-}, S_5^{2-}	Polysulphides	-2/3, -1/2, -2/5
S_2^{2-}	Bisulphide	-1
S^{2-}	Sulphide	-2
H_2S	Hydrogen Sulphide	-2

2.7.1. *Presence of sulphur dioxide in the electrolyte*

The high negative reduction potential of manganese makes it difficult to deposit and recover the metal at increased current efficiencies. There were attempts to increase the current efficiency by introducing additives such as selenium in the form of selenium oxide (SeO_2) or selenious acid (H_2SeO_3) (Padhy *et al.*, 2015; Zheng *et al.*, 2018). The formation of α-MnSe is a key factor in increasing the % C.E., in which the Se^{4+} is reduced to Se^0 during the electrodeposition process and adsorbs on the cathode (Sun *et al.*, 2011). However, the adsorption of selenium on the manganese cathode affects the quality of the material and has a negative impact on the environment and health of the workers (Padhy *et al.*, 2015). Therefore, sulphur compounds such as SO_2 have been sought and applied in industrial production of electrolytic manganese despite the low % C.E., to eradicate the detrimental effect of the additives.

According to Gamali *et al.* (1964), the % C.E. is found to be between 60 – 65% when 0.1 g/L of SO_2 is added in pure manganese electrolyte. Jacobs et al. (1946), established that adding 0.10 to 0.15 gram per litre (g/L) of SO_2 to the cell feed is beneficial in preventing hydrolysis of manganese in the solution during handling and storage. In addition, the manganese produced from measured quantities of SO_2 is deposited in the α-phase and can be readily separated from the cathode. However, a relation between SO_2 content in the electrolyte and sulphur content in the metal as illustrated in Table 2.8 exists when 0.1 gram per litre of SO_2 is added. The sulphur in the metal is in the sulphide sulphur and not in the sulphate sulphur because the electrolyte becomes occluded (Jacobs et al., 1946). Furthermore, Jacobs et al. (1946), indicated that the presence of sulphite (SO_3^{2-}) increases the relative amount of non-concluded sulphur impurity in the deposited $Mn_{(s)}$, existing in the form of sulphide or polysulphides.

Table 2.8 The composition of sulphur content in the metal (Jacobs *et al.*, 1946)

	Total S	**Sulphide S**
No. 1 with sulphur dioxide	0.046	0.041
No. 2 without sulphur dioxide	0.042	0.002

In support of Jacobs *et al.* (1946), Saunders and Ribane (1986), also established that when the sulphite concentration is increased, the sulphur is also increased in a linear form as indicated in Figure 2.4.

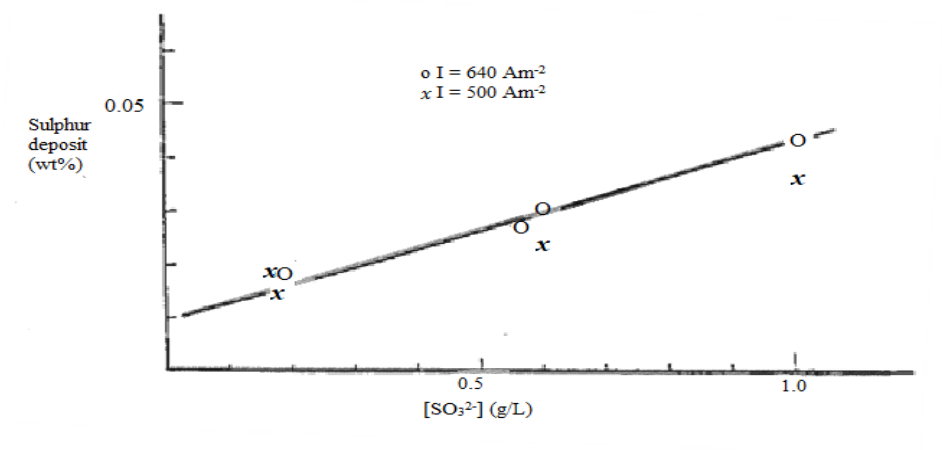


Figure 2.4 The concentration of sulphite vs sulphur in metal (Saunders and Ribane, 1986)

The sulphite is immediately formed when SO_2 reacts with water content in the solution after dosing as indicated in Equation 2.18 (Murray et al., 1994).

$$SO_{2(g)} + H_2O_{(l)} \rightarrow {SO_3}^{2-}{}_{(aq)} + 2H^+{}_{(aq)} \qquad (2.18)$$

2.7.2. *Thiosulphate in aqueous solutions*

According to Murray et al. (1994), concentrations of about 100 ppm of thiosulphate have been detected at MMC. Thiosulphate is generated when elemental sulphur $S_{(s)}$ reacts with sulphite according to Equation 2.19 or in the purification section through Equation 2.10.

$${SO_3}^{2-}{}_{(aq)} + S_{(s)} \rightarrow {S_2O_3}^{2-}{}_{(aq)} \qquad (2.19)$$

Thiosulphate can be present in the cathode compartment by transportation through diffusion as neutral complexes of $MnS_2O_3{}^0$ and $MgS_2O_3{}^0$. This may be electrolytically reduced at the cathode to form equimolar quantities of sulphite and sulphide (Murray et al., 1994). In addition, thiosulphate decomposes rapidly in acidic solutions forming sulphate and a mixture of $S_{(s)}$, H_2S, H_2S_n and SO_2. Furthermore, thiosulphate is readily reduced on various cathodes to equimolar concentrations of sulphide and sulphite (Cotton and Wilkinson, 1988). Saunders and Ribane (1986), confirms that the presence of thiosulphate in the solution does influence the sulphur contained in the electrodeposit as indicated in Figure 2.4.

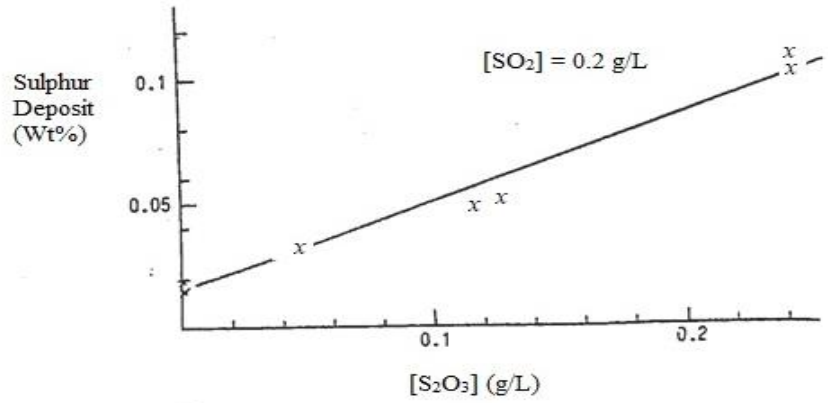


Figure 2.5 The concentration of thiosulphate vs sulphur in metal (Saunders and Ribane, 1986)

It was further established that treating synthetic catholyte or plant catholyte with H_2S to give a pink precipitate produced a very poor, thin, black, and high sulphur deposit with % C.E below 20% (Saunders and Ribane, 1986). When the plant catholyte is treated twice with ammonium sulphide to improve the purification process, the plated metal illustrated high level sulphurs (Lebakeng *et al.*, 2002). The reasons for the poor performance demonstrated by both workers when a sulphide media was added in excess was not clear, although Saunders and Ribane (1986), suspected the presence of organic additives.

2.8. **Impact of Hydrogen Embrittlement on Metal Characteristics**

The ease in knock-off of the brittle α-Mn is achieved by a combination of hydrogen embrittlement, sulphur speciation on grain boundaries and hydrogen bubble formation on dislocations (Murray and Wade, 1998). Smialowski (1962), defines hydrogen embrittlement as the degree to which ductility of the electroplated manganese is decreased. Embrittlement is regarded as a serious problem in the steel and iron industry as it leads to structural failure. However, in the case of manganese production, embrittlement is beneficial to ease metal removal of the deposited product from the cathode.

In the steel industry, sulphide species play a role in the embrittlement through a process known as the sulphide steel cracking (SSC). The SSC is a progressive type of failure that produces cracking at stress levels that are well below the tensile strength of the material (NACE, 2002).

According to NACE (2002) this is a cracking process that develops in the presence of water, corrosion and surface tensile stress were hydrogen ions are a product of the corrosion process (see Figure 2.6). These ions pick up electrons from the base material producing solely hydrogen atoms in which other hydrogen atoms combine to form a hydrogen molecule.

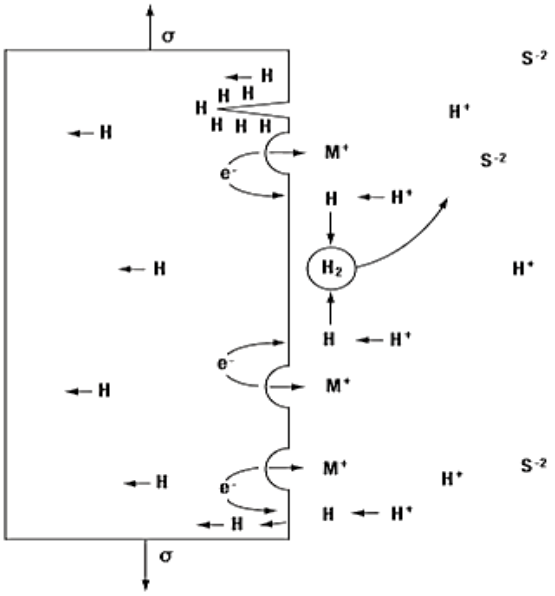


Figure 2.6 Schematic Showing the Generation of Hydrogen Producing SSC (NACE, 2002)

Murray and Wade (1998), made a distinction between the production of hydrogen molecules and hydrogen gas. Whereby, hydrogen gas is formed when the solubility of the hydrogen molecules is exceeded. Although, most molecules collect to form hydrogen bubbles and float away without any negative impact on the metal, a percentage of the hydrogen atoms diffuses into the base metal and embrittle the crystalline structure. The hydrogen bubbles of optimum size hinder the motion of dislocations, increasing strength and lowering ductility.

The build-up of hydrogen in the strain fields around lattice defects, in the dislocation core and in the micro-voids further reduces ductility and often causes embrittlement (Merchant, 1995). In addition, the formation of hydrogen gas during the electroplating of manganese metal results into current inefficiencies. Furthermore, when low alloy and medium alloy steel types are subjected to stress and corrosive action of acidified brine-hydrogen sulphide solutions, varying degrees of embrittlement are shown when measured by ductility loss in the bend tests (Snape, 1967). To restore the ductility of the metal, an amount of hydrogen is required to be removed from the metal after exposure (Snape, 1967; Maciejewski, 2015). NACE (2002), identified that

H_2S does not actively participate in the SSC reaction, however, sulphides act to promote the entry of the hydrogen atoms into the base material. The sulphate component is not reduced at potentials involved by cathodic polarisation of iron and, therefore, sulphate does not influence the absorption of hydrogen. The presence of sulphites may also be reduced to sulphide ions on the cathode compartment which do influence absorption. Sulphide has been referred to as a "poison of the recombination reaction" (Smialowski, 1962).

According to Liu *et al.* (2014), "the susceptibility of both the 13Cr stainless steel and P110 steel to the SSC was significantly promoted by increasing H_2S partial pressures in solutions containing 4 MPa CO_2 and different P_{H2S} (0-0.3 MPa)". In addition, fracture toughness found to be lowered 25–50% with increased sulphide concentrations. However, Maciejewski (2015), found that "the sulphur content has on the notch toughness in the longitudinal direction, but transverse notch ductility decreased significantly as indicated by a change in anisotropy ratio by 260%".

2.9. **Summary**

This study is aimed at establishing the impact of excess sulphide on the electrodeposition of manganese metal. This chapter provided a theoretical background around the important role that the sulphur species play in the manganese solution. It was established in this chapter that the presence of these sulphur species in the process solution results from the addition of sulphuric acid (for ore dissolution), sulphide (purification of the solution) and SO_2 (to stimulate metal phase change).

The presence of unwanted metal ions or impurities in the solution (after leaching of the calcined ore) will need to be removed prior to electrodeposition. This is because metal ions have a deleterious impact on the electroplating process i.e. low current efficiencies due to low electrode-reduction potential of manganese. Therefore, ionic precipitation of the impurities using various sulphide reagents is preferentially used for solution purification. Due to complexity of the purification step, a significant excess manganese in the solid phase or precipitate is used as an end point to indicate effective purification. This is done by addition of excess sulphide to the solution thus for manganese with low solubility to precipitate as manganese sulphide. Furthermore, excess sulphide is also added to increase the particle size of the precipitate to eliminate any seepage of fine particles through the filters. The presence of fines in the electrolyte tends to re-dissolve and cause challenges in the electrodeposition of the

metal. However, for industrial practice, the addition of excess sulphide should be carefully controlled to avoid areas of high local sulphide concentration because the formed precipitate tends to re-dissolve into solution. It is extensively illustrated in the literature review that the metal sulphides re-dissolve to form polysulphides when excess sulphide is added.

In the presence of oxygen or an oxidizing media, and pH value between 7 – 12, polysulphides react to form thiosulphate and sulphide. In addition, the SO_2 gas added in the electrolyte (to convert manganese from the γ-Mn to the more suitable α-Mn) hydrolyse to form sulphite. The sulphite reacts with solid sulphur to form additional thiosulphate, which is transported to the cathode compartment through diffusion to form complexes. In this review, therefore, it was indicated that both thiosulphate and sulphite can play a role in the increase of the sulphur content. In addition, the presence of sulphite and sulphide causes embrittlement on metallic components, whereby in the steel industry the term 'hydrogen embrittlement' is regarded as a serious challenge. This occurs when the sulphide acts to promote the absorption of hydrogen atoms into the base material, resulting into cracking of the material.

3. CHAPTER THREE: MATERIAL, EQUIPMENT AND METHODS

3.1. Introduction

The test programme involved the installation, commissioning and operation of the laboratory sized electrolytic cells (labcells). The design of the labcells is a direct scale-down of the cells used in the Manganese Metal Company (MMC) cellhouse. The labcells were operated with the same procedure adopted in the plant to simulate the electrowinning process. This method of testing on the laboratory scale was preferred to an on-line full-scale test work as it is more sensitive, the results are immediate, handling of solution is manageable, low risk due to reduced power or current requirements and less labour intensive.

The investigation was divided into two sections. Firstly, the solution preparation stage that was conducted to manipulate the sulphide content in the feed solution and determine the impact at varied concentration. In addition, the introduction of oxygen by bubbling the solution with compressed air is used to determine the degree of thiosulphate formation. Secondly, the electroplating process (i.e. using the laboratory electrolytic cells) was used to indicate the performance and the change in morphology of the metal with the change in the sulphide concentrations.

This chapter gives a detailed description on the equipment, experimental methods, experimental design, and analytical techniques employed in the study. Data analysis methods are discussed in the study. A summary is subsequently provided to wrap-up the chapter.

3.2. Materials: Solution Preparation

3.2.1. *Feed solution*

The solution for the test program was collected at the plant cell feed, an area known as the F-bank rotameter manifold. The solution at this stage was already treated with Sodium Hydrogen Sulphide (NaHS) and impurities been removed as a form of insoluble metal sulphide precipitate. The removal of the precipitate was done using the thickening and filtration processes from the MMC plant to ensure that there is no presence of fine particles in the solution. As illustrated in Figure 3.1, a valve was connected at the rotameter area to make it easier for collecting the solution.



a) **b)**

Figure 3.1 Solution collection point a) Valve at F-bank rotameter. b) Installed valve for solution collection

The solution was collected using a calibrated (i.e. clearly marked volumetric levels on the drum using a 5-litre beaker) 25-litre drum or holding tank, which was thoroughly rinsed using the feed solution to minimise contamination. The plant feed solution was chosen over the synthetic solution, as it was necessary to simulate the labcells close to the performance of the plant. In addition, the sulphur values of labcells metal can be compared to plant metal for standard runs performed on fresh plant solution only (Glück and Pieterse, 1997). The plant catholyte was also used to start-up the labcells. The selection criteria of the catholyte was based on the performance of plant cells according to a higher cell feed rate, a higher current efficiency (% C.E) and lower cell voltage.

3.2.2. *Reagents*

The reagents used in the study were collected from the plant and others were added in the solution according to the desired electrowinning process specification. This included the addition of a polyacrylate flocculant (also known as magnafloc 351 or magna floc) smoothing agent. In the plant, the magna floc is used to control the intensity of metal cracking as a smoothing agent. The Sulphur dioxide (SO_2) gas produced from the SO_2 plant located at MMC,

was bubbled into the solution at the plant feed tank. The 24% NaHS reagent was sourced from the plant holding tank known as the T155. This was already mixed and ready to be used in the plant for purification purposes and a required volume was collected for the test program (see Figure 3.2). The sodium silicate (Na_2SiO_3) used in the test program was collected from the plant immediately after preparation. The sodium silicate is a release agent applied to allow ease in removal of the manganese (Mn) metal from the cathode plate during harvesting.

3.2.3. *Reagent dosing setup*

The set up for the solution-preparation is illustrated in Figure 3.2. The preparation of the solution according to the test program was conducted in a fume cupboard to avoid direct contact with the NaHS during aeration. The direct contact may lead to headache, drowsiness, dehydration, or serious health related issues especially when the pH drops to acidic range and results in the formation of hydrogen sulphide gas. A 5-litre beaker was used to carefully measure the required volume in the holding tank. A 25-litre holding tank was chosen to contain and allow the preparation of 20 litres volume of solution for the test. A 10 mm glass cylinder was used to measure the desired amount of NaHS reagent.

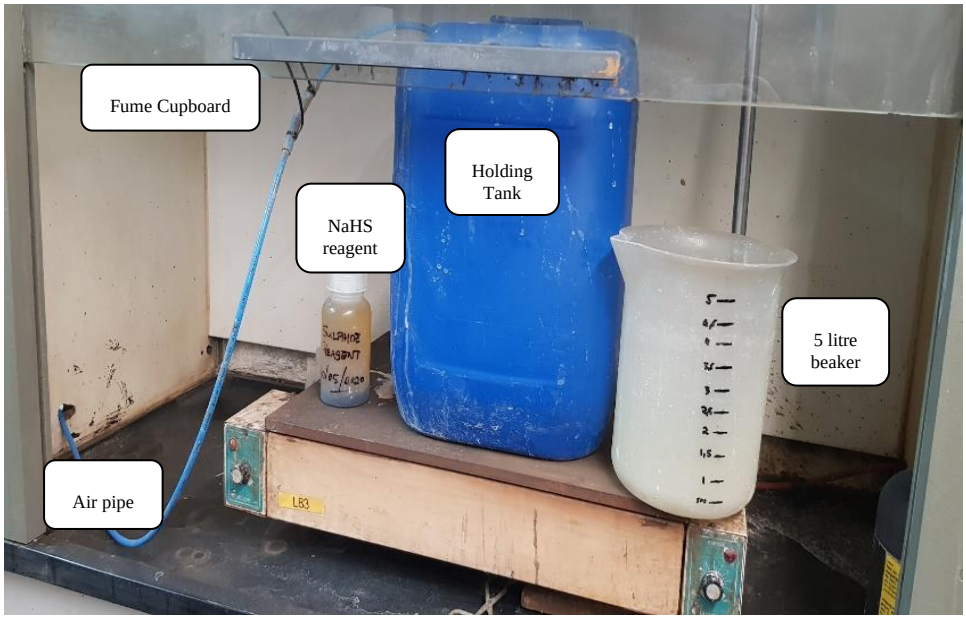
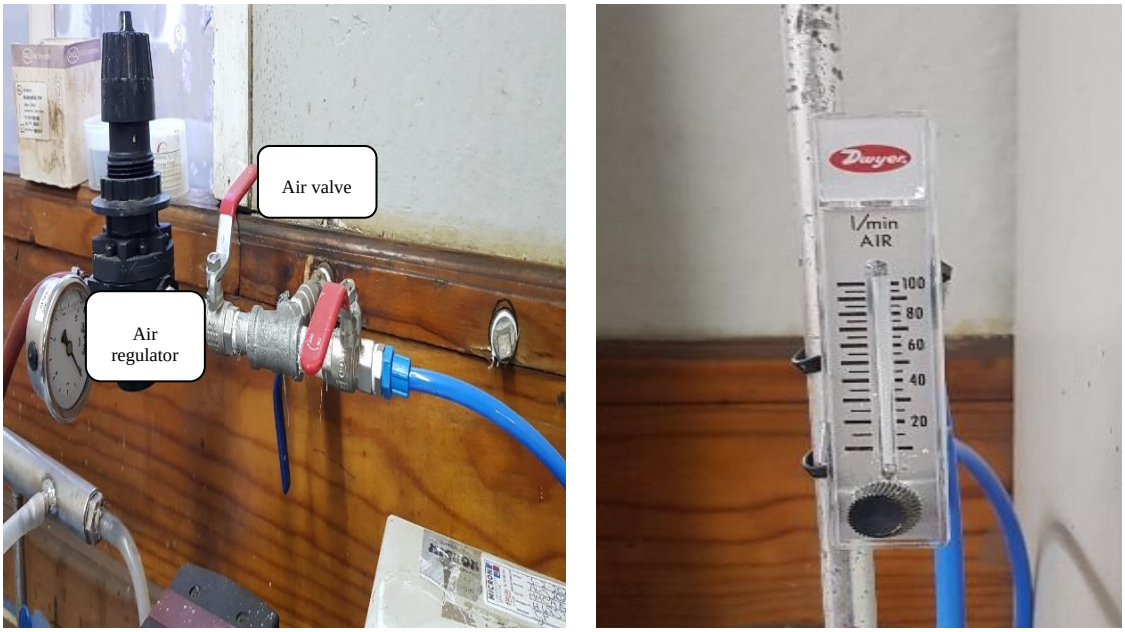


Figure 3.2 Test setup for solution preparation

3.2.4. *Solution aeration*

A compressor was installed to supply the required volume of air in the research laboratory (research lab). Figure 3.3 (a) illustrates an air regulator that was installed in the research lab to control the air pressure to a maximum of 600 kPa for both solution aeration and filtration unit. The controlled air was transferred to the holding tank to induce aeration using a 12 mm diameter pipeline that was connected to an air control valve. The flow rate of the air was measured in litres per minute on an air flow meter as indicated in Figure 3.3 (b). A stopwatch was also used to measure time for aeration.



a) **b)**

Figure 3.3 Materials used to control the aeration of solution a) High-pressure airline for oxidation. b) Airflow meter

3.2.5. *Filtration equipment description*

A Macsalab filter, as illustrated in Figure 3.4, was used for the removal of fine particles. The filter vessel had a 9.7 litre volume capacity and consisted of a base that is fabricated with carbon steel, a yoke and a 304 stainless steel grade vessel. The solids were separated from the solution using a Whatman filter paper with a grade of 602h. This was a dense filter paper designed to collect fine particles above 2µm.



Figure 3.4 Macsalab filter press for solid separation

A 12 mm diameter pipeline was connected at the discharge point below the base to collect the filtrate into a holding tank.

3.3. **Equipment: Laboratory Electrolytic Cells**

The test program was conducted at the research lab available at MMC where two labcells denoted as Cell A and Cell D as illustrated in Figure 3.5, were located.

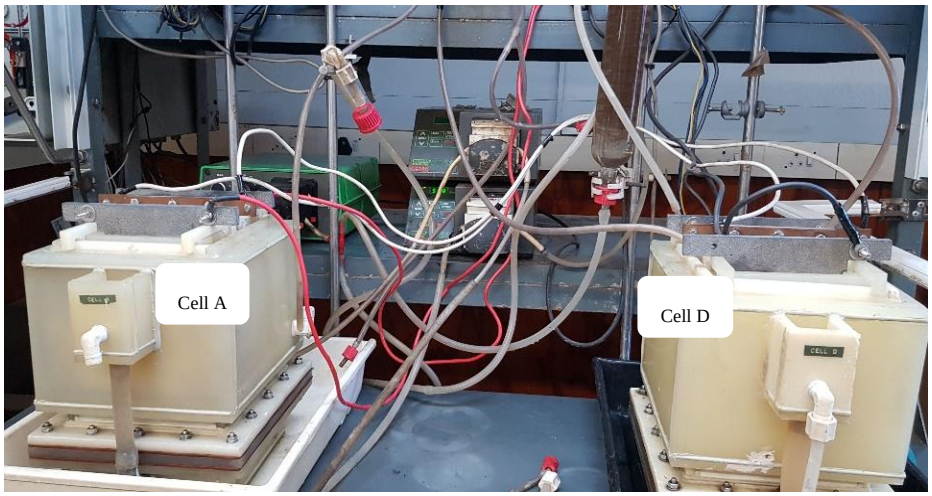
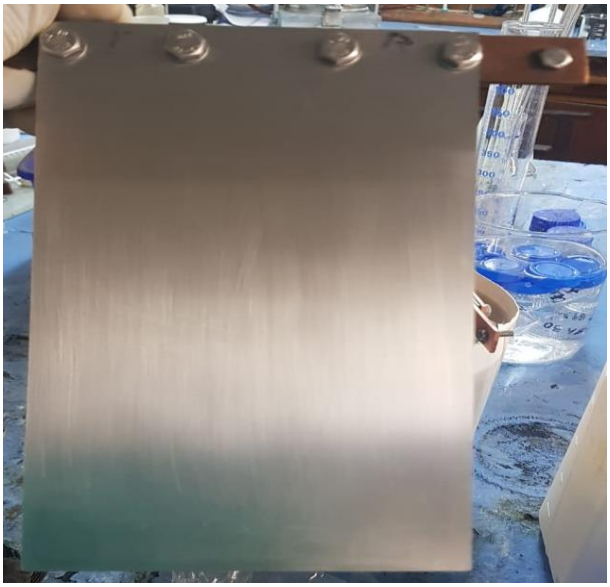


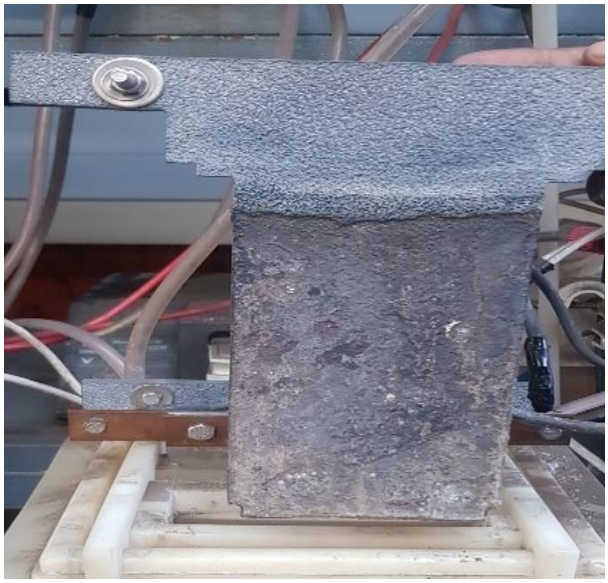
Figure 3.5 Laboratory electrowinning cells A and D

The labcells were manufactured from a polypropylene material with a total volume capacity of 5 litres (i.e. length (160 mm), width (160 mm), height (160 mm) and a 1 litre false bottom). A false bottom is a compartment in the labcell that is used to collect and re-circulate the catholyte.

Each cell can accommodate one cathode (316 stainless steel material) and two anodes (Pb-1% Ag grade) as illustrated in Figure 3.6 (a) and (b) respectively.



a)



b)

Figure 3.6 Types of electrodes used in the labcells a) Stainless Cathode Plate b) Anode Plate

3.3.1. *Electrical current connection and flow*

The current flow through the circuit was supplied using a direct current (DC) rectifier (see Figure 3.7) to make the electrowinning process possible.



Figure 3.7 Direct Current Power Supply

The electrical current moved through the electrodes (i.e. cathode and anode) using positive and negative electrical cables. The red and black cables represented positive and negative electrical potential, respectively, as indicated in Figure 3.5. The white cables allowed a positive potential to be distributed from the cathode plates of cell A to the anodes of cell D (Figure 3.5). This follows the setup that best represents the connection in the plant as described in Appendix A.

The ‘Banana’ socket and plugs were used to ensure that the electrical contact was made on the electrodes. The current and voltage flowing from the rectifier through the electrodes and power cables were measured using an AC-DC BM853A multimeter.

3.3.2. *Temperature control*

The temperature in the cells was measured using a red mercury thermometer with an upper temperature limit of 50℃. A water bath containing heating elements (see Figure 3.8.a) was used in this test program to minimize heat losses through the cells. The warm water in the water bath was supplied to a glass condenser (indicated by Figure 3.8.b) using peristaltic pumps to exchange heat with the catholyte and feed solution. The catholyte was recirculated through the inner coil of the glass condenser and returned to the cell at the desired temperature.



a) **b)**

Figure 3.8 Equipment to control the temperature of the cells a) Elemental water bath b) Glass condenser for heat exchange

3.3.3. *Solution supply and control*

The Watson-Marlow 500 series peristaltic pumps were also used to supply the filtrate or feed solution through the glass condenser to the catholyte compartment of the cells. The anode boxes were covered with the diaphragm cloth on both sides, attached using a silicone sealant. The function of the diaphragm cloth was to attain control over the flow of solution and movement of ions through the cell. The box was then connected to the false bottom via a rubber tube, to effectively separating the anolyte (pH of ±1.0) from the catholyte (pH of ±8.3) as indicated by Figure 3.9.

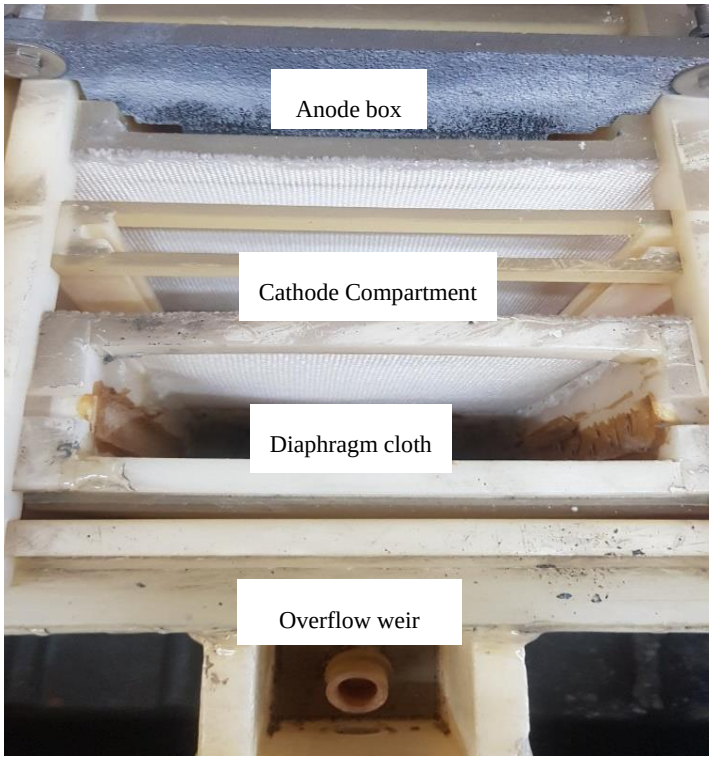


Figure 3.9 The top-view of the lab-cells section

An overflow weir indicated on Figure 3.9 was installed to control the level of catholyte in the cell and the collection of the anolyte. An extension pipe was connected at the outlet to collect the anolyte into a holding tank.

3.4. **Analytical Techniques**

Various materials and methods were adopted to collect data that best describes the test programme by analysing the solution or Mn metal. The following were analysed i.e. pH or Eh, sulphur, surface morphology, SO_2 content, thiosulphates, excess sulphide, and manganese concentration.

3.4.1. *pH measurements*

The pH levels of the test solution were measured using a Hanna pH/ORP meter with an electrode HI – 9125. The pH meter was calibrated with pH buffers 4, 7 and 10; and checked on a regular basis to ensure accurate readings.

3.4.2. *Sulphur analysis in metal content*

The analysis of elemental sulphur in the manganese metal samples was conducted using the LECO CS744 S/N:20036 analyser indicated on Figure 3.10. This method is also adopted at the MMC plant to determine the sulphur and carbon content in the Mn metal, and powder samples for plant quality control and certification. The Mn metal sample was crushed to -20 μm size and mixed. The bulk material was split to select a representative sample of which 1 gram was weighed using a calibrated scale and placed into a crucible. The LECO analyser was first calibrated using a certified reference standard sample. The sample in the crucible was then carefully placed into the furnace of the LECO machine and analysed.



Figure 3.10 LECO CS744 sulphur content analysis

3.4.3. *Scanning electron microscope analysis*

The Mintek, Mineralogy Division was approached to conduct analysis on the Mn metal samples produced from the test programme. This was done to reveal the mineralogical information such as the type of phase present in the Mn metal plates, the mineral association and texture or morphology of the Mn metal. The Carl Zeiss Evo MA15 Scanning electron microscope (SEM) with a Bruker energy dispersive spectrometry (EDS) system was used to analyse the samples. The SEM observations were demonstrated with a suitable backscattered electron (BSE) images and with relevant semi-quantitative EDS data. The higher the accelerating voltage on the EDS, the more penetration into the sample will occur.

3.4.4. *Determination of the SO_2 content using titration*

The prepared feed solution was titrated in a 0.03 molar potassium iodide (KIO_3) to determine the concentration of SO_2. This was a redox titration method where the solution was diluted with a measured volume of distilled water and followed by the addition of concentrated hydrochloric acid (HCl). The KIO_3 titrant was added until the solution turned blue in colour to indicate the endpoint. The volume of the titrant used was measured to determine the concentration of SO_2.

3.4.5. *Determination of the thiosulphate content using titration*

The presence of thiosulphate in the solution was measured by redox titration with a standard 0.01 molar iodine solution. Since the presence of sulphide, sulphur dioxide or sulphurous acid reacted with iodine, it was necessary to remove or mask the components before titration. A strong acid was added to displace the weak acids as hydrogen sulphide (H_2S) and SO_2 gas. Any other trace elements of SO_2 remaining were also masked with formaldehyde. The volume of the iodine solution was used to determine the concentration of thiosulphate. The sulphur was produced during the decomposition of polysulphides present.

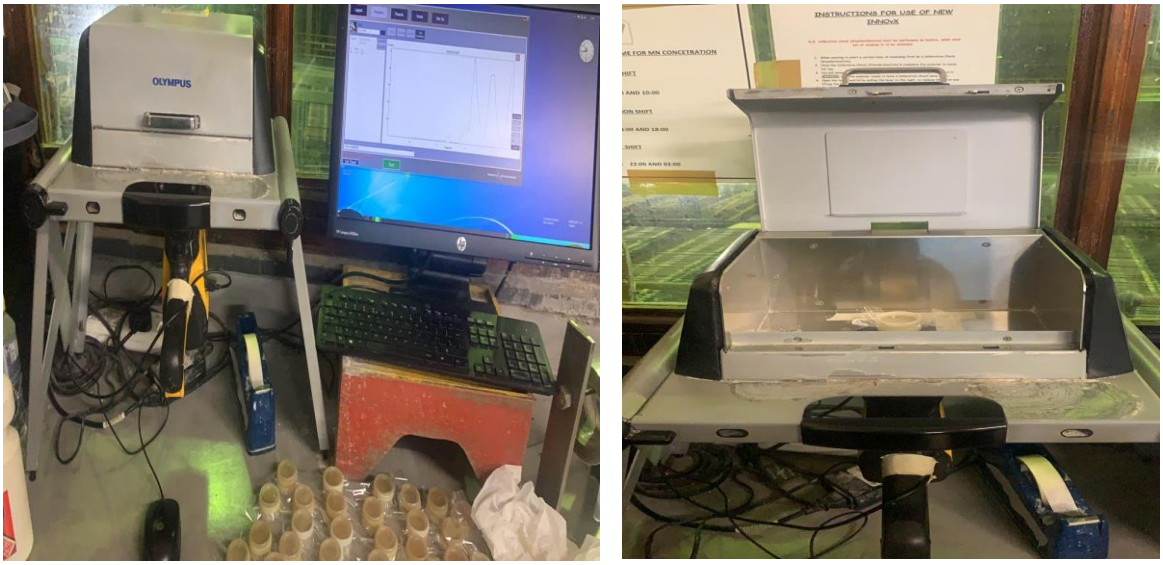
3.4.6. *Determination of excess sulphide using lead acetate test*

The test was conducted to qualitatively determine the presence of sulphide in the test solution. The H_2S and soluble sulphide are released from the solution when reacted with a strong acid. Therefore, the presence of excess sulphide was detected when a paper soaked with lead acetate was contacted with the H_2S. The colour formed on the surface of the filter paper was considered and related to the degree to which the excess sulphide is present (i.e. nil, faint, medium or dark stain).

3.4.7. *Analysis of manganese concentration in the solution*

The Mn content in both the catholyte and cell feed solution were determined using the Innovex system. This is an X-ray fluorescence (XRF) elemental analysis equipment located at MMC plant and the setup is indicated on Figure 3.11 a) and b). The materials needed for the Innovex system were capsules to collect the samples, a screen monitor to control (stop, start and calibrate options) and results indication, and a test stand or compartment to ensure that the fluorescent light is contained to minimize the measurement variation. A 10ml sample was collected into a capsule and carefully wrapped with a film plastic. The wrapped sample was

inserted into an Olympus test stand compartment and the lid was closed for the analysis to commence.



a) **b)**

Figure 3.11 Manganese analysis equipment a) Innovex setup for manganese in solution b) Olympus test stand compartment

3.5. **Design of Experiments**

The design of experiment (DOE) was selected as a tool in this experiment to provide guidance in investigating the effect of input variables (factors) on an output variable (response) simultaneously. The DOE is a process improvement tool that is normally used to identify the process conditions and product components that affect the quality and determine the factor settings to optimize results (MiniTab, 2020). The experiment consisted of a series of runs whereby purposeful changes were made to the input variables and data was collected at each run. The Minitab statistical software was used in the DOE as it offered five types of designs i.e. screening, factorial, response surface, mixture, and Taguchi designs.

A factorial design tool was selected as a better option in this experiment to determine the impact of experimental factors on the response. The experimental design had three level settings for sulphide dosing (i.e. 0, 0.5, 1) and two-level settings for aeration of the solution (i.e. 0, 1) as indicated by Table 3.1. The runs were done in a set of six and repeated three times to determine reproducibility of the impact these variables influence the concentration of thiosulphate, sulphur in the metal and metal cracking.

Table 3.1 Definition of factors and levels

Factors	Level Settings of the Factors		
NaHS	Setting 1	Setting 0.5	Setting 0
Aeration	Setting 1	N/A	Setting 0

Since there were only two levels for the aeration of the solution, the output had two data points when aeration was the factor considered. For sulphide addition, the graph had three data points. Table 3.2 shows the factorial design matrix that was generated using the Minitab software. This resulted into a total of 18 test runs that were generated from the factorial design.

Table 3.2 Factorial design and design matrix for test program

Cycle	Run Order	Cell Type	Solution type	Sulphide Setting	Aeration Setting
Cycle 1	1	A	Plant Fresh	0	0
	2	D	Solution Preparation	0	1
	3	A	Solution Preparation	0.5	0
	4	D	Solution Preparation	0.5	1
	5	A	Solution Preparation	1	0
	6	D	Solution Preparation	1	1
	7	A	Plant Fresh	0	0
	8	D	Solution Preparation	0	1
	9	A	Solution Preparation	0.5	0

Cycle 2	10	D	Solution Preparation	0.5	1
	11	A	Solution Preparation	1	0
	12	D	Solution Preparation	1	1
Cycle 3	13	A	Plant Fresh	0	0
	14	D	Solution Preparation	0	1
	15	A	Solution Preparation	0.5	0
	16	D	Solution Preparation	0.5	1
	17	A	Solution Preparation	1	0
	18	D	Solution Preparation	1	1

3.6. **Data Analysis Method**

Graphical techniques were used to display, interpret, and identify patterns to investigate further and understand the data. The following tools were selected to best represent the data analysis method which was used in this test programme i.e. scatter plot, null hypothesis and p-value, line graph or time series, boxplot, and two-sample t-test.

3.7. **Method: Solution Preparation**

The DOE provided guidance into the test programme whereby six different solution types were identified and used. The NaHS dosing and aeration differentiated the solution type used in the labcells. Figure 3.12 illustrate a process map that was followed during the solution preparation of the test programme. The NaHS dosing setting at 1.0 represented a dosage at 100% of the reagent as established from the plant historic data. At 0.5 setting, NaHS was dosed at 50% volume. This was done to produce any form of polysulphides in the solution according to Shea

and Helz (1988). However, due to the banning on the use of asbestos for laboratory use, the analysis of polysulphide was omitted from this experimentation. This is because the analytical method required crucibles manufactured from asbestos. The 0 NaHS setting represented the fresh plant solution whereby NaHS was not dosed in the solution.

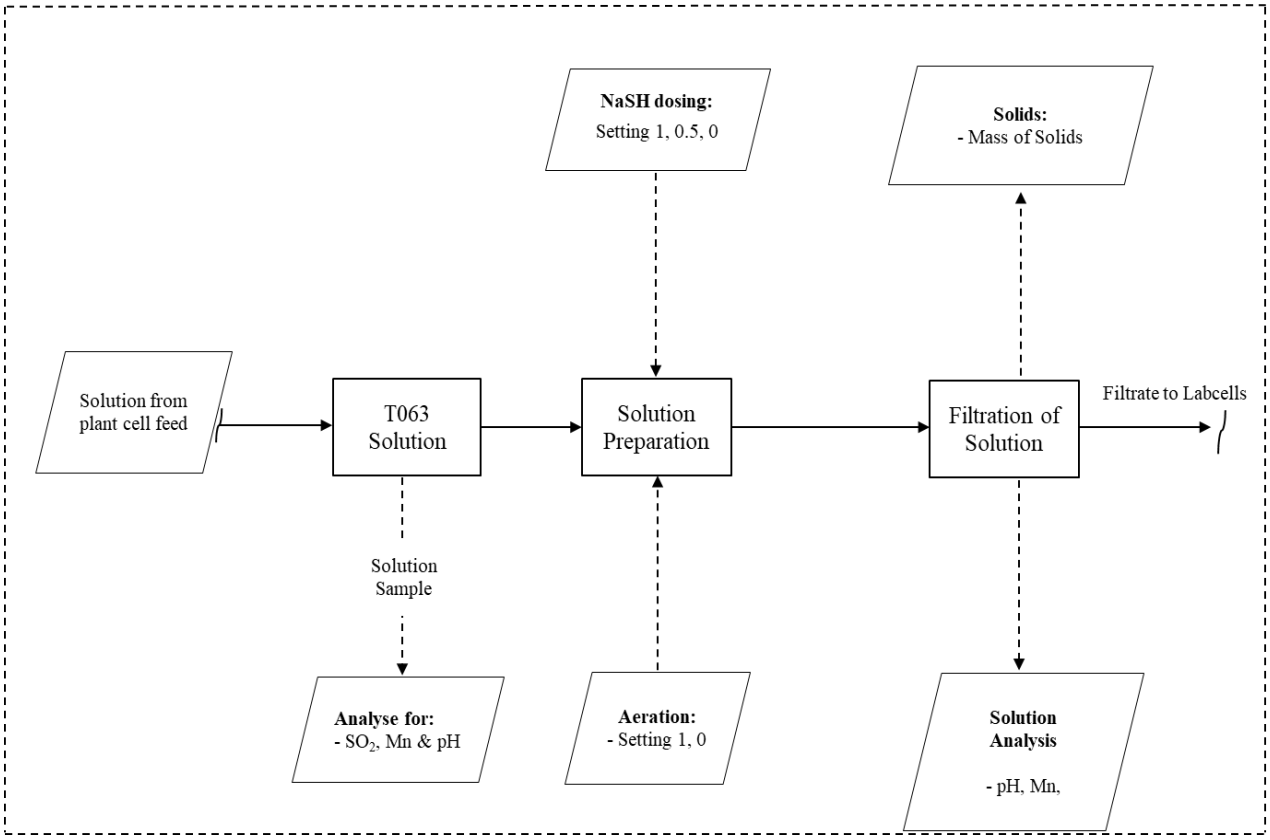


Figure 3.12 Flow diagram for the solution preparation experiments

The aeration of the solution was conducted at airflow of 80 L/min for 2 hours, which represents the residents time at the launder. This represented an aeration setting at 1.0, whereas at 0 settings, no aeration was introduced into the holding tank. Aeration was introduced to establish the formation of thiosulphate in the solution according to Steudel *et al.* (1986).

3.7.1. *The feed solution quality*

The solution collected at the F-bank rotameter manifold consisted of standard chemical composition as indicated in Table 3.3. The specification of the solution quality is necessary as it is the main reason for the variance of the day-to-day cellhouse performance. As described in Chapter 2, the impurities present in the feed solution have a negative impact on the performance of the labcells i.e. % C.E, pinholes on the surface of the metal and sulphur quality.

Silica (Si) and magna floc are also constituents of the electrolyte necessary in determining the quality of the solution. It is well known from MMC plant personnel and proven with experience that silica and magna floc are required in the solution to prevent "hard knock-offs" of the manganese electroplated on the stainless-steel cathodes. The silica and magna floc content were maintained between 9.5 – 11.5 g/L and 0.32 – 0.41 g/L respectively, because any concentration above this will result into cracking and flaking of the labcells.

Table 3.3 Specification of fresh plant solution

Chemical name	Specification
Mn ($\frac{g}{L}$)	29.5 – 30.5
Si ($\frac{mg}{L}$)	9.5 – 11.5
$(NH_4)_2SO_4$($\frac{g}{L}$)	125 – 130
SO_2 ($\frac{g}{L}$)	0.3 – 0.4
Magna floc ($\frac{mg}{L}$)	0.3 – 0.4
Turbidity (NTU)	0 – 2
pH	6.8 – 7.0
eH (mV)	-50 – 180

Therefore, to rule out the metal cracking or any variation of the metal sulphur content, the solution quality was an aspect that received special attention when running the labcells.

3.7.2. *Volume of NaHS required for dosing*

The volume of the sulphide required for dosing in the test programme was determined from the historical plant data. About 705 data points were extracted from the MMC central data system. T-test was used to analyse the data and to compare the NaHS dosing between T102A and T102B of the purification circuit (see Figure D.4 for a description of the T102A and T102B). The t-test, as indicated in Figure D.2 and Figure D.3 of Appendix D, also provided a descriptive analysis as illustrated by Table 3.4. The mean of both the sulphide dosing rate and the solution flow were calculated and used as a basis for the dosing ratios in the test programme.

Table 3.4 Descriptive Statistics

Sample	N	Mean	StDev	SE Mean
T102 A Sulphide (l/min)	705	1.22	0.36	0.01
T102 B Sulphide (l/min)	705	1.17	0.41	0.02
T102 A Flow [m³/h]	705	94.76	8.02	0.30
T102 B Flow [m³/h]	705	94.95	7.92	0.30

A volumetric flowrate for the NaHS and solution were identified 1.2 L/min and 95 m^3/hr, respectively. The units of the sulphide dosing rate in the plant were manipulated to establish an equal unit, thus to determine the ratio. The ratio of the sulphide flow to solution was calculated using Equation 3.1.

$$Ratio = \frac{\text{NaHS (m3/hr)}}{\text{Solution (m3/hr)}} \qquad (3.1)$$

$$= \frac{0.072}{95} = 0.000758$$

This was regarded as the NaHS dosing setting of 1.0 according to the requirements of the DOE.

3.7.3. *Tests performed*

The preparation of the solution for labcells trial run was conducted according to the design established by the DOE. The following provides a full description of the methodology which was followed. This includes the first six runs denoted as a cycle i.e. 0 NaHS and 0 aeration, 0 NaHS and 1 aeration, 0.5 NaHS and 0 aeration, 0.5 NaHS and 1 aeration, 1 NaHS and 0 aeration, and 1 NaHS and 1 aeration. Therefore, 150 litres bulk solution was collected at the F bank rotameter manifold for the first six trial runs and sampling.

0 NaHS and 0 Aeration

About 20 litres of solution was measured in a holding tank using a 5-litre beaker. This was a fresh plant solution that was necessary to establish a baseline of the experiments. The holding tank was labelled, and the feed pipes of Cell A were inserted in the holding tank for solution supply to the cell.

0 NaHS and 1 Aeration

To determine the impact of aeration on the fresh plant solution, about 20 litres of solution was measured in the holding tank. The solution was placed in a fume cupboard where an air pipe was connected. The air control valve was opened, and airflow was controlled at 80 l/min. The air pipe was carefully placed in the holding tank and solution was bubbled for 2 hours. The 2 hours represents the resident time of the solution from the sulphide thickener exit launders to the filtration feed (T171 launder). After 2 hours, the air control valve was closed, the tank was carefully removed from the fume cupboard. The holding tank was labelled, and the feed pipes of Cell D were inserted in the holding tank for solution supply to the cell.

0.5 NaHS and 0 Aeration

To determine the impact of the presence of excess sulphide or polysulphide, about 20 litres of solution was measured in the holding tank. A sample was collected, and the Mn concentration measured using the Innovex before the dosage of NaHS and recorded. The solution was carefully placed in a fume cupboard to avoid any exposure to NaHS fumes. Using the calculated ratio of NaHS to solution flow, about 7.6 mL of NaHS was measured using a 10mL glass measuring cylinder and added in the 20-litre holding tank. After the dosing, the tank was fully closed, and the solution was mixed manually by shaking the holding tank for less than 2 minutes. This was repeated every 30 minutes for 2 hours to ensure that the NaHS and distributed evenly throughout the tank. This frequency showed to be effective as the cloudiness in the solution (i.e. formed when NaHS is mixed with a manganese sulphate solution) was evenly distributed throughout the holding tank. After 2 hours, the tank was carefully removed from the fume cupboard and the solution was filtered. The holding tank was labelled, and the feed pipes of Cell A were inserted in the holding tank for solution supply to the cell.

0.5 NaHS and 1 Aeration

To determine the impact of the presence of excess sulphide or thiosulphate, about 20 litres of solution was measured in the holding tank. A sample was collected, and the Mn concentration measured using the Innovex before the dosage of NaHS and recorded. The solution was carefully placed in a fume cupboard to avoid any exposure to NaHS fumes. Using the calculated ratio of NaHS to solution flow, about 7.6 mL of NaHS was measured using a 10mL glass measuring cylinder and added in the 20-litre holding tank. After the dosing, the air control valve was opened, and airflow was controlled at 80 l/min. The air pipe was carefully placed in the holding tank and solution was bubbled with air for 2 hours. The 2 hours represents the

resident time of the solution from the sulphide thickener exit launders to the filtration feed (T171 launder). After 2 hours, the air control valve was closed, the tank was carefully removed from the fume cupboard and the solution was filtered. The holding tank was labelled, and the feed pipes of Cell D were inserted in the holding tank for solution supply to the cell.

1 NaHS and 0 Aeration

To determine the impact of the presence of excess sulphide or polysulphide, about 20 litres of solution was measured in the holding tank. A sample was collected, and the Mn concentration measured using the Innovex before the dosage of NaHS and recorded. The solution was carefully placed in a fume cupboard to avoid any exposure to NaHS fumes. Using the calculated ratio of NaHS to solution flow, about 15.2 mL of NaHS was measured using a 20mL glass measuring cylinder and added in the 20-litre holding tank. After the dosing, the tank was fully closed, and the solution was mixed manually by shaking the holding tank for less than 2 minutes. This was repeated every 30 minutes for 2 hours to ensure that the NaHS is distributed evenly throughout the tank. After 2 hours, the tank was carefully removed from the fume cupboard and the solution was filtered. The holding tank was labelled, and the feed pipes of Cell A were inserted in the holding tank for solution supply to the cell.

1 NaHS and 1 Aeration

To determine the impact of the presence of excess sulphide or thiosulphate, about 20 litres of solution was measured in the holding tank. The Mn concentration was measured using Innovex before dosing of NaHS and the concentration was recorded. The solution was carefully placed in a fume cupboard to avoid any exposure to NaHS fumes. Using the calculated ratio of NaHS to solution flow, about 15.2 mL of NaHS was measured using a 10mL glass measuring cylinder and added in the 20-litre holding tank. After the dosing, the air control valve was opened, and airflow was controlled at 80 l/min. The air pipe was carefully placed in the holding tank and solution was bubbled with air for 2 hours. After 2 hours, the air control valve was closed, the tank was carefully removed from the fume cupboard and the solution was filtered. The holding tank was labelled, and the feed pipes of Cell D were inserted in the holding tank for solution supply to the cell.

3.7.4. *Solution filtration procedure*

The filtration of the solution was done using a Macsalab filter press to remove the presence of fine particles. The impact of fine particles is detailed in section 2.5.4 of Chapter 2; which indicates that, fine particles causes an increase in sulphur content and redissolution of the plated

metal. Therefore, this was considered during the test programme to ensure that a clear solution is attained to avoid any external variation. The mass of the dry filter paper was weighed and recorded before placing into the vessel. The vessel was filled with solution until full and the top cover was repositioned, the ball valve was closed, and the yoke was tightened.

A holding tank was placed underneath the vessel. The air control valve was slowly opened to the air pipe and measured at 80 l/min. The valve was kept opened until the filtrate was completely discharged into the holding tank. Once the vessel was empty, the air supply was closed. The air was slowly released from the vessel via the ball valve located on the top cover. The yoke was then released and placed into the resting position to remove the top cover. The cycle was repeated with the same filter paper until the batch solution was completely filtered. The dry cake was recovered and placed in an oven to dry. The solids and filter paper were weighed, and the mass was recorded. A sample from the filtrate was collected to measure the Mn concentration after dosing. Other components that were analysed on the filtrate sample were excess sulphide, thiosulphate, and pH of the filtrate.

3.7.5. *Oxidation of the solution in the plant*

Murray *et al.* (1994), indicated that oxygenation or aeration does seem to be occurring in the steep launder or supertube (indicated by Figure 3.13) at MMC immediately after leaving the sulphide thickener. However, the oxygenation challenge was not investigated as the precipitate removal efficiency in the thickener was denoted as the remedial action to resolve challenges of the sulphur quality.



Figure 3.13 Supertube launder

Therefore, since not much effort was previously placed in confirming the oxidation of the sulphide species at the super-tube, a pH/eH probe was installed at the bottom of the launder at an area known as the T171 (see Figure 3.14a and Figure 3.14b). The data recorded by the probe was logged on the MMC central data system. The probe at the T102 exit (before the supertube or steep launder) was already installed and the eH was measured in the plant.



(a)



(b)

Figure 3.14 (a) T171 launder with no eH/pH probe (b) T171 launder eH/ pH probe installed

3.8. **Method: Laboratory Electrolytic Cells**

The filtrate was used in the labcells according to Figure 3.15, a flow diagram describing the setup and running of the test program. The labcells were operated for 18 – 22 hours and data was collected to determine the correlation of the response to the varied factors on each run. The data was collected on a 2 hourly basis during test run was on the catholyte and electrode potential. Subsequently, at the completion of each run, the anolyte and Mn metal were also analysed. The following sections provides the methodology that was followed in preparing the cells, operating the cells, metal harvesting and determination of cell performance.

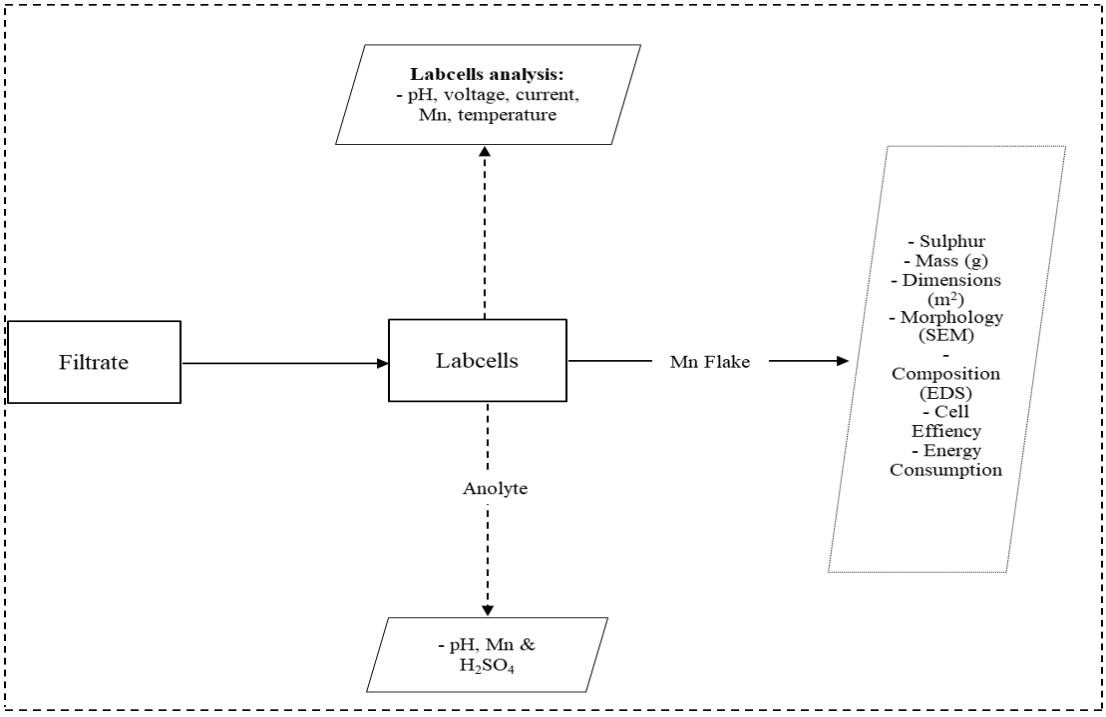


Figure 3.15 Flow diagram for the labcells operations

3.8.1. *Preparation of the labcells material*

The preparation of the cells, electrodes and diaphragms were carried out to minimise the introduction of external variations due to the sensitivity of the labcells.

Laboratory electrolytic cells preparation

After stripping the cathodes at the end of a cycle run, the rectifier was switched off, the anodes were disconnected and removed from the anode boxes. The anode boxes were disconnected from the rubber tube connecting to the false bottom, thus allowing the anolyte to drain and mix with the catholyte. The frames holding the cathode plates were also removed from the cells. The discharge valve at the back of the labcells was opened to drain the anolyte-catholyte solution. The cells were washed with running water and soaked in cleaning solution (i.e. a mixture of 4% hydrogen peroxide and 6% sulphuric acid) to remove the manganese hydroxide ($Mn(OH)_2$) scale in the glass condenser, diaphragm cloth and re-circulation pipes.

Preparation of anodes

The anodes were cleaned under running water and the loose manganese dioxide (MnO_2) layer was gently scrapped off, thus leaving behind the lead dioxide (PbO_2) layer and any adherent MnO_2. The PbO_2 is a hard, stable, and protective layer that is insoluble in water or weak acid.

Anode box diaphragm preparation

During the operation of the cells, a catholyte head of 2 – 3 mm was maintained since the flowrate of solution through the diaphragm is determined by the permeability of the diaphragm. In cases where the head was above specification, this meant that the electrolyte flow through the diaphragm was hindered because of partial blinding. The blinding was caused by the presence of $Mn(OH)_2$ on the diaphragm during operation. Therefore, on the completion of the cycle, the diaphragm was soaked in the cleaning solution and washed off with running water. The anode boxes and diaphragm were also inspected to ensure that there were no leakages available. The leakages are normally caused by Mn metal, which has flaked off the cathode or blinding due to ingrained precipitates. This was done to avoid the seepage of the anolyte into the catholyte compartment.

Cathode Preparation

The pre-treatment of the cathodes was one of the most important factors to be considered as it affects the plating conditions. After harvesting the metal, the cathode plate was fully soaked in the cleaning solution until the dissolution (denoted by the bubbling of the catholyte) has stopped. Careful consideration was taken to avoid prolonged exposure of stainless steel in H_2O_2 solution as it results in the pitting. The plate was rinsed with running water and smoothened using a scotch brite pad to ensure that the surface is smooth. The cathode was rinsed with running water and soaked in a solution of 3.2 – 3.4 g/L Na_2SiO_3 and allowed to drip-dry for at least 2 hours prior to usage.

Preparation for start-up of the cells

Cell A and D were filled with catholyte solution from the cellhouse. This was done using a 10-litre drum to ensure that both cells have the same catholyte solution. The anodes were inserted, and the electrical conductors were connected without starting the power supply. The water bath was heated to 40 ℃ and circulated through the glass condenser. The catholyte recirculation pumps were started to allow the heating of the cell contents to approximately 37 – 40 ℃.

3.8.2. *Operation of the labcells*

The pre-treated cathodes were inserted, connected and the power supply on the rectifier was switched on. The feed pumps were immediately started to supply feed solution (or filtrate) to the catholyte compartment. As soon as the cells were started, the process parameters were measured and logged i.e. time, total voltage, voltage over diaphragms, catholyte pH, catholyte temperature, catholyte manganese concentration, feed rate to the cell, current through

conductors and contacts. These parameters were also measured continuously throughout the period of electrowinning.

The operating conditions indicated in Table 3.5, were used to establish a baseline for the performance of the labcells. The catholyte samples were collected every 2 hours during the operation of the labcells to determine the pH, temperature, and Mn concentration. The pH measurements were taken immediately outside the cells to avoid the electromagnetic field in the cells from affecting the results. The feed flowrate was also measured every 2 hours. The flowrate is used to control the Mn concentration in the cell when above or below specification. However, in this test programme minimal adjustments were made to the feed flowrates. Refer to Appendix B.1 on the impact of flowrate on the Mn concentration during hot commissioning of the cells.

Table 3.5 Standard experimental parameters

Parameter Type	Specification
Cell catholyte Mn content	10.5 – 12.5 g/L
Catholyte pH	8.2 – 8.6
Mn removed from freed (Delta Mn)	20 g/L
Operating temperature	40 – 42 ℃
Current input	19 A
Deposition time	20 – 22 hours
Operating cell voltage	4.8 to 5.1 V
Catholyte recirculation flow	100 ml/min
Cell Feed rate	8 – 12 ml/min

A multimeter was used to monitor the voltage and current and recorded on the log-sheets every 2 hours. The test runs were operated at an average current density of 610 A/m^2 which was equivalent to the rectiformer setting of 54 KA (i.e. this is the same settings used in the plant at the time of the experiment) or 19.0 A of the labcells. A total of six runs of cell A and Cell D were conducted without stopping the electricity or solution feed to the cells thus representing one cycle. The change in each run was conducted by changing the cathode plate. Upon the completion of each cycle, the rectifier and feed solution were switched off, the labcells and solution piping were then completely disassembled, acid treated and rinsed before being assembled for the following cycle. This was done to maintain diaphragms in a fixed condition of minimum scale build-up.

3.8.3. *Metal harvesting*

The cathode was removed from the cells after plating and rinsed to wash off the crystals or sulphur species present on the surface of the metal. This is because unwashed metal samples, whether rough or smooth, have high sulphur content than washed samples (Glück and Pieterse, 1997). Therefore, washing of the metal samples was standardised to minimise the contamination of the results or data. In addition, this is a standard operating procedure applied in the plant where water is sprayed on the surface of the metal before the drying, dehydrogenation, and packaging.

The rinsed cathode with the deposit was dried in an oven set at 60 ℃ for 30 minutes and was carefully removed, allowed to cool down before visual inspections (i.e. grading) was done. The dimensions of the metal i.e. width, length and thickness were measured using a digital vernier caliper to determine the surface area. The harvesting of the deposit from the cathode plate, through the knock-off process, was followed. During the metal knock-off, direct hammer blows of the cathode were avoided as it may cause the shape of the plate to be deformed. To avoid this, a diaphragm cloth from the plant was used to protect the plate during knock-off. The cathode plate was placed flat on a stable table and a hammer was used to hit directly onto the diaphragm and stopped as soon as all the Mn metal was recovered. The weight of the deposit was measured to determine the current efficiency, energy consumption and current density. In addition, samples were taken to determine the sulphur content, morphology, and the composition.

3.9. **Calculations**

The following calculations were used to determine the yield of reactions, number of moles, molar concentration, deposition time, plating area, current density, current efficiency, and energy consumption.

3.9.1. *Yield of reactions*

Yield is a measure of the performance of a reactor or a plant (Sinnott et al., 2005). For a reactor the yield is measured as follows:

$$Yield = \frac{mols\ of\ product\ produced \times stoichiometric\ factor}{mols\ of\ reagent\ converted} \quad (3.1)$$

Stoichiometric factor = stoichiometric mols of reagent required per mol of product produced

3.9.2. *Determination of the deposition time*

It is a general principle of the electrowinning process that the current efficiency of the deposition decreases with increasing plating hours. The start time and end time of the experiment were recorded.

The deposition time was calculated by deducting the end time from the start time according to Equation 3.2.

Deposition time = End time- Start time (3.2)

3.9.3. *Determination of the current density*

The relative rates of the cathodic and anodic reactions are dependent on the current density at the surface of the cathode with a maximum % C.E existing at some optimum current density. At low current densities (<200 A/m^2) hydrogen evolution is thermodynamically preferred (Glück and Pieterse, 1997). Therefore, an increase in the current density raises the electrode potential and make metal deposition more favourable. Glück and Pieterse (1997), further indicated that at much higher current densities, above 500 A/m^2, the hydrodynamics and electro-kinetics of the two competing reactions determine the % C.E as the metal deposition rate becomes limited by the diffusion of manganese ions to the cathode surface. The hydrogen ion reduction rate is not diffusion limited and a drop in current efficiency is obtained with

increasing current density. Therefore, the current density was then determined in the test programme for every run by first calculating surface area of the electroplated material using Equation 3.3.

$$Area\ plated = \frac{(length\ (mm) \times Width\ (mm) \times 2)}{1000000} \quad (3.3)$$

Therefore, the current density is determined by dividing the average current through the electrodes by the area plated as illustrated by Equation 3.4.

$$Current\ density = \frac{Total\ current}{Area\ plated} \quad (3.4)$$

3.9.4. *Determination of current efficiency and energy consumption*

The current efficiency was measured determine the effective use of current to produce the Mn metal. This also provided the performance of the cells and the presence of any foreign substance in the feed solution.

The % C.E was determined using Equation 3.5.

$$\%\ Current\ Efficiency = \left(\frac{Mass\ Mn\ Metal}{(deposition\ time \times total\ current \times 1.025)}\right) \times 100 \quad (3.5)$$

The amount of energy consumed which is increased with a reduction in the current efficiency was determined using Equation 3.6.

$$Energy\ consumption\ (kWhr/ton) = \frac{Average\ voltage \times 100 \times 975.7}{\%\ current\ efficiency} \quad (3.6)$$

3.10. **Summary**

This chapter presented and discussed the materials and methods that were used in the study. In particular, the focus of this chapter was on the following activities that constitutes the laboratory testing aspect of the study:

1. Feed solution and reagent dosing.
2. Aeration and non-aeration of solution in the formation of thiosulphates and polysulphides.
3. Fines removal through filtration.

4. DOE procedures to establish the best experimental setting.
5. Procedure for preparation of the labcells for test run.
6. Operations of the labcells.
7. Data collection and recording procedures.
8. Data interpretation and analysis, identification of the relationships in the data using images, graphical, analytical, and empirical methods.

4. CHAPTER FOUR: RESULTS AND DISCUSSION

4.1. Introduction

This chapters discuss the results obtained during the simulation of the Manganese Metal Company (MMC) plant on a laboratory scale test programme. The results include the following: the oxidation of the manganese solution at the MMC plant, formation of the thiosulphate and other sulphur species, the impact of these products on the performance of the lab cells, the change in the morphology and sulphur content in the metal.

4.2. Determination of the degree of oxidation and behaviour of sulphur species

This section focuses on identifying the impact the presence of sulphide species and oxidative environments on the purified Mn^{2+} solution. The first section presents results on the investigation of oxidation on the process launder (supertube). Furthermore, the behaviour of the sulphide species at different concentration after thickening was also studied. This section considers the species that forms when constant aeration is introduced on the solution in the process launder and the plant fresh feed.

4.2.1. *Solution oxidation in the process launder*

The oxidation at the T102 exit and T171 (supertube launder) was closely studied after the installation of an Eh probe at the launder. The data was recorded at an hourly period and the Minitab software was used to determine the significance of the oxidation at the supertube launder. The t-test was conducted and a summary report is in Figure D.1 in Appendix D. The figure shows that the mean eH (-83.26 mV) at T171 is significantly different from the mean eH (-309.03 mV) at T102 exit as the p-value < 0.05. The difference in Eh measured at the two points is between 221.89 - 229.64 mV at a confidence interval of 95%. Therefore, substantial oxidation of the solution occurs at the supertube launder in the MMC plant. The observed oxidation can be explained by considering the gas-liquid mass transfer model as presented by Lewis and Whitman (1924). Whereby, the transfer of a gas film (i.e. air) into the liquid film (i.e. solution) depends on the physical properties of the air, solution, and the prevailing hydrodynamics. The reactions become significant regardless of the 20.4 metres distance between the probes as the launder is at a 48º angle, creating an increased velocity of the solution. The residence time in the launder until the cellhouse feed tank is 2 hours, at an average solution flowrate of 180 m^3/hr.

The three modes in which air can be introduced into the solution at the launders are described by Perry (1963).

1. The air is dispersed as bubbles in the solution at the launder, see Figure 4.1.

2. As the flowrate of the solution increases the solution becomes dispersed as droplets in the air. The dispersion is increased when the solution encounters the wall of the launder and the crystal build-up.

3. The solution and air are brought in contact as thin films over the side or top wall of the steep launder.



(a) **(b)**

Figure 4.1 Observation of the solution at the inlet and exit of the supertube (a) Solution at supertube inlet (b) Solution at supertube exit

Therefore, the design of the steep launder promotes the mass transfer of air into the solution thus resulting in the oxidation of the solution. The presence of the crystal build-up is likely to increase the rate of oxidation at the supertube.

4.2.2. *The oxidation of T102 solution in various hydrogen sulphide concentration*

The solution at the T102 exit (i.e. before the supertube launder) was sampled, dosed with a sodium hydrogen sulphide (NaHS) reagent at various molar concentrations and bubbled at airflow of 80 L/min for 2 hours. The results are in Table 4.1, excess sulphide or thiosulphate was not detected on the plant fresh feed solution. However, when the molar concentration of NaHS in the solution at 3.3 mmol/L (indicated by test 3 in Table 4.1), a dark stain appeared. In addition, when the sulphide increased to 7.42 mmol/L as indicated by test 1, no stain was detected. Furthermore, a medium stain attained as soon as the concentration was reduced to 5.77 mmol/L as shown by test 2. When the concentration was further reduced to 1.65 mmol/L, the stain test showed that there was no excess sulphide in the solution. Nevertheless, the results show that the concentration of thiosulphate increases with increase in the concentration of NaHS.

Table 4.1 Oxidation of sulphide in manganese sulphate solution

Test No.	Solution Volume (L)	NaHS (mL)	Molar Conc. (mmol/L)	Stain Test	Thiosulphate (mg/L)
Test 1	5	9	7.42	Nil	0.13
Test 2	5	7	5.77	Medium	0.10
Test 3	5	4	3.30	Dark	0.05
Test 4	5	2	1.65	Nil	0.04
Test 5	5	0	0.00	Nil	0.00

The chemical oxidation of sulphide forms several reaction products i.e. sulphur, thiosulphate, sulphite, and sulphate; as described by the following reactions (Lens and Pol, 2000).

$$HS^-_{(aq)} + \frac{1}{2}O_{2(g)} \rightarrow S^0_{(s)} + OH^-_{(aq)} \quad (4.1)$$

$$HS^-_{(aq)} + O_{2(g)} \rightarrow \frac{1}{2}{S_2O_3}^{2-}_{(aq)} + \frac{1}{2}H_2O_{(l)} \quad (4.2)$$

$$HS^-_{(aq)} + \frac{3}{2}O_{2(g)} \rightarrow {SO_3}^{2-}_{(aq)} + H^+_{(aq)} \quad (4.3)$$

$$HS^-_{(aq)} + 2\,O_{2(g)} \rightarrow {SO_4}^{2-}_{(aq)} + H^+_{(aq)} \quad (4.4)$$

According to Equation 4.2, a ½ molar concentration of thiosulphate (${S_2O_3}^{2-}$) is formed when 1 mole of hydrogen sulphide reacts with ½ mole of oxygen. Figure 4.2 shows the variation of ${S_2O_3}^{2-}$ concentration as a function of the molar concentration of NaHS for test 1 to 5. It can be observed that a 1 mmol change in NaHS concentration results in a 0.0095 mmol change in ${S_2O_3}^{2-}$ concentration. The R-squared indicates that 98.37% of the data fits the straight line and can be used to explain the model.

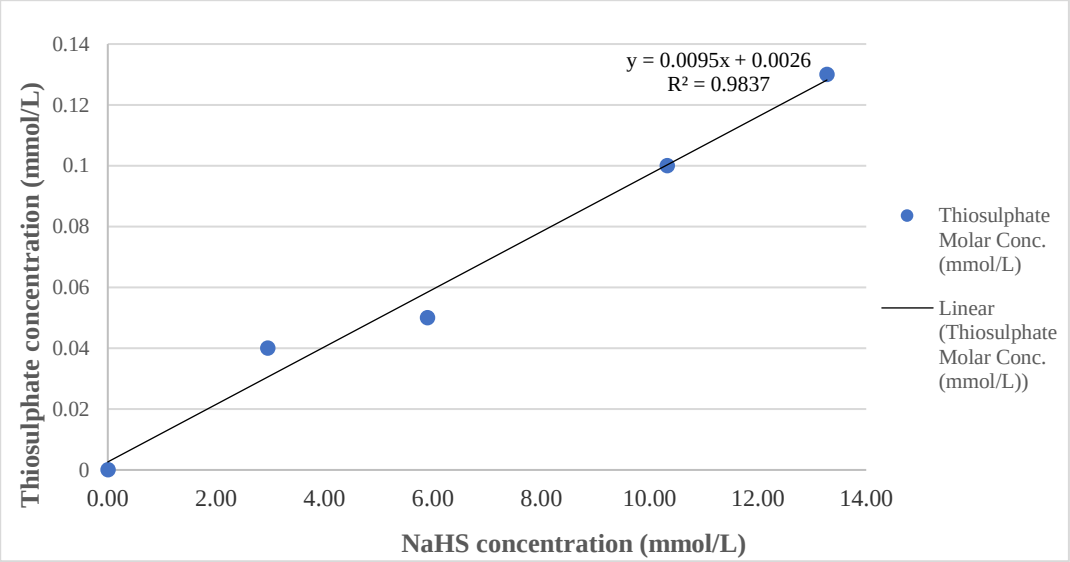


Figure 4.2 Thiosulphate and NaHS concentration for T102 solution

4.2.3. *The presence of polysulphides during excess sulphide oxidation*

Lens and Pol (2000) observed that polysulphide ions are formed as intermediates when the elemental sulphur formed in Equation 4.1 further reacts with the hydrogen sulphide. Shea and Helz (1988), indicated the reaction between the elemental sulphur and the hydrogen sulphide (See Equation 2.8 in Chapter 2). The inability to detect any form of stain, especially on test 1 and test 4, is caused by the further oxidation of polysulphide into [${S_2O_3}^{2-}$] as indicated in Equation 2.10 in Chapter 2. The polysulphide was not measured in the solution because the method of analysis required the use of asbestos, a material that is banned from industrial use.

The increase in $S_2O_3^{2-}$ can be explained by Equation 2.10 in chapter 2 which shows that polysulphide can be oxidised into elemental sulphur and $S_2O_3^{2-}$. This is because the dark stain attained on test 3 indicates the presence of unreacted sulphide ion resulting from incomplete reactions, hence the reduced % yield of $S_2O_3^{2-}$. The yield of $S_2O_3^{2-}$from the chemical oxidation of sulphide is determined and compared with the stain test in Figure 4.3. It is indicated that the excess sulphide is not detected on the sample comprising of the highest yield of $S_2O_3^{2-}$ i.e. test 4. However, at a minimum yield of thiosulphate, a dark stain is established illustrating the presence of excess sulphide at higher concentrations. Therefore, the concentration of excess sulphide is reduced with an increase in the yield of the thiosulphate. This occurs regardless of the molar concentration of the sulphide.

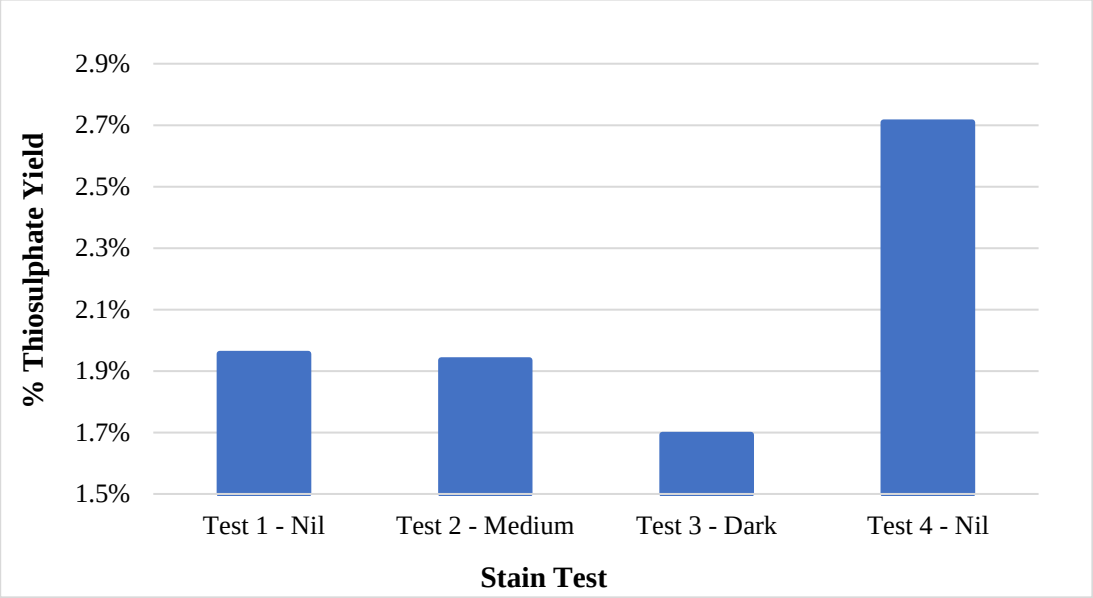


Figure 4.3 Percent yield for T102 solution and stain test

Kleinjan et al. (2005) stipulated that the oxidation of polysulphide occurs more rapidly than the oxidation of sulphide ions, therefore, $S^{2-}{}_x$ species catalyse the oxidation of sulphide.

4.2.4. *The impact of the presence of SO_2 on the excess sulphide oxidation*

An outline of the sulphur species present in the feed solution to the labcells is indicated in Table 4.2. The conditions differ with the presence and absence of forced aeration at various sulphide and sulphur dioxide concentrations. For example, run 7 was a fresh feed solution collected at the F-bank rotameter and it is noted that the $S_2O_3^{2-}$ concentration was already measured at 0.02 mmol/L. This differs significantly with the concentration of the thiosulphate from test 5, measuring at 0.00 mmol/L. It is of importance to note that the solution collected at this stage

was already treated with NaHS and impurities had been removed as a form of insoluble metal sulphide precipitate by the thickeners and filters in the MMC plant. Therefore, the presence of the thiosulphate in run 7 is the oxidation of the sulphide at the supertube launders.

When sulphide was added to the solution at a concentration equivalent to test 3 in Table 4.1, run 10 and run 16 results in thiosulphate concentrations of 5.4 – 7.4 times more than that of test 3. This is likely because of the added oxidation of run 10 and run 16 solution occurring at the supertube and laboratory, as compared to test 3 which was only oxidized in the laboratory. In contrast, the stain test reveals that there are similarities between test 3 and both run 10 and run 16 regarding the presence of excess sulphide in the solutions. The stain test (faint, medium or dark) was obtained when a solution containing 3.66 mmol/L of sulphide was aerated.

Table 4.2 The behaviour of the sulphur species with the change in the solution type

Run Order	Aeration	Stain Test	M_{NaHS} (mmol/L)	Mass of MnS (g)	Thiosulphate (mmol/L)
Run 7	No aeration	Nil	0	0	0.02
Run 9	No aeration	Nil	3.66	11.5	0.10
Run 10	Aeration	Medium	3.66	8.1	0.27
Run 11	No aeration	Nil	7.31	18.5	0.18
Run 12	Aeration	Nil	7.31	10.5	0.38
Run 15	No aeration	Nil	3.66	9.4	0.08
Run 16	Aeration	Faint	3.66	7	0.37

When sulphide is added in the solution at various concentrations in the absence of air, the concentration of $S_2O_3^{2-}$ in the solution is increased by 4 – 9 times as indicated by run 9, run 11 and run 15. For example, the thiosulphate concentration is increased from 0.02 mmol/L to 0.10 mmol/L when 3.66 mmol/L of NaHS is added in the solution. This is because the SO_2 that is added in the feed solution to achieve a phase change during electroplating dissolves readily in water to give solutions of SO_3^{2-} and H^+ as stipulated by Equation 2.18 in chapter 2.

Heunisch (1977), studied the impact of sulphite species in a medium containing HS^- ions in the absence of oxygen. It is observed that free SO_3^{2-} reacts with HS^- ion at room temperature and the overall reaction is depended upon hydrogen ion concentration to form thiosulphate ($S_2O_3^{2-}$). Nevertheless, the formation of $S_2O_3^{2-}$ in the presence of HS^- and SO_3^{2-} occurs in a two-step mechanism as indicated by the following reactions (Heunisch, 1977).

$$2HS^-_{(aq)} + HSO_3^-{}_{(aq)} \rightarrow 3S_{(s)} + 3OH^-_{(aq)} \qquad (4.5)$$

$$S_{(s)} + HSO_3^-{}_{(aq)} \rightarrow S_2O_3^{2-}{}_{(aq)} + H^+_{(aq)} \qquad (4.6)$$

The overall reaction is regarded as:

$$2HS^-_{(aq)} + 4HSO_3^-{}_{(aq)} \rightarrow 3S_2O_3^{2-}{}_{(aq)} + 3H_2O_{(l)} \quad (4.7)$$

This is shown by the increased formation of the thiosulphate in the absence of air in Figure 4.4. For example, about 0.27 mmol/L of hydrogen sulphide reacted with 0.54 mmol/L of sulphite to produce 0.41 mmol/L thiosulphate (i.e. run 11), when Equation 4.7 is applied to determine the stoichiometric factor. Furthermore, when the sulphide concentration is doubled, the thiosulphate formation is increased by a factor of 1.8.

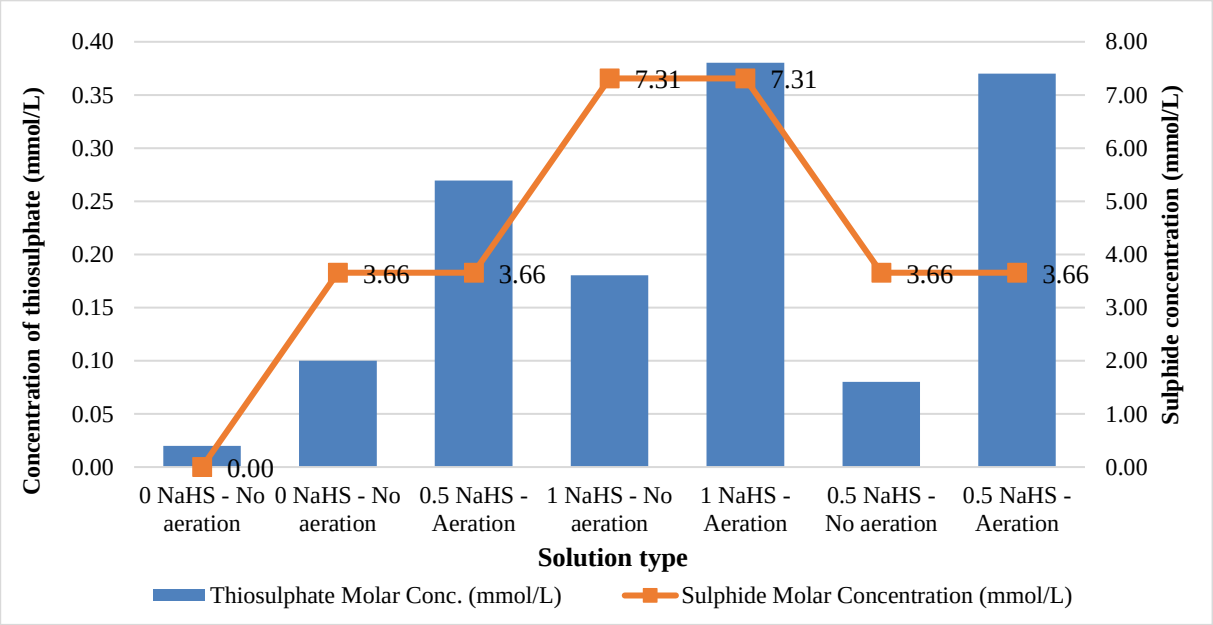


Figure 4.4 The relation of the thiosulphate with change in aeration and sulphide

It is established that in the presence of oxygen, the formation of thiosulphate is intensified. For example, at a dosing setting of 0.5, the concentration of thiosulphate increases by a factor of 2.7 – 4.6 when air introduced as indicated in Figure 4.4. In addition, a strong hydrogen sulphide odour was noted during the analysis of the samples for run 10, run 12 and run 16 as compared to other tests. It was also established that during the preparation of run 12 feed solution, the solution turned milky in colour consisting of bubbles (see Figure 4.5). The filtration of this solution through a < 2 µm filter paper was difficult due to the presence of fine white precipitate i.e. cloudy in appearance. Similar observations were made by Heunisch (1977), whereby after the increase of the HSO_3^-/HS^- molar ratio (i.e. by addition of the excess HSO_3^-), the finely divided, white precipitate was formed. Heunisch (1977) identified the white precipitate as elemental sulphur when analysed using an infrared measurement. As indicated, HSO_3^- is formed when the sulphide ion is bubbled with air, as shown in Equation 4.3 (Murray *et al.*, 1994).



Figure 4.5 Solution appearance for preparation run 11 and run 12

When excess sulphide was added in the absence of air, the mass of manganese sulphide (MnS) content peaked as illustrated by run 11 in Figure 4.6. However, it is also noted that when oxygen was introduced into the circuit, as shown in run 12, the mass of the MnS precipitate was drastically reduced. This trend was also noted on Run 9 – 10 and run 15 – 16. The presence or absence of aeration in the solution will have an impact on the formation of MnS precipitate when HS^- is added. Therefore, the formation of the white precipitate, which Heunisch (1977) associated with elemental sulphur, could have resulted in the reduction of the MnS precipitate. It can also be deduced that, in the absence of an oxidising media, the sulphide is used mostly to precipitate the manganese as manganese sulphide according to Equation 4.8.

$$Mn^{2+}{}_{(aq)} + S^{2-}{}_{(aq)} \rightarrow MnS_{(s)} \qquad (4.8)$$

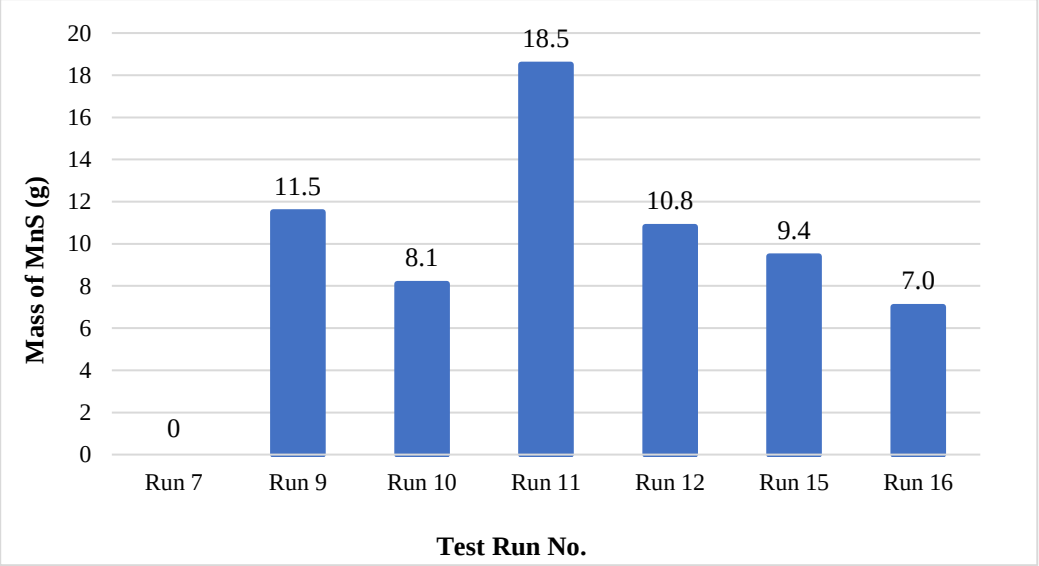


Figure 4.6 Mass of Manganese precipitated in each run

4.3. **Performance of the Labcells**

The following section provides an overview of the performance of the labcells with different solution types. This includes the performance of the labcells using the solution produced directly from the plant (i.e. standard solution) and the aerated plant solution. In addition, the performance of the labcells at a setting of 0.5 and 1.0 for NaHS dosing and aeration is also discussed. The performance is based on the change in the catholyte concentrations, physical characteristics of the metal and the sulphur content. Furthermore, the current efficiency or energy consumption for each solution type is also discussed.

4.3.1. *Overall performance of the labcells*

The overall performance of the test runs, based on the Mn concentration and feed-rate is shown in Figure 4.7. The figure shows that the feed-rate is increased from 7.6 mL/min to 8.6 mL/min after run 1 and run 2 of cycle 1, to accommodate the low Mn concentrations in the cells. Subsequently, the feed-rate is maintained at a close range within 8.4 mL/min up until run 9 and run 10. The sudden increase in the feed-rate at run 9 and 10, is due to the metal comprising of a burnt surface as indicated in Figure D.9 in Appendix D. These normally occurs when the start-up Mn concentration of the catholyte is below 9 g/L. Furthermore, the feed rate was slightly reduced in the middle of run 15 as the average Mn concentration in the cell was above 13 g/L.

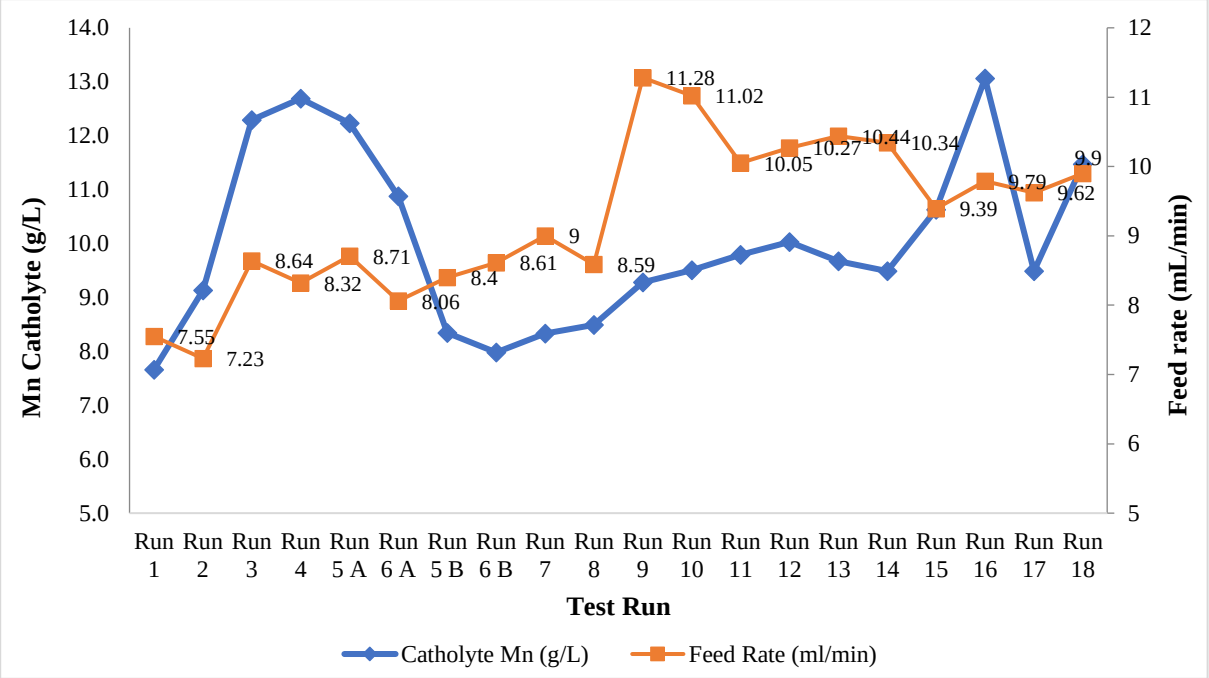


Figure 4.7 The average manganese catholyte of the test programme

Jacobs *et al.* (1946), indicated that if the Mn concentration is held below 10 g/L continuously, burning of the deposit results. If the manganese is raised above 14 g/L, excessive treeing followed by burning occurs and formation of manganese hydroxide begins. It is indicated in Figure 4.8 that the pH in the catholyte differed for each run. A significant difference is noted in cycle 3, where the pH is increased from an average 8.6 between cycle 1 and cycle 2 to pH 9.0 in cycle 3. This is because the labcells were started up using the catholyte solution from the preceding test run i.e. cycle 2 (run 11 and run 12). Therefore, it is deduced that the sudden increase in the pH due to the formation of the manganese hydroxide as the labcells were online for an extended period. It is also indicated from Figure 4.8 that the pH of the catholyte is reduced for aerated feed solution. However, the two-sample t-test in Figure D.5 in Appendix D, illustrates that there is no significant difference between the catholyte pH of both aerated and unaerated feed solution.

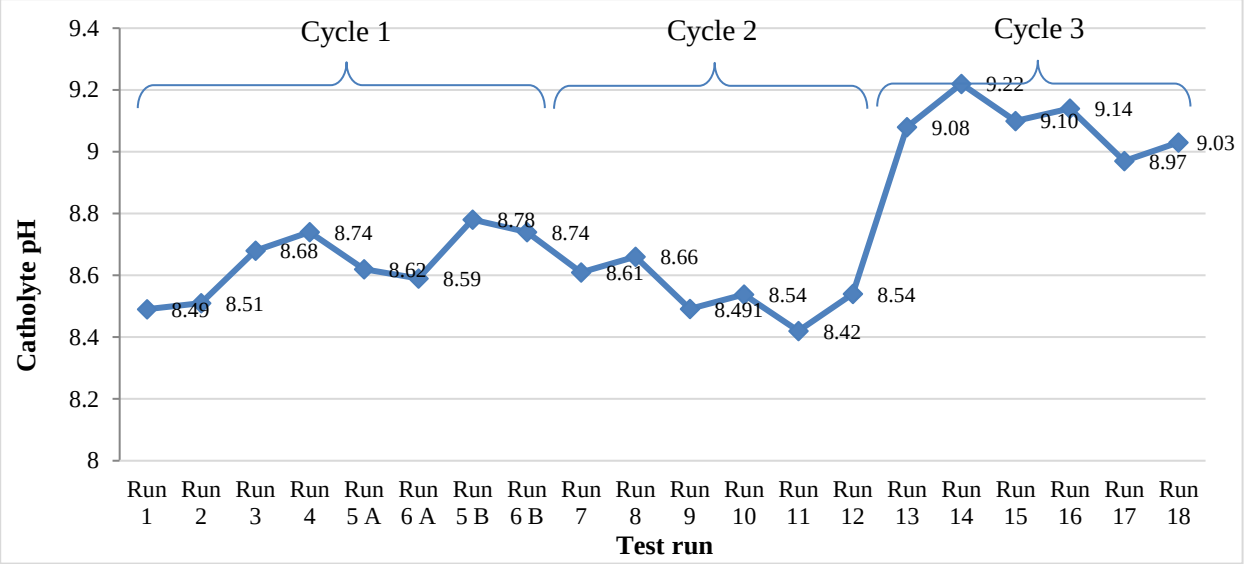


Figure 4.8 The average catholyte pH of the test runs

It can be deduced that a solution that is aerated will have a high chance of metal cracking, causing a fluctuation in the Mn concentration. The low current efficiencies result when the pH of the catholyte is above 8.90 and the Mn concentration are fluctuating. In addition, the high efficiencies result when Mn concentration is stable during the deposition period (Lebakeng, 2002). The fluctuation or increase in the pH of the catholyte is generally caused by the metal flaking and re-dissolving into solution due to the stress factor and cracking on the metal.

4.3.2. *Performance of the labcells at standard and aerated solution*

Catholyte concentration

The typical Mn concentrations of the catholyte from both the standard and aerated solutions are illustrated in Figure 4.9. It can be noted that the catholyte concentrations followed a similar pattern upon start-up and during the period of metal deposition. Firstly, a drop in the concentration of the cells is noted in the first 6 hours of starting up all test runs. This is because, the rate of Mn consumption is increased when a new cathode plate is inserted, as the electric field or migration is increased due to minimal resistance (Gluck and Pieterse, 1997). Subsequently, the Mn concentration of most of the test run increases gradually over a period until an apex is reached where the concentration becomes stable as shown in Figure 4.9. It can be noted from the figure that run 2 and run 8 shows catholyte concentration of Mn is still increasing at the end of the test. The increase in the concentration is associated with the presence of dendrites on the metal surface (see Figure 4.10) during run 2 and the blockage of the overflow weir during run 8 (see Figure D.7 in Appending D). The maximum concentration at end of the plating period is found to be below 12 g/L, which is well within specification.

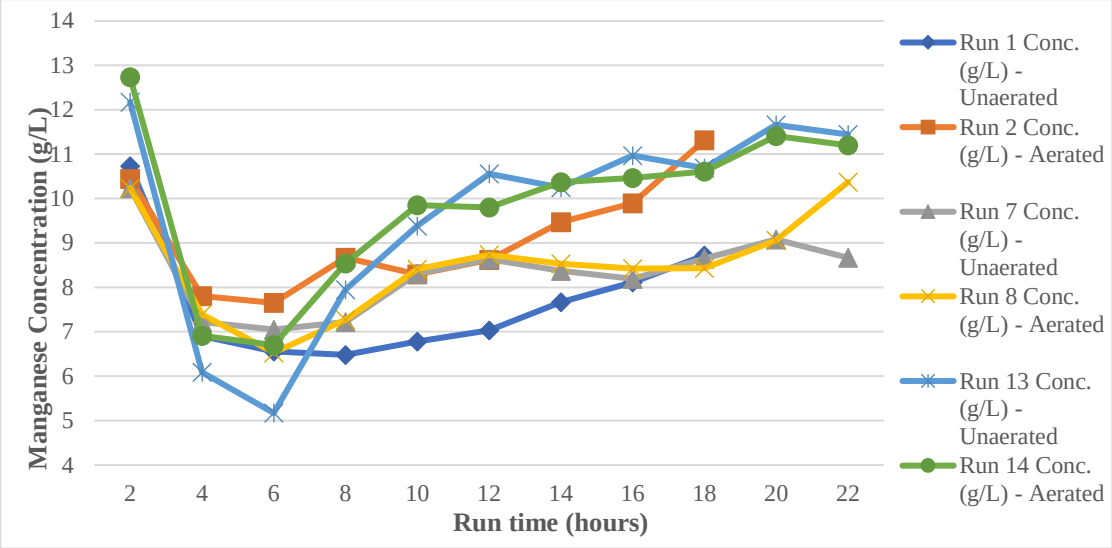


Figure 4.9 The catholyte concentration for runs at fresh feed and aeration

Although the start-up concentrations of run 1-2 were equivalent in the first 6 hours of deposition, the concentrations differed by 2.60 g/L upon completion of the test period. This is because of the increase in the concentration of run 2. The presence of dendrites observed on the surface of the metal upon stripping, might have caused this rise in the concentration since the solution feed rate was kept constant at average 7.20 ml/min. The dendrites are in a typical multi-branching, tree-like form that is easier to remove, thus falling and re-dissolving into the cell. Figure 4.10 provides a clear indication of some of the metal that fell from the bottom half of the deposit.



Figure 4.10 Physical characteristics of metal run 1 and run 2 before stripping

The total mass of the deposit recovered from the run provides a clearer indication of the loss of metal due to redissolution, as run 1 and run 2 produced 154 and 117.6 grams of metal respectively. Therefore, it can be deduced that about 36.4 grams of metal re-dissolved in the catholyte due to the formation of dendrites on the surface of the metal.

Characteristics of the manganese deposit

The harvesting of the metal from the cathode plate for both run 1 and run 2 was found to be difficult due to an increased number of hammer strikes required. The removal of the metal was stopped to avoid distorting the cathode plate and the metal was classified as a hard knockoff (HKO). The material that is difficult to remove from the cathode plates of both run 1 and run 2 is shown in Figure 4.11. The metal deposit that was successfully recovered from the cathode plate was found to be crystalline and good metallic lustre. Similar observations were made on the deposit recovered from run 7-8 and run 13-14, however, HKOs were not observed during the harvesting.

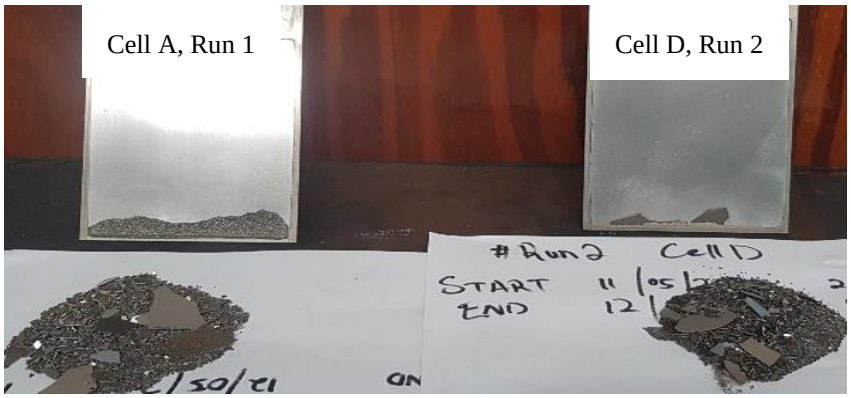


Figure 4.11 Physical characteristics of metal run 1 and run 2 after stripping

It was also established that the metal recovered from the cellhouse in the same period as run 1 and run 2, recorded a spike in the number of HKOs produced (see Figure D.6 in Appendix D). This is because; both the labcells and plant cells used the same feed solution at the time. In addition, the labcells used the catholyte from the plant cell as a start-up catholyte. Hence, the outcome from the plant performance compares closely with the standard runs of the labcells.

Sulphur content and current efficiency

The impact of the HKOs observed in both run 1 and run 2 are illustrated in Table 4.3. The % C.E was found to be 42.16% and 32.08% respectively. The low current efficiency or increased energy consumption observed in both runs is due to the loss of the metal from HKOs, whereas, run 2 is due to both HKOs and metal loss due to redissolution. Nevertheless, the sulphur content is in-specification for run 2 and ultra-low for run 1 (i.e. Table 1.1 provides a classification of the sulphur content). An improved quality and current efficiency were observed in both run 7 and run 8. Although, the quality of the deposits from run 13 and run 14 is off specification, the current efficiency was found to be the highest at 58.29% and 60.88% respectively. The low

quality of the metal from run 13 and run 14 probably due to the use of the catholyte from the run 11 and run 12 (1.0 setting) to start up the test run. This is similar to the procedure applied in the electrowinning process of the plant, whereby, the harvesting occurs by only changing the cathode plate. For instance, only the catholyte from run 12 was used to start up the run 14. Consequently, run 12 solution consisted of white particles identified as elemental sulphur species, which were difficult to filter. However, it is indicated in Table 4.3 that the use of the standard feed solution results in the production of good quality metals (i.e. average 0.033%) and minimal energy requirements (i.e. 10349.92 KWhr/ton).

Table 4.3 Performance of the labcells at 0 NaHS – Aeration and No aeration

Run type	Aeration status	% Current Efficiency	% Sulphur	Power consumption KWhr/ton)
Run 1	Not aerated	42.16	0.012	11437.97
Run 2	Aerated	32.08	0.028	15601.49
Run 7	Not aerated	50.52	0.014	9590.07
Run 8	Aerated	50.11	0.017	9471.10
Run 13	Not aerated	58.29	0.052	8296.96
Run 14	Aerated	60.88	0.073	7701.9
Average		**49.01**	**0.033**	**10349.92**

4.3.3. *NaHS dosing at 0.5 setting and aeration*

Catholyte concentration

The typical performance of the labcells from a solution containing 3.66 mmol/L of NaHS (i.e. 0.5 setting) is illustrated in Figure 4.12. A significant fluctuation in the Mn concentration is observed with each run. For example, the catholyte concentration of run 3 and run 4 comprised of a standard deviation of 3.79 and 2.29 respectively, as compared to run 1 at 1.37 and run 2 at 1.24. Furthermore, it is deduced that when the feed solution contains 3.66 mmol/L of NaHS, the Mn concentration of the catholyte will increase. This occurs regardless of whether the

solution is aerated or not. The phenomenon can be shown by run 3, run 4, run 15 and run 16, whereby, the concentration of the runs at the end of the test period is above 12.5 g/L. It is observed that the metal on the cathode plate tends to crack or flake into the catholyte when a solution containing 3.66 mmol/L of NaHS was pumped into the labcells. It was observed during the actual run (see Figure D.8 and Figure D.9 in Appendix D) that the cracking of the metal occurs instantaneously, especially when the aerated solution is fed into the labcells (i.e. the Mn concentrations of run 4, 10 and 16). On the contrary, the cracking of the metal is delayed and occurs over a period when the non-aerated solution is fed into the labcells (i.e. the Mn concentrations of run 3 and run 15).

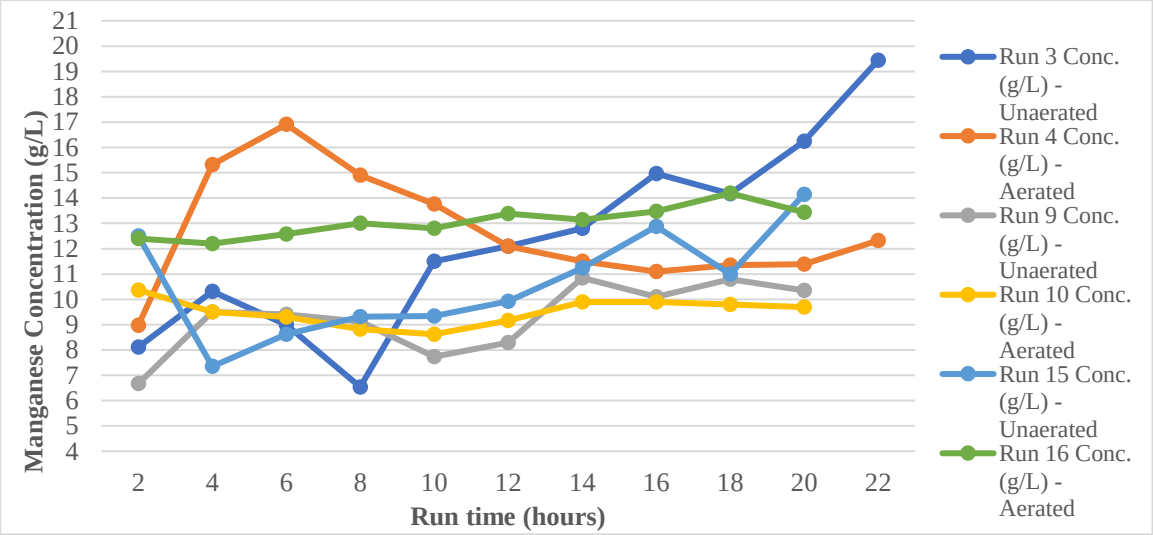
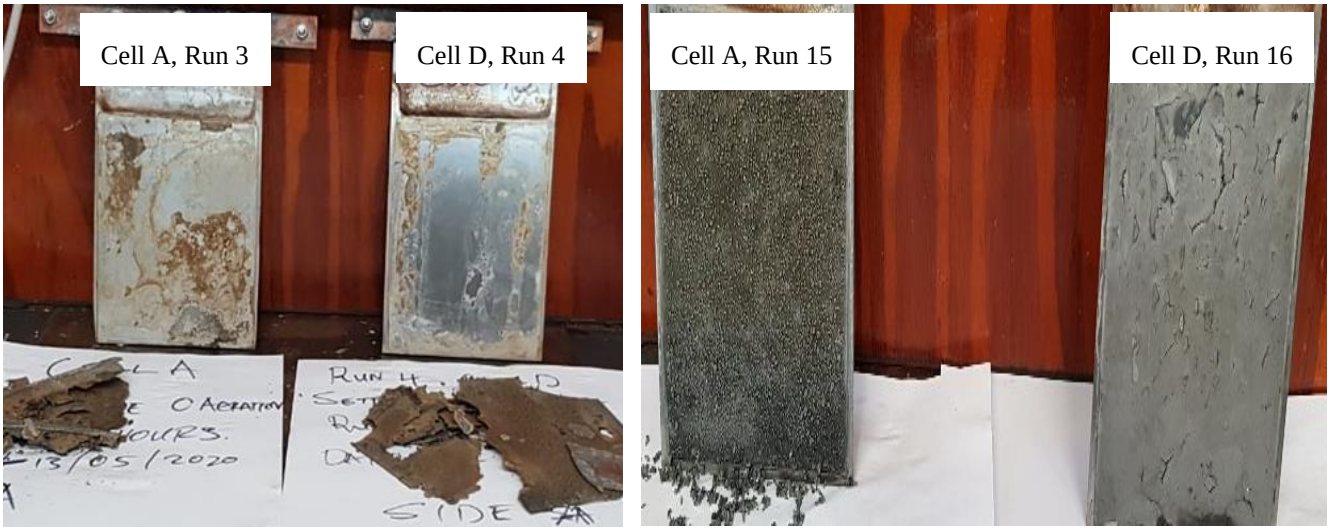


Figure 4.12 The catholyte concentration for runs at 0.5 NaHS and aeration

A fizzy or effervescent sound was also detected in the cells as soon as the current and the feed solution were started. This was detected mostly at run 4, as the sound was higher as compared to other test runs. The effervescent sound can be associated with the change in the characteristics of the feed solution or the redissolution of the metal. For example, the catholyte concentration of run 4 increased from 9.0 g/L to 17 g/L within 6 hours i.e. as soon as a solution prepared at 3.66 mmol/L NaHS was introduced. This instantaneous increase in the Mn concentration due to the change in the feed solution occurred at the same period as the effervescent sound. A gradual reduction in the Mn concentration was noted after 6 hours of starting up the cells.

Characteristics of the manganese deposit

The characteristic of the metal produced from the feed solution comprising of 3.66 mmol/L NaHS is illustrated in Figure 4.13. This shows the cracking and flaking that forms on run 3 and run 4 when this solution type is used. The catholyte solution used to start-up the cells were that of run 1 and run 2 i.e. the test run that resulted in HKOs. On the contrary, the deposits produced from both run 3 and 4 were more brittle (i.e. breaks easily) with a bronze lustre and had a dull characteristic. Furthermore, the stripping or recovery of the deposit from the cathode plate was done – effortlessly – by rubbing off from the cathode plate without any need of the hammer. Furthermore, similar characteristics were also observed in run 15 and run 16 as indicated in Figure 4.13.a. Run 15 produced large dendrites deposit and run 16 produced a metal that is flaking and difficult to handle. Generally, the harvesting of the deposit from a feed solution comprising of 3.66 mmol/L of NaHS required no effort.



(a) **(b)**

Figure 4.13 a) Characteristics of deposit from run 3 and run 4 b) Characteristics of deposit from run 15 and run 16

Sulphur content and current efficiency

It can be deduced that the performance of the labcells was reduced when a solution comprising of 3.66 mmol/L of NaHS was fed into the cells. This is illustrated in Table 4.4, which shows that the average sulphur content in the metal was at 0.23%, current efficiency at 35.20% and energy consumption at an average of 17900.94 KWhr/ton. The flaking observed during run 3 and run 16 resulted in an increased level of sulphur in the metal at 0.248 and 0.697% respectively. Glück and Pieterse (1997), associates these types of sulphurs as the flaked metal

sulphurs (see Table E.1 in Appendix E). The flaked sulphurs are incorporated by the cracking of the metal and dissolution during electroplating and can be minimized by controlling the metal hardness and internal stress. It was established that the performance of run 3 and run 16 was the lowest in the experiment. The current efficiency was at 17.18 and 13.1% for run 3 and 16 respectively. Moreover, the energy consumption in run 16 is higher at 36520.81 KWhr/ton, a significant difference when compared with run 15 at 9577.96 KWhr/ton. The only difference between the two runs is that air was introduced in run 16 and not in run 15.

Table 4.4 Performance of the labcells at 0.5 NaHS – Aeration and No aeration

Run type	Type	% Current Efficiency	% Sulphur	Power consumption (KWhr/ton)
Run 3	No Aeration	17.18	0.248	28180.68
Run 4	Aeration	38.90	0.139	12172.64
Run 9	No aeration	45.49	0.053	10478.15
4Run 10	Aeration	45.29	0.089	10475.4
Run 15	No aeration	51.25	0.156	9577.96
Run 16	Aeration	13.10	0.697	36520.81
Average		**35.20**	**0.23**	**17900.94**

The current efficiencies for run 9 and run 10 compare closely, however, an increased level of sulphur was measured in run 10. Run 15 was found to be the best performing cells based on the current efficiencies and power consumption, however, the sulphur content was off specification at 0.156%.

4.3.4. *NaHS dosing at 1.0 and aeration*

Catholyte concentration

The tests conducted with the feed solution prepared at a sulphide concentration above 7.3 mmol/L (or 1.0 setting) are illustrated in Figure 4.14. It can be noted that stable conditions in the labcell were attained at a period between 10-12 hours of deposition in all the test runs. The stable catholyte concentration occurs in-spite of the previous performance of the process where the Mn concentration was found to be fluctuating (i.e. generated from the 3.66 mmol/L NaHS feed solution). At an average cell feed rate of 9.2 mL/min, the total volume of feed solution supplied to the labcells in 10-12 hours was 5.5-6.6 litres as illustrated in Table C.1 in Appendix C. This is almost equivalent to the total volume of the labcells, including the false bottom, measuring at 5 litres. It was deduced that the stable condition occurs upon the displacement of the catholyte. Therefore, the introduction of a feed solution prepared at a sulphide concentration above 7.3 mmol/L resulted in a more stable Mn concentration in the cells. For example, the cell concentration of Mn for run 5B and 6B was maintained between 8 – 9 g/L with a standard deviation of 0.59 and 0.35. The run 5B and 6B is the continuation of run 5A and 6A. Therefore, when the cells were started up with a catholyte generated from feed solution at 1.0 settings, the standard deviation of the Mn concentration is negligible over a period.

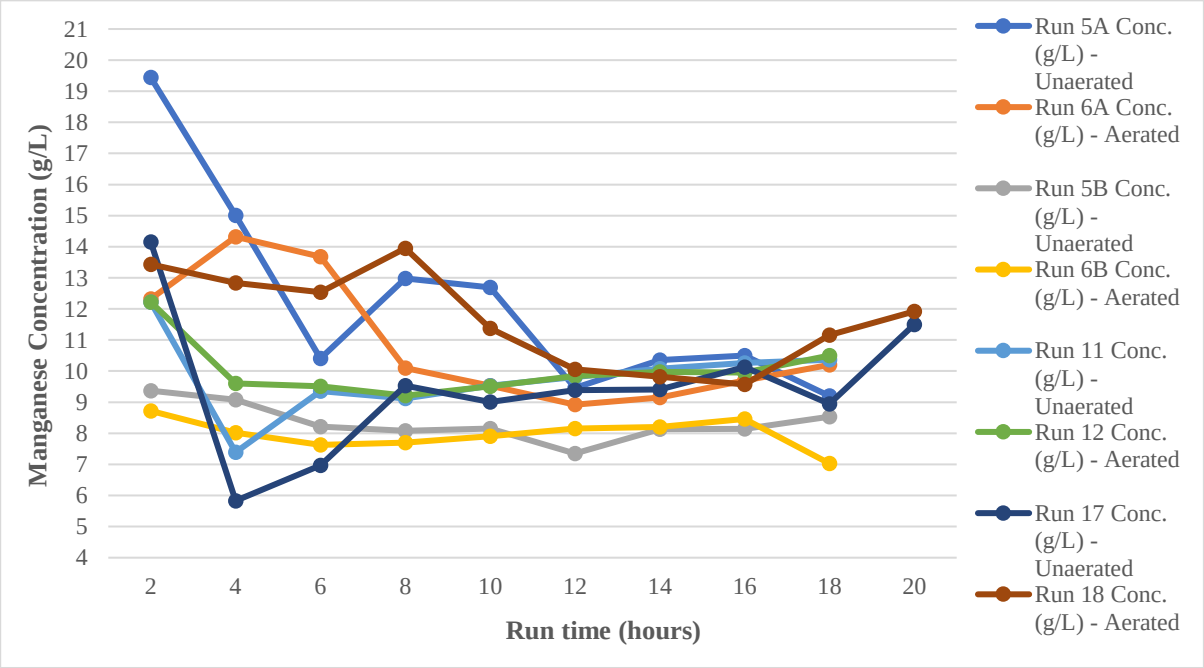


Figure 4.14 The catholyte concentration for runs at 1.0 NaHS and aeration

Characteristics of the manganese deposit

The metals produced from the solution type had a solid adherence with a full coverage on the cathode plate as indicated in Figure 4.15. The decision to repeat run 5A and run 6A was due to a suspicion that the experiments were conducted without the presence of the magna floc. This occurred because, the expected presence of cracking or flaking of the metal deposit was not observed. Therefore, about 22 mL of magna floc was added into the feed solution and a rerun was conducted denoted as run 5B and run 6B. It was noteworthy that the harvesting of these material still required the use of a hammer and the effort of recovery remained unchanged like that of run 5A and run 6A. Although, the metal deposited were fully recovered in a form of metal sheets, the deposit is found to be soft and brittle.



Figure 4.15 Physical characteristics of metal run 5B and run 6B

The impact of the white solid particles (i.e. elemental sulphur) found in the filtrate during the preparation of the feed solution for run 12 is illustrated in Figure 4.16. A white powder or paste was formed on the surface of the deposit and the metal required a hammer to strip from the cathode plate and no cracking is observed.

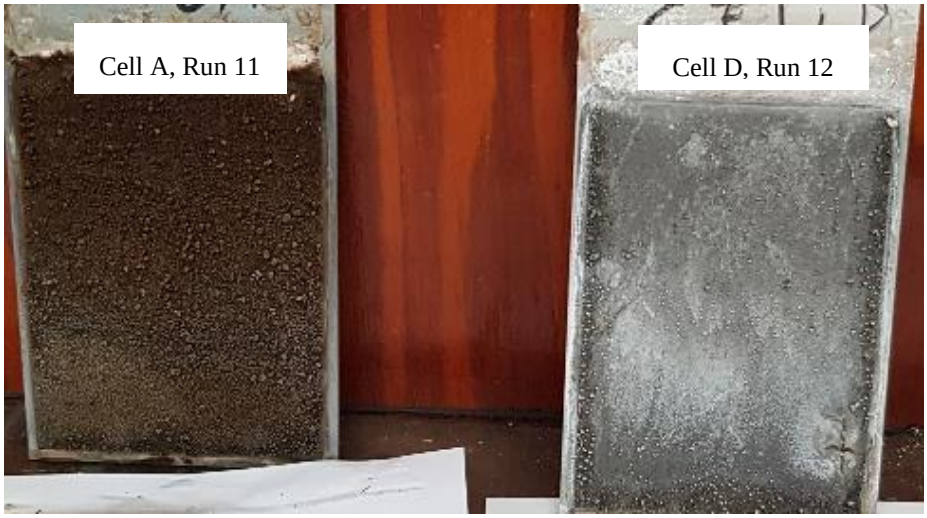


Figure 4.16 Digital images of manganese metal produced in run 11 and run 12

Sulphur content and current efficiency

The performance of the labcells when a solution of 7.3 mmol/L of NaHS was supplied in the labcells is indicated in Table 4.5. It shows that the solution type resulted in an increased performance of the labcells as compared to the other test runs. The average current efficiency and power consumed was 52.691% and 9073.513 KWhr/ton respectively. However, the presence of sulphur in the metal remained high at average 0.123% i.e. off specification. It was also observed that the level of sulphur in the metal is consistent between 0.054 – 0.97 % on almost all the runs excluding run 12. It was, therefore, deduced that the paste on the surface of the run 12 deposit, resulted in the high levels of sulphur in the deposit at 0.45%. The power consumption of run 12 is lower at 9380.1 KWhr/ton despite the high sulphur content.

Table 4.5 Performance of the labcells at 1.0 NaHS - Aeration and No aeration

Run	Type	% Current Efficiency	% Sulphur	Power consumption (kWhr/ton)
Run 5A	No aeration	52.23	0.054	9070.12
Run 6A	Aeration	54.29	0.065	8600.16
Run 5B	No aeration	57.54	0.089	8310.35
Run 6B	Aeration	55.81	0.072	8426.84
Run 11	No aeration	53.58	0.097	9087.50
Run 12	Aeration	50.41	0.45	9380.10
Run 17	No aeration	46.27	0.089	10596.80
Run 18	Aeration	51.40	0.072	9116.23
Average		**52.69**	**0.12**	**9073.51**

Although the solution at a sulphide concentration of 7.3 mmol/L results in stable conditions and improved current efficiencies, the quality of the material remains off specification.

4.3.5. *The overall comparison of the labcells performance*

The performance of the labcells at different solution types used is described in Table 4.6. It is shown that the performance of the labcells varies with the change in the solution characteristics i.e. varying the sulphide content and aeration. The introduction of air into the feed solution (i.e. standard solution or excess sulphide) reduced performance of the labcells and increased sulphur content in the metal. For example, when standard feed solution is oxidized, the current efficiency was 47.69% and sulphur was off specification at 0.040%. Whereas, when the similar solution was not aerated, the current efficiency was 50.32% and the sulphur content was measured at 0.026%.

Table 4.6 Comparison of the labcells performance at different solution types using power consumption and sulphur content

Solution type	Average Current Efficiency (%)	Average power consumption (kWhr/ton)	Average sulphur content (%)
0 NaHS - No aeration	50.32	9775	0.026
0 NaHS - aeration	47.69	10924.83	0.040
0.5 NaHS - No aeration	37.97	16078.93	0.15
0.5 NaHS - aeration	32.43	19722.95	0.31
1 NaHS - No aeration	54.45	8822.66	0.080
1 NaHS - aeration	53.50	8802.37	0.20

Similarly, it was observed that when sulphide was in excess at 1.0 settings and no air introduced, the current efficiency of the cell was at 54.45% and the sulphur content at 0.0798%. However, when similar solution was oxidized, the current efficiency reduced to 53.5% and sulphur content increased to 0.20%. The greatest impact was observed when the solution comprise of sulphide at an excess of 0.5 settings. It was established that the sulphur content in the metal increased to 0.31% and current efficiency decreased to a low 32.43% when the solution was oxidized. However, when aeration was excluded, the sulphur content in the metal was at 0.15% and the current efficiency at 37.97%.

4.4. **Surface morphology and EDS analysis**

It has been illustrated that the drastic change in the performance of the laboratory cells, the physical and chemical content of the metal can be associated with the change in the sulphide concentration. Therefore, changes in the surface morphology are expected with the change in the sulphide concentration. The morphology of the manganese metal is studied in this section. Six samples were collected (i.e. run 7, run 9, run 10, run 12, run 15 and run 16) to represent the overall test runs as set out in the design of experiment (DOE).

4.4.1. *Sample characteristics and examination*

Representative pieces of the samples were selected (see Figure 4.17) and mounted on the holder and carbon coated in preparation for SEM analysis. The samples were examined using a Zeiss Evo Scanning Electron Microscope (SEM) with a Bruker Energy Dispersive Detector system (EDS) operated at 25 kV accelerating voltage and 10 nA beam current. Backscattered electron (BSE) images and the corresponding semi quantitative energy dispersive X-ray microanalyses EDS data were captured to illustrate the metallic and non-metallic phases observed in the samples. It should be noted that some of the BSE images show bad visuals due to the uneven surface of the samples. Some samples developed pointed spheres that are larger and higher than other particles, thus creating a height difference and uneven surface for analysis.

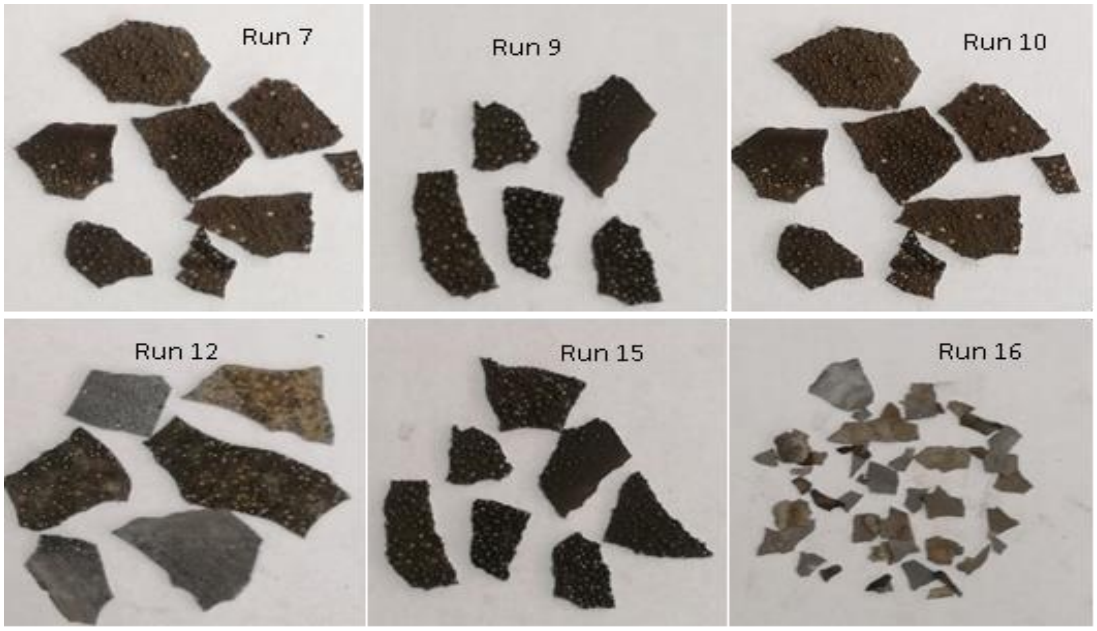


Figure 4.17 Sample photographs for SEM analysis

4.4.2. *Morphology of the metal at 0 NaHS setting and 0 aeration*

The run 7-sample piece was generated from a standard solution and the analysis of the morphology is given in Figure 4.18. It is clearly illustrated from the BSE images that the grains are compacted with spheres of Mn metal in a "Cauliflower" like texture. The manganese metal flakes show poorly developed prisms and ridges that can be associated with increased rate of nucleation (Murray and Wade, 1998). This could be due to the increased hydrogen overpotential as the standard solution consists of less impurities or foreign ions. The ridges between the prisms are coated with manganese oxide, consisting of a semi-bright and shaded

colour denoted as D. In addition, a few relatively large particles of discrete Mn metal flakes are observed at the top view of the image denoted as C.

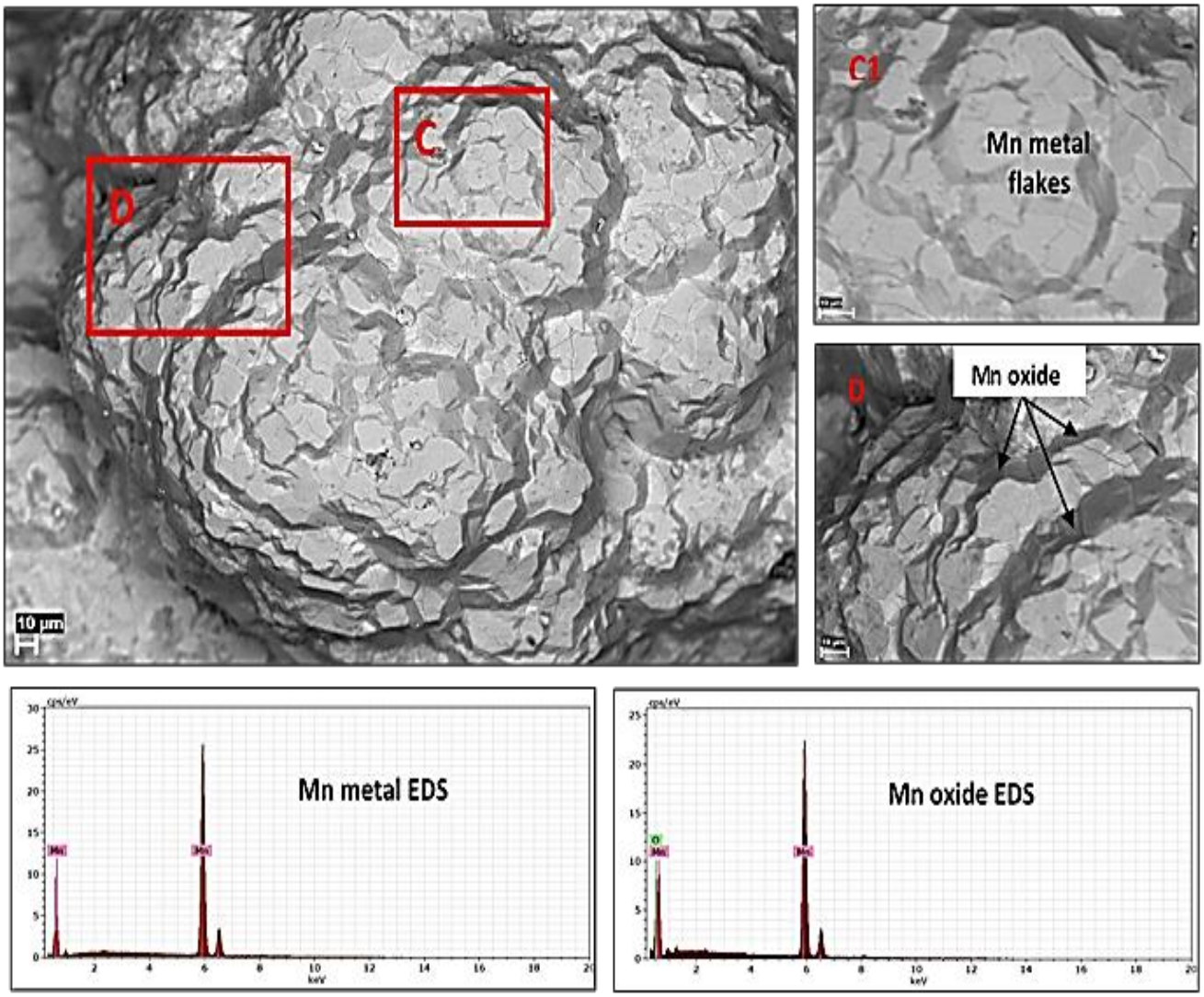


Figure 4.18 BSE images and EDS spectrum of manganese metal flakes and manganese oxide in run 7

It is also illustrated in Table 4.7 and the 25 KV EDS images that the manganese metal deposited from the standard sulphate solutions is of a very high purity. This is because; there are no occluded or inherent sulphur species (see Table E.1 in Appendix E on the forms of sulphurs in the metal) identified in both the Mn metal flakes and Mn oxide phase. However, the analysis conducted using the LECO CS744 S/N:20036 analyser indicated 0.014% sulphurs in the metal i.e. ultra-low metal. These sulphurs can be associated with the surface sulphurs, which forms during the precipitation of sulphate salts from plating solutions and can be removed by effectively washing the deposit with clean water after stripping.

Table 4.7 Chemical composition and speciation of the Mn Metal produced at run 7

Sample	Phase	Elements, wt %				
		O_2	Na	Mg	S	Mn
Run 7	Mn metal					100.0
	Mn oxide	22.6				77.4

4.4.3. *The Morphology of the metal at 0.5 NaHS setting and 1 aeration*

It has been established that the performance of the labcells is reduced when the cell is supplied with a solution comprising of 3.66 mmol/L sulphide, i.e. current efficiency at 35.20 % and sulphur content at 0.230%. The loss in the metal due to cracking and flaking into the catholyte contributed mostly to the low performances of the cell when this solution type was used. As described in Chapter 2 section 2.8, the extra embrittlement that is necessary to attain ease in knock-off is achieved by a combination of hydrogen embrittlement, sulphur precipitation on the grain boundaries and hydrogen bubble formation on dislocations (Murray and Wade, 1998).

The sulphide stress cracking (SSC) is a cathodic cracking process that develops in the presence of water, corrosion, and surface tensile stress where hydrogen ions are a product of the corrosion process (NACE, 2002). In support of NACE (2002), Tapas and Mena (2012), noted that the atomic hydrogen either combines to form hydrogen gas (H_2) at the metal surface or diffuses into the metal matrix. However, in the presence of sulphide the amount of atomic hydrogen combining to form H_2 is reduced (Smialowski, 1962). This tends to increase the amount of diffusion of atomic hydrogen into the metal matrix (Tapas and Mena, 2012).

Once hydrogen has entered the interstices in the metal crystal through the diffusion process, a local strain in the lattice develops, thus the metal becomes susceptible to cracking and flaking (Smialowski, 1962). Smialowski (1962), established that in steel the sulphate is not reduced at potentials involved by cathodic polarization of iron. Therefore, sulphate does not influence the absorption of hydrogen. It can then be deduced that the ductility of the metal produced from the standard solutions of manganese (for example, run 7) is due to the inability of the sulphate solution to influence absorption of hydrogen. However, when sulphide is added in the standard feed solution to a concentration of 3.66 mmol/L, a manganese sulphide or manganese sulphide

coating (MnS) phase was observed on the surface of the deposit as illustrated in Table 4.8. The presence of sulphur in the various phases was observed at a high concentration on both run 15 and run 16, where the EDS measure the sulphur at 19.2 % and 22.0 % respectively. This effect was also observed in steel, whereby; pyrophoric iron sulphide (FeS) was formed when iron reacted with hydrogen sulphide (Walker *et al.*, 1987). It was also shown that the unaerated solution of run 15 resulted in an increased level of both sodium (Na) and Magnesium (Mg) on the MnS phase as compared with the aerated solution of run 16. The reasons for the increase in the Mg and Na level is unclear, although the nodular (run 15) and cracking (run 16) indicates high levels.

Table 4.8 Chemical composition and speciation of the Mn Metal produced

Sample	**Phase**	**Elements, wt %**				
		O_2	**Na**	**Mg**	**S**	**Mn**
Run 9	Mn metal sheets					100.0
	Mn oxide flakes	22.6				77.4
	Mn sulphide	25.3			2.9	71.9
Run 10	Mn metal					100.0
	Mn sulphide	30.1			8.1	61.9
Run 15	Mn oxide					
	Mn sulphide	31.1			9.1	59.8
	Mn sulphide coatings	42.2	3.3	5.4	19.2	29.9
Run 16	Mn metal					100.0
	Mn sulphide	43.7		2.0	22.0	32.4

A mechanism involving SSC and hydrogen embrittlement is proposed to explain the cracking phenomenon on the Mn metal. In the case of electroplating, the electrochemical reactions resulting in the impact of corrosion or cracking of Mn metal are amplified. This is because, the energy required is supplied in the form a large negative potential. For example, the electrolysis of water (see Equation 2.13 in Chapter 2) occurs as part of the cathodic reactions during the deposition of manganese to form 1 molar H_2 and 2 molar OH^-. The formation of the hydrogen gas at the metal surface is described by hydrogen overpotential i.e. the difference in potential between that at which visible hydrogen gas evolution commences and the theoretical reversible potential (Murray and Wade, 1998).

Hampel (1964), indicated that the hydrogen overpotential can be significantly influenced by foreign ions. In support of Hampel (1964), Murray and Wade (1998), noted that the adsorbed anions decrease the overpotential while adsorbed cations increase it. In addition, sulphite ions were reduced to sulphide ions on the surface of the steel (Smialowski, 1962). Furthermore, thiosulphate is readily reduced on various cathodes to equimolar concentrations of sulphides and sulphites (Cotton and Wilkinson, 1988). Kappes (2011), also proved that the H_2S or sulphide is produced when thiosulphate reacted with the electrons of a corroded carbon steel.

It is indicated in Table 4.9 that the yield of thiosulphate and excess sulphide varied for each solution type. For example, run 10 and run 16 comprised of a high yield in the thiosulphate and concentration of excess sulphide. This is a solution that consists of sulphide at 0.5 settings and continuously aerated. Whereas, run 7 and run 9 comprised of the lowest yield of thiosulphate, and run 11 and run 12 illustrated a medium yield. It can be noted that the yield is increased with the introduction of aeration.

Table 4.9 The percent yield of thiosulphate and excess sulphide using the stain test at various feed solution type

Run Order	Aeration	% Yield of thiosulphate	Stain Test
Run 7	0 NaHS - No aeration	0	Nil
Run 9	0 NaHS - No aeration	5.46%	Nil
Run 10	0.5 NaHS - Aeration	14.73%	Medium
Run 11	1 NaHS - No aeration	4.93%	Nil
Run 12	1 NaHS - Aeration	10.39%	Nil
Run 15	0.5 NaHS - No aeration	4.37%	Nil
Run 16	0.5 NaHS - Aeration	20.22%	Faint

Kappes (2011), showed that a carbon steel specimen exposed to $S_2O_3^{2-}$ forms an FeS and cementite film on the surface and cannot conduct electrons, however, the film controlled the rate of hydrogen absorption on the steel. Therefore, the poor performance observed in run 16, i.e. low current efficiency and high sulphur content can be ascribed to the increased presence of thiosulphate and sulphide. In addition, the cracking and flaking observed at both run 3 and run 4, can also be associated with the increased film formation of MnS, resulting in an increased hydrogen embrittlement. The following section provides a description of resultant morphology of the deposits produced from the feed solution at sulphide dosing at 0.5 setting with the aerated and unaerated solution i.e. run 9, run 10, run 15 and run 16.

Run 9

The typical BSE images of the run 9 are illustrated in Figure 4.19 with the EDS spectrum in Figure 4.20. It shows that the spheres of MnS films were starting to develop at the grain boundaries close to the Mn oxide prisms. The manganese metal flakes and oxide phase consists of larger particle which are clearly visible. The accelerated voltage of the sulphur in the MnS film is found to be at 10 KV and Table 4.8 indicating a sulphur content of 2.9%. Therefore, the MnS film at an unaerated solution containing 3.66 mmol/L is marginal, hence, the absence of flaking during electrodeposition of the metal.

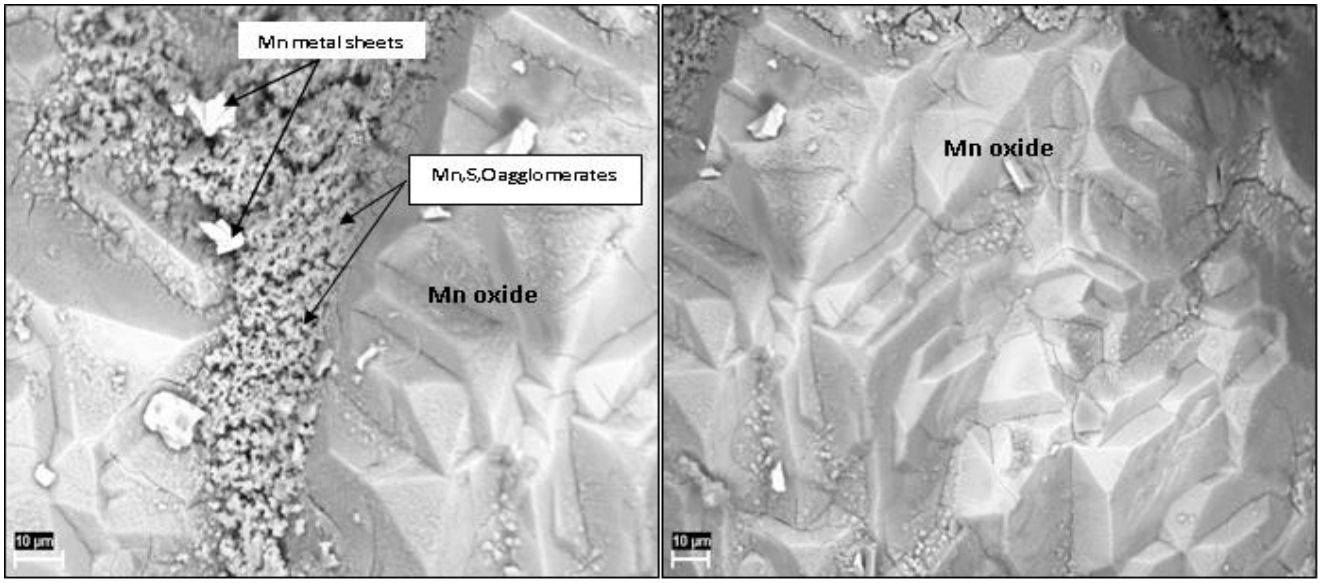


Figure 4.19 BSE images of fine discrete manganese metal sheets, manganese oxide prisms and manganese sulphide agglomerates in Run 9

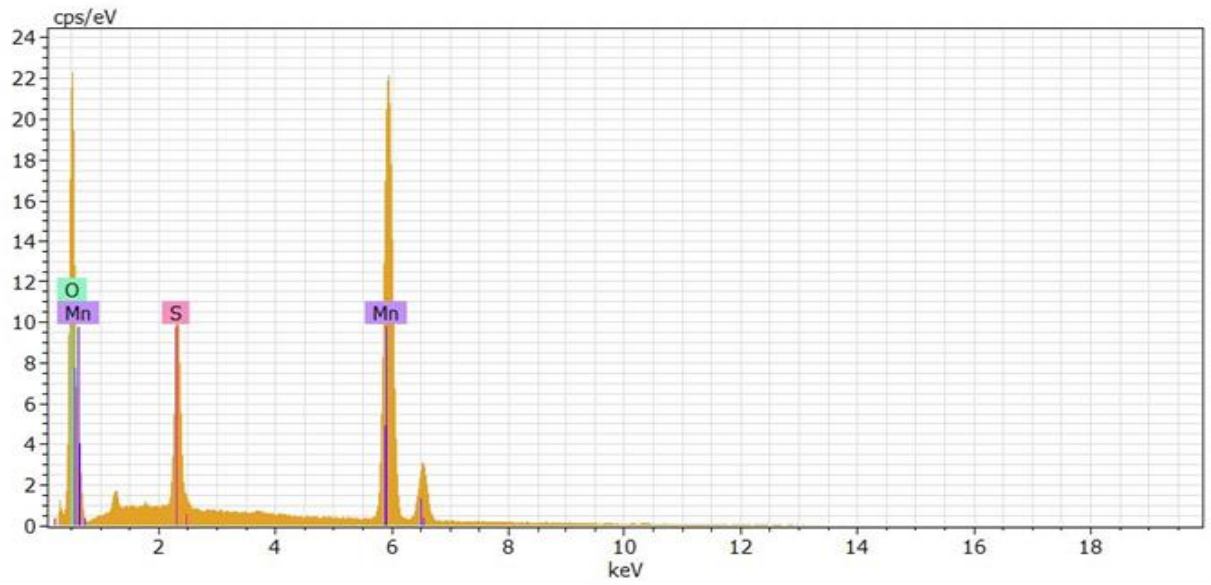


Figure 4.20 EDS spectrum of manganese sulphur agglomerates in Run 9

Run 10

It is illustrated in Figure 4.21 that the MnS films is spread across the Mn metal prisms and the grain boundary, where the spheres are larger in size compared to that of run 9. The difference between the two runs is that run 9 was unaerated and run 10 was aerated. The EDS images illustrated in Figure 4.22, shows that the amount of sulphur in the MnS phase in run 9 is found to be almost two times that of run 10 when the solution is aerated. The results presented in Table 4.8 measure the sulphur levels in this phase at 8.1 %, thus, sulphur type is associated

with both the inherent (interstitial) and intergranular grain boundary as indicated in Table E.1 in Appendix E (Gluck, 1997). Relatively large particles of manganese metal sheets are scattered within the developed spheres of manganese sulphide.

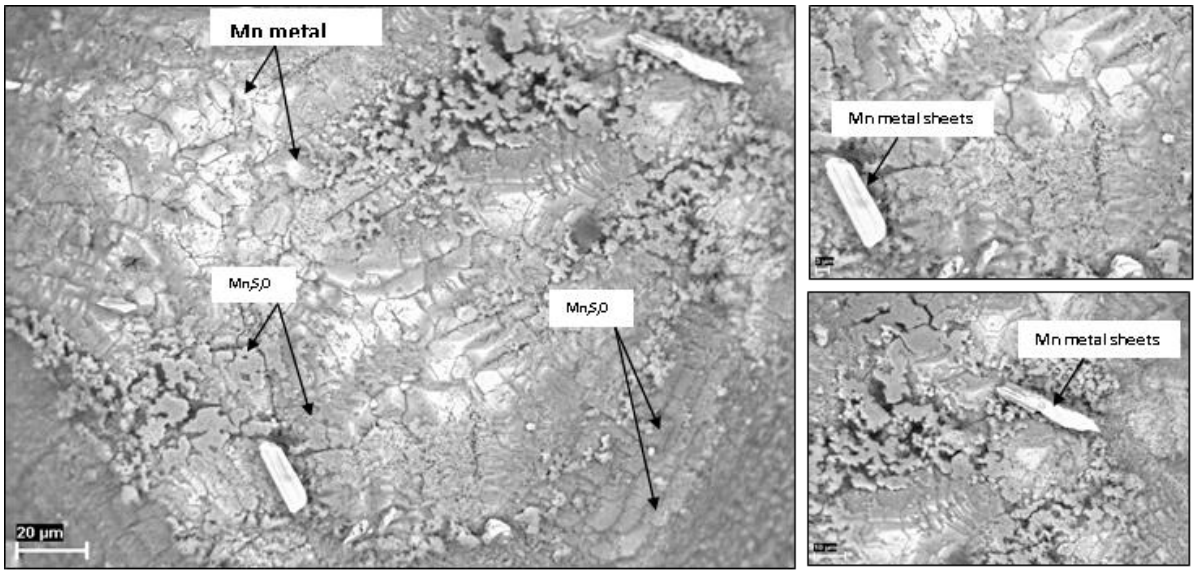


Figure 4.21 BSE images of developing Mn metal prisms with surface coated by manganese sulphide and fine discrete manganese metal sheets in Run 10

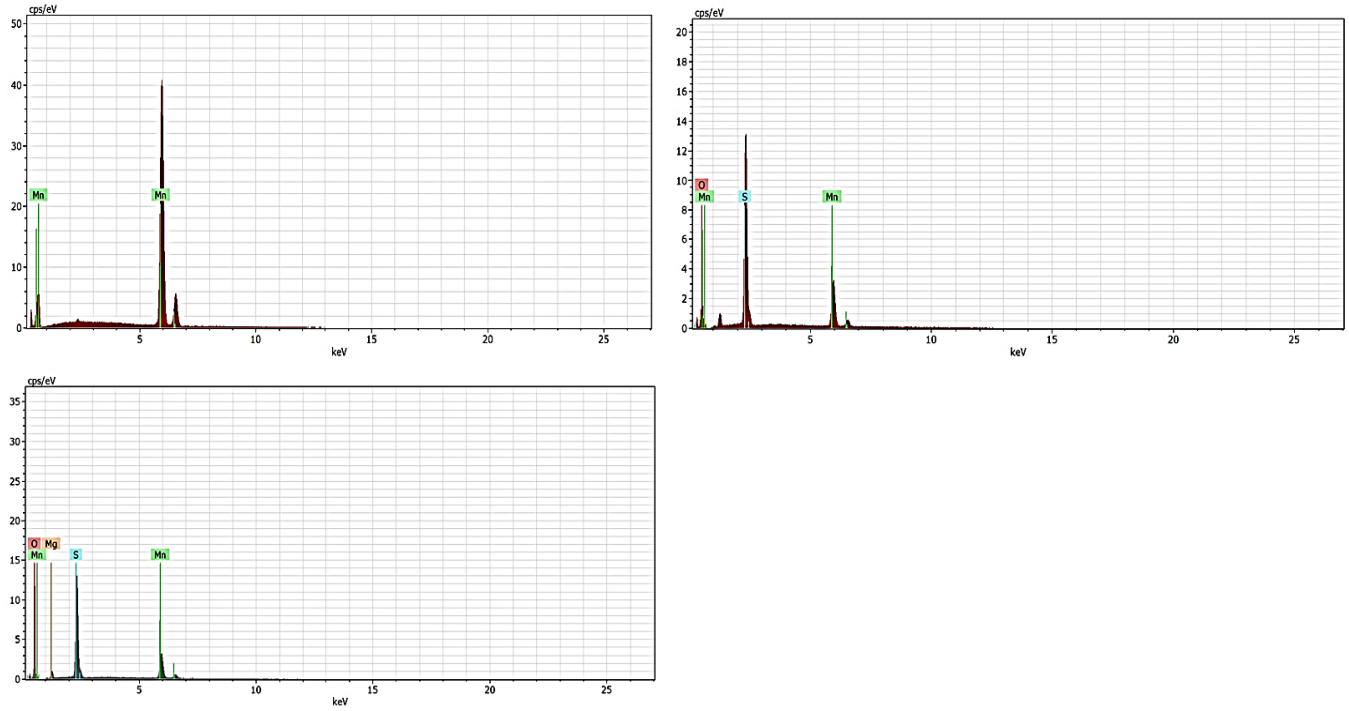


Figure 4.22 EDS spectrum of manganese sulphur agglomerates in Run 10

Run 15

The manganese sulphide matrix is settling between the ridges of manganese oxide prisms and Mn metal ridges as indicated in Figure 4.23. Relatively large particles of manganese metal are scattered within the manganese sulphide matrix. The BSE images also indicate the presence of the cracking on the MnS film. The EDS images (see Figure 4.24) indicate that the sulphur species also exists in the Mn oxide phase at an accelerated voltage of 10 KV. Hence, the increased concentration of sulphur in the metal measured at 0.156% when using the LECO CS744 S/N:20036 analyser.

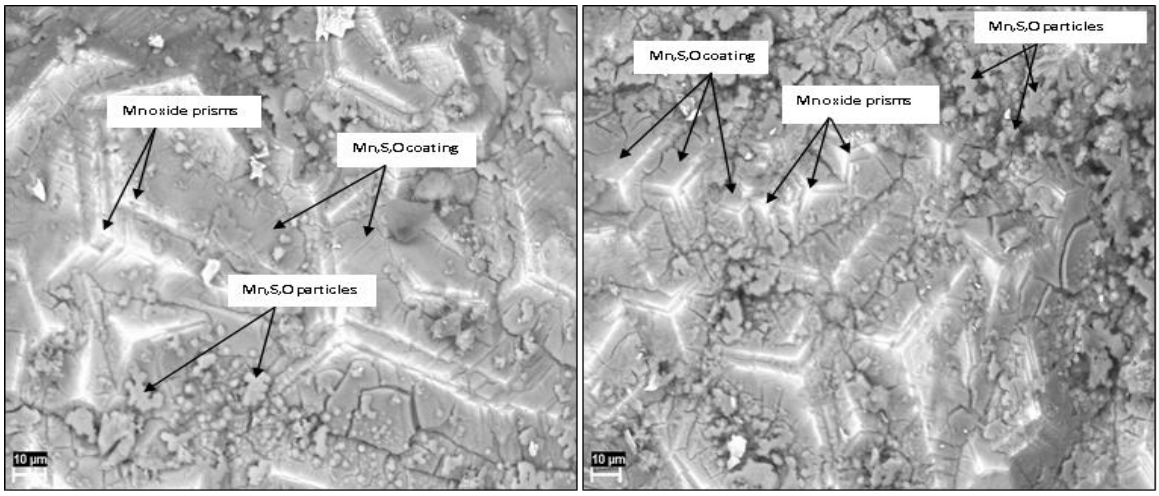


Figure 4.23 Detailed BSE images of well-developed manganese oxide spheres with the surface coated by manganese sulphide in material in Run 15.

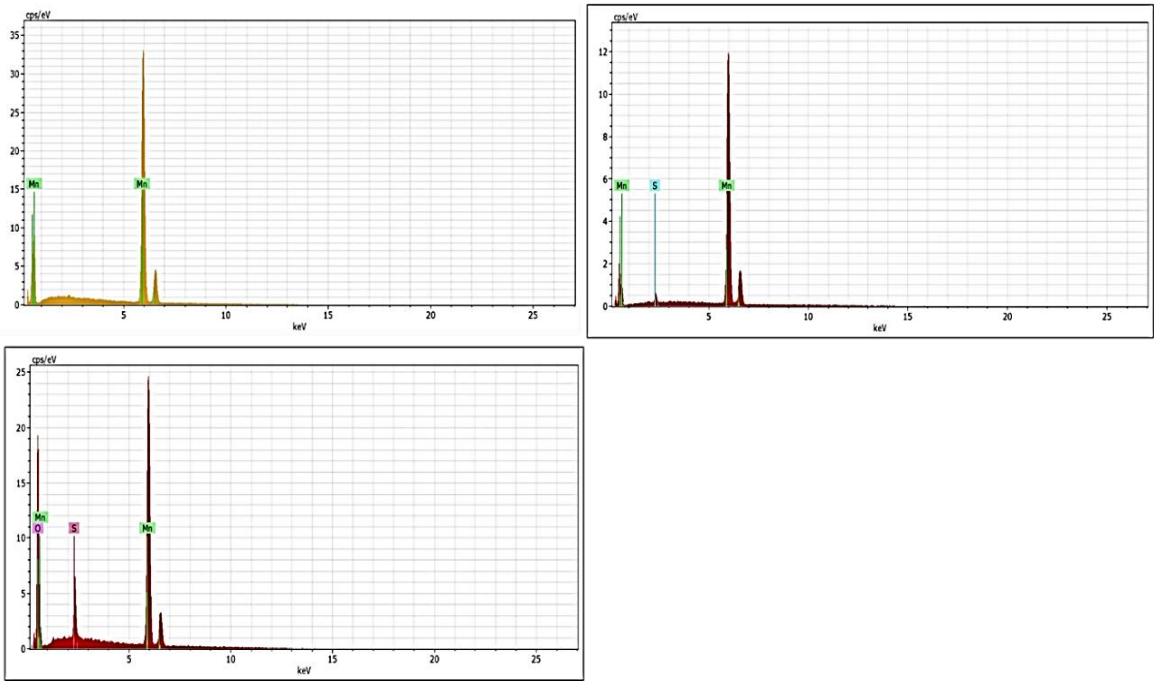


Figure 4.24 EDS spectrum of manganese sulphur agglomerates in Run 15

As indicated in Table 4.8, the MnS coating film in run 15 had various elements i.e. sodium (Na), Magnesium (Mg) and Sulphur at the grain boundaries. The grain boundary phenomenon provides clarity to the presence of these impurities at the film. Ohring (2002), states that the loosely bound atoms prevail by bonding at the grains as the normal atomic bonding terminates, thus, causing the grain boundary to be a more heterogenous region. This is where various atomic reactions and processes such as solid-state diffusion and phase transformations, precipitation, corrosion, impurity segregation and mechanical relaxation are favoured or accelerated (Ohring, 2002).

Since the adsorbed cation has the potential to increase the hydrogen overpotential (Murray and Wade, 1998), the hydrogen formed evolves as hydrogen gas on the cathode. The formation of the hydrogen gas occurs regularly in the plant, and hydrogen fires (see Figure D.10 in Appendix D) emerge as soon as a spark is generated during the insertion of the plates. Therefore, this provides clarity to the increased current efficiency at 51.25% as the potential for hydrogen to diffuse into the metal matrix (i.e. causing the material to crack or flake) is reduced. This occurred regardless of the increased levels of sulphur as indicated in Table 4.8 i.e. 9.10% in the MnS phase and 19.20% in the MnS coating phase.

Run 16

The typical BSE and EDS images of the deposit from run 16, produced from an aerated feed solution comprising of sulphide at 3.66 mmol/L, are indicated in both Figure 4.25 and Figure 4.26. The Mn oxide metal prisms is not identified because the ridges are covered up with the MnS films of fibrous texture. The increased flaking that resulted in the low performance of the cell at run 16 is indicated by the BSE images with the increased presence of MnS films. Smialowski (1962), indicated that the presence of the sulphide films on the metal surface is formed by reducing sulphite to sulphide. Therefore, the increased flaking can be associated with hydrogen embrittlement because the reduction of sulphite to sulphide influences absorption of hydrogen into metal crystal (Murray and Wade, 1998). In addition, the electron transfer is impeded at the grain boundary or metallic sulphide film (Ohring, 2002 and Kappes, 2011), the tensile strength is increased thus resulting in the flaked metal sulphur (Glück and Pieterse, 1997). The EDS operated at an accelerating voltage of 25KV, shows a higher sulphur content at run 16. Saunders and Ribane (1986), confirmed the higher sulphur in a 25KV accelerating voltage as an integral part of the deposit. Table 4.8 illustrates that the elemental sulphur in the film is at 22% as well as Mg impurity measured at 2%. Moreover, the deposit

produced from run 16 consisted of the highest total sulphurs at 0.697% when measured on the LECO.

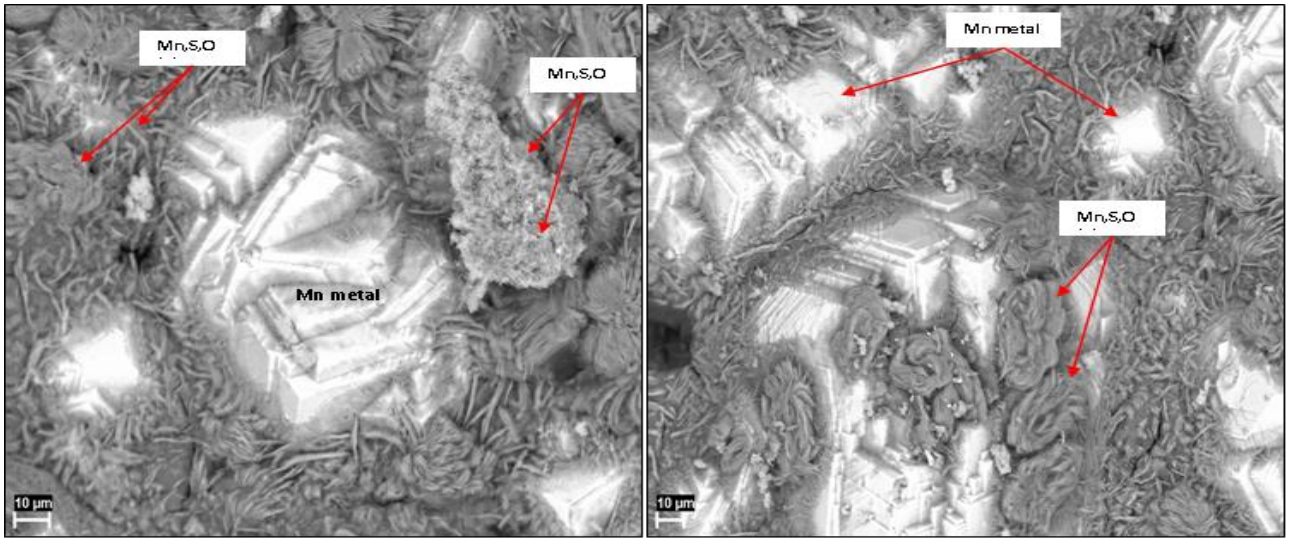


Figure 4.25 Detailed BSE images of well-developed manganese metal prisms with the surface and ridges coated by fibrous manganese sulphide particles in Run 16

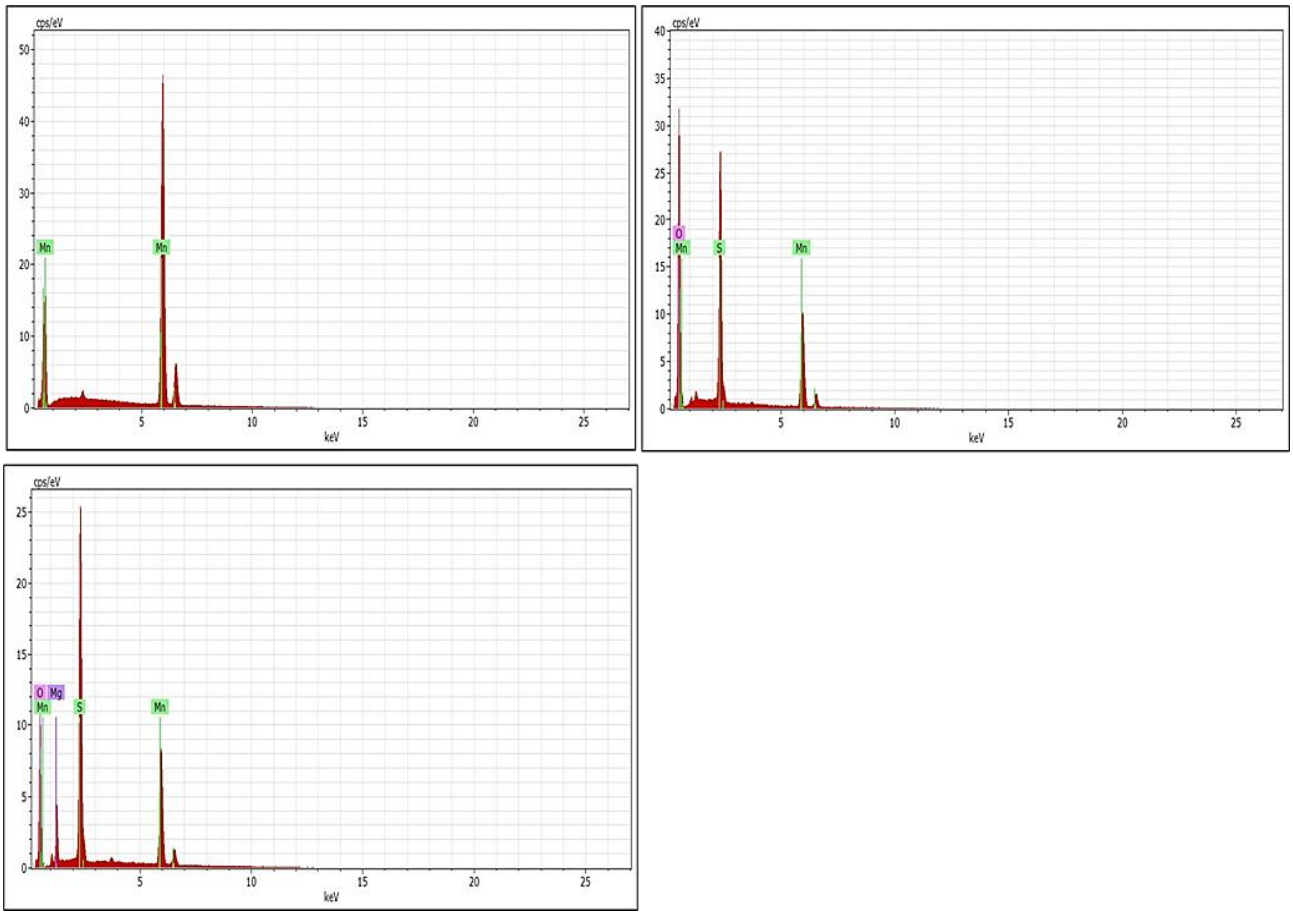


Figure 4.26 EDS spectrum of manganese sulphur agglomerates in Run 16

4.4.4. *The Morphology of the metal at 1.0 setting and aeration*

The run 12 solution produced a white paste on the surface of the deposit resulting in increased levels of total sulphurs in the metal at 0.45% when measured using the LECO. However, Table 4.10 indicates that the MnS species that exist on the surface of the metal comprises of sulphurs at 3.9%. In addition, the MnS that exist on the grain boundaries constitute of sulphur of 5.0%. This is lower than that of run 10 at 8.1% and it is regardless of the observation that the solution used in run 12 consisted of white precipitate identified as elemental sulphur. It can be deduced that the total sulphurs at the deposit are the surface sulphur. The current efficiency of the run 12 is almost equivalent to the other runs conducted using sulphide at concentration of 7.33 mmol/L. Therefore, the surface sulphurs do not result in the cracking or flaking of the deposit, whereas, the inherent or intergranular sulphurs do.

Table 4.10 Chemical composition and speciation of the Mn Metal produced at run 12

Sample	**Phase**	**Elements, wt %**				
		O_2	**Na**	**Mg**	**S**	**Mn**
Run 12	Mn metal					100.0
	Mn oxide	26.2			3.9	69.8
	Mn sulphide	27.3			5.0	67.7

A well-developed spherical structure of manganese oxide with prism texture on the surface is illustrated in Figure 4.27. The spheres are cemented or joined by the MnS on the grain boundaries and few MnS particles are observed on the surface of the Mn metal prisms. The EDS in Figure 4.28 illustrates an accelerated voltage equivalent to that of run 10 on the sulphur content and Mg is also present.

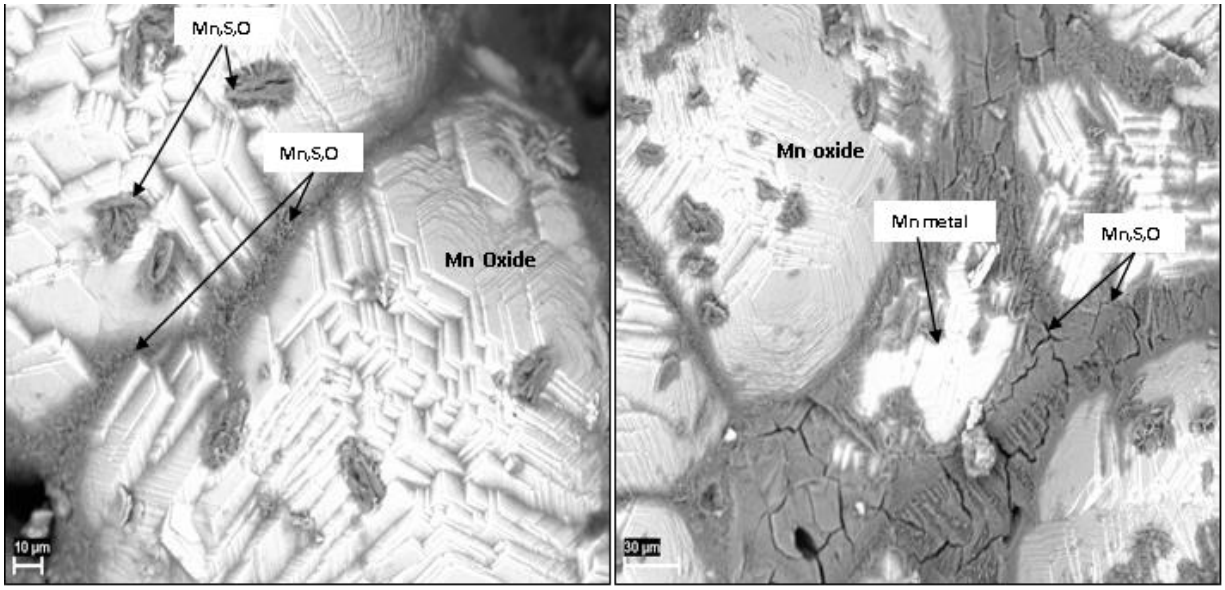


Figure 4.27 Detailed BSE images of well-developed manganese oxide spheres, and the cementing material manganese sulphide, in Run 12

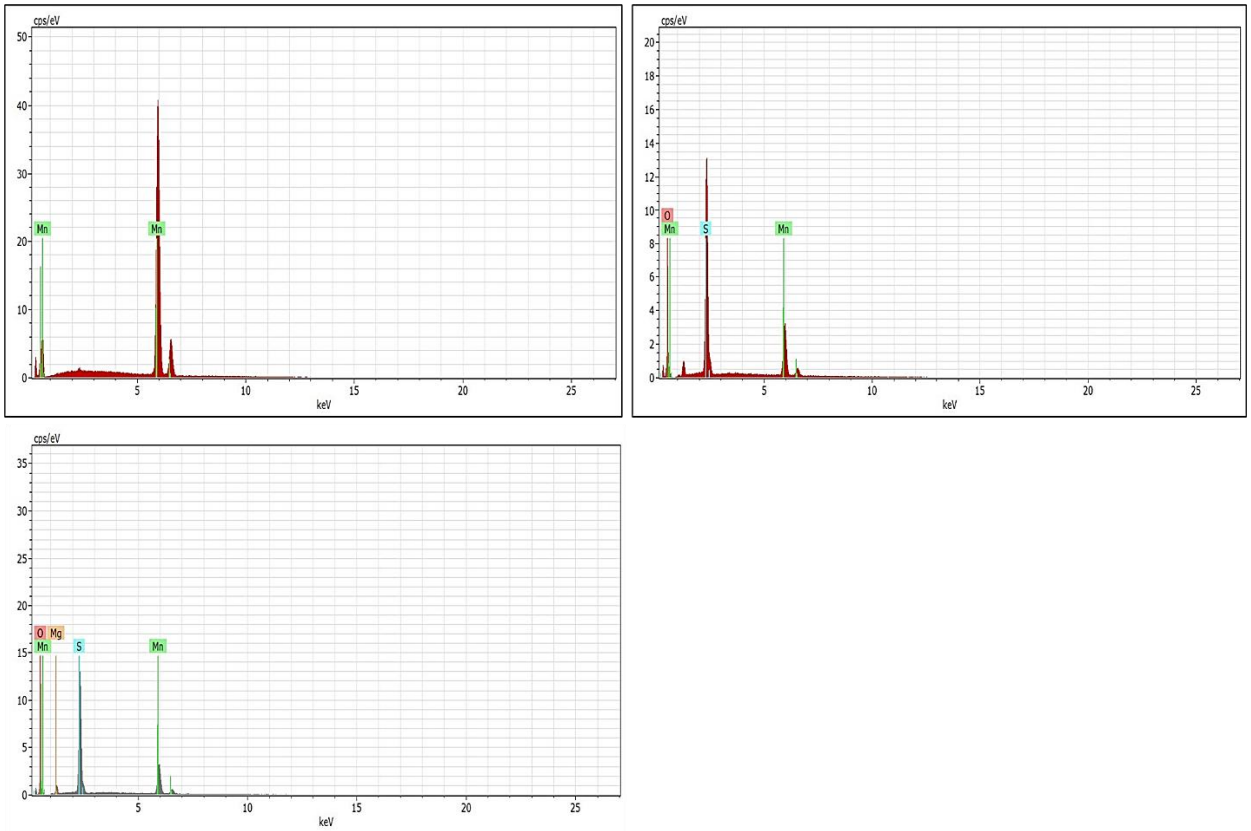


Figure 4.28 EDS spectrum of manganese sulphur agglomerates in Run 12

4.5. **Summary**

The commissioning and optimisation of the labcells (see Appendix B and Appendix C), were factors requiring close monitoring to minimize any form of outliers and variations. These factors affected both the yield of manganese metal and the level of sulphur in the metal. Therefore, the basic principle of operating the labcells was established and the data gathered during the actual test programme was close to reliable with minimal contamination (See Appendix C). For example, the trial test indicated that non-uniform current on the cathode plate resulted in the loss of metal due to high material cracking and increase in catholyte concentration. In addition, the buffing of the plates before starting the labcells was considered an essential task. This was because, unbuffed plates resulted into material cracking and increased levels of sulphurs in the form of trapped, cavity or flaked metal sulphur (see description in Table E.1 in Appendix E). Therefore, it was necessary to ensure that the cathode plates were effectively buffed, and contacts were continuously checked to minimize any form of cracking or increased levels of sulphurs.

The oxidation of the solution at the transfer launders of the MMC plant was closely studied after the installation of an Eh probe. The t-test indicated that the oxidation of the solution was significant at an area known as the T102 exit and T171 transfer launders (i.e. supertube launder). The transfer launders are situated immediately after the sulphide purification thickeners, designed to deliver the solution to the filtration circuit. Since the purification of the manganese solution was denoted as a complex step, one of the methodologies employed to attain a pure solution was to ensure that a significant excess Mn was in the solid phase or precipitate. To attain this, excess sulphide was added for manganese with low solubility to precipitate manganese sulphide. However, the level of excess sulphide needs to be carefully controlled as it may result in the negative impact of downstream processes.

It was indicated that a 1 mmol change in NaHS concentration will result in a 0.0095 mmol change in thiosulphate concentration. These results were deemed valid as the R-squared indicated that 98.37% of the data fits the straight line. In general, the intensity of the stain was increased when the concentration of the sulphide is increased. However, it was also indicated that the colour of the stain becomes nil when the concentration of the sulphide reagent was increased to above 7.3 mmol/L. When the sulphide reagent was dosed at above 7.3 mmol/L in a solution consisting of Sulphur Dioxide (SO_2), the stain was found to be nil on most runs except that of run 17 and run 18 as indicated in Table D.2 in Appendix D. It was also indicated

that the intensity of the stain was increased with the reduction in the yield of $S_2O_3^{2-}$ on the solution collected after the purification. On the contrary, the solution comprising of SO_2 resulted in high stain when the yield of $S_2O_3^{2-}$ was increased.

When sulphide was added at various concentrations in the absence of air - in an SO_2 containing solution, the concentration of $S_2O_3^{2-}$ in the solution is increased by 4 - 9 times (i.e. as compared to the solution collected after the purification section). In addition, when the sulphide concentration was doubled, the thiosulphate formation was increased by a factor of 1.8 in an anaerobic condition. The formation of $S_2O_3^{2-}$ was intensified (increased at 2.7 – 4.6 times compared to that of an anaerobic solution) when sulphide reagent was added in an SO_2 containing solution in the presence of oxygen. In addition, a strong hydrogen sulphide odour was noted during the analysis of some of the samples, and one of the solutions was difficult to filter through a $\leq$ 2 μm filter paper. The filtrate was found to contain white particles. Furthermore, it was also noted that when oxygen was introduced into the circuit, the mass of the MnS precipitate was reduced drastically.

The aerated and unaerated solutions were separated in three different parts according to the Design of Experiments (DOE) and supplied to the labcells to determine the performance of the labcells for each feed solution type. The concentration of sulphide was adjusted as follows:

1. Standard feed solution normally supplied to the main cellhouse (0 setting)
2. Sulphide concentration at 3.66 mmol/L (0.5 setting)
3. Sulphide concentration at 7.33 mmol/L (1.0 setting)

The performance of the labcells at standard feed solution, both aerated and unaerated, resulted in a deposit that was difficult to recover from the cathode plate i.e. regarded as a Hard Knockoff (HKOs). However, the metal deposit that was successfully recovered from the cathode plate was found to be ductile, crystalline, and good metallic lustre. Furthermore, the use of the standard feed solution resulted in the production of good quality metals (i.e. average 0.033%) and minimal energy requirements (i.e. 10349.92 KWhr/ton). The average cell efficiency was at 49% due to the unrecovered material, however, about 60.88% cell efficiency was attained for runs where the deposit was fully recovered. A sample was collected to determine the morphology of the deposit at a standard feed solution. It was established using the BSE images that the ridges between the prisms were coated with manganese oxide phase, and a few relatively large particles of discrete Mn metal flakes were observed. In addition, the 25 KV EDS images indicated that the manganese metal deposited from the standard solutions is of a

very high purity as there were no occluded or inherent sulphur species identified in both the Mn metal flakes and Mn oxide phase. The sulphur content established using the LECO CS744 S/N:20036 analyser was associated with the surface sulphurs, which forms during the precipitation of sulphate salts from plating solutions and can be removed by effectively washing the deposit with clean water after stripping.

The performance of the labcells using a feed solution comprising of sulphide at a concentration of 3.66 mmol/L resulted in significant fluctuation of the catholyte Mn concentration in the labcells. In addition, the Mn concentration of the catholyte increased, regardless of whether the solution is aerated or not. The increase and fluctuation in the Mn concentration was because the deposit on the cathode plate tends to crack or flake into the catholyte. The cracking of the metal occurs instantaneously, especially when the excess sulphide solution was aerated. This resulted in a material comprising of average sulphur content of 0.23%, current efficiency at 35.20% and energy consumption at an average of 17900.94 KWhr/ton. A mechanism involving the sulphide steel cracking (SSC) and hydrogen embrittlement was proposed to explain the cracking phenomenon on the Mn metal. The low current efficiency and high sulphur content can be ascribed to the increased presence of thiosulphate and sulphide in the solution. In addition, the cracking and flaking was associated with the increased film formation of manganese sulphide (MnS), resulting in an increased hydrogen embrittlement. It was established that the presence of the metallic sulphide films on the surface of the metal promotes the diffusion of hydrogen through the matrix.

The BSE images indicated that there were spheres of MnS films developing at the grain boundaries close to the Mn oxide prisms when an unaerated solution was used. The MnS films of fibrous texture were spread across the Mn metal prisms when the feed solution comprising of sulphide concentration at 3.66 mmol/L was aerated. The deposit produced from run 16 (denoted as a poor performing test run) consisted of the highest total sulphurs at 0.697% and a lower current efficiency at 13.1%. The EDS indicated that sulphur was present in both the oxide and MnS phase at an accelerated voltage above 25 kV. The elemental sulphur in the MnS film was measured at 22% as well as an Mg impurity measured at 2%.

A stable Mn concentration of the catholyte was attained in all the test runs when a solution consisted of sulphide at a concentration of 7.33 mmol/L. This was despite the fluctuation of the Mn concentration found in the preceding performance. The metals produced from the solution type had a solid adherence with a full coverage on the cathode plate and the harvesting

of these materials required the use of a hammer. The average current efficiency and power consumed is 52.69% and 9073.51 kWhr/ton. However, the presence of sulphur in the metal remained high at average 0.12% i.e. off specification.

The test run comprising of a solution that was difficult to filter produced a white paste on the surface of the deposit resulting in increased levels of total sulphurs in the metal at 0.45% when measured using the LECO analyser. However, the EDS indicated that the elemental sulphur was at 3.9% and 5.0% in both the Mn oxide and MnS phase. These were found to be lower than other test runs that produced lower sulphurs when measured under using the LECO analyser. These are considered as surface sulphurs and it is deduced that surface sulphurs do not play a role result in the cracking or flaking of the deposit, whereas the inherent or intergranular sulphurs do. The BSE images indicated a well-developed spherical structure of manganese oxide with prism texture on the surface. The spheres were cemented or joined by the MnS on the grain boundaries and few MnS particles are observed on the surface of the Mn metal prisms.

5. CONCLUSIONS AND RECOMMENDATIONS

5.1. Conclusions

Metal cracking in the manganese (Mn) electroplating process is vital to ease the recovery of manganese metal from the cathode compartment. However, when this phenomenon becomes uncontrollable, the recovery of Mn metal is reduced as metal tends to flake-off the cathode and redissolves into catholyte solution. The report is an investigation to establish the causes of production losses through uncontrollable cracking and unacceptably high levels of sulphur in the deposit encountered at Manganese Metal Company (Pty) Ltd (MMC). The literature review and experiments were centred around understanding the chemistry of excess sulphide in an oxidative environment, the degree of oxidation in the MMC steep launder and effect of excess sulphide on metal cracking or flaking and high level of sulphur in the metal.

It is concluded from the experimental results that the oxidation of the process solution at MMC was significant at the process launder known as The Supertube. It was found that, statistically significant oxidation takes place at The Supertube. Subsequently, the results presented in this study have shown that thiosulphate was formed when the solution of excess sulphide was oxidized. In addition, when 1 mmol/L concentration of sulphide was increased, the formation of thiosulphate increased at a slope of 0.0095. Furthermore, the concentration of thiosulphate was increased by 4 – 9 times in the absence of aeration when sulphur dioxide was added to the solution. Lastly, the formation of thiosulphate was increased by above 10 times when the similar solution was in an oxidative environment.

It was indicated that a solution comprising of increased concentrations of thiosulphate and sulphide or sulphite, promotes the absorption of hydrogen in the metal crystals. Consequently, the presence of hydrogen in the metal crystals results in the cracking phenomenon known as hydrogen embrittlement. In addition, the spheres of manganese sulphide film were found to be developing at the grain boundaries close to the manganese oxide prisms for a metal produced from a solution (i.e. comprising of a sulphide concentration of 3.66 mmol/L) that was not aerated. When the similar solution was aerated, the manganese sulphide film became more fibrous in texture and was spread across the manganese metal prisms. The level of the elemental sulphur measured in the manganese sulphide film on the grain boundaries was between 8.1 - 22%, thus the sulphur was considered as occluded or interstitial. Furthermore, the results presented also showed that the cracking and flaking is associated with the increased film formation of manganese sulphide. On the contrary, the results indicated that the metal became

difficult to recover when the sulphide concentration was increased to concentrations above 7.33 mmol/L. In addition, the cell efficiencies became higher when this solution type was used although the metal deposit consisted of increased levels of sulphurs. The increased levels of sulphurs in the metal were found be surface sulphurs. It was indicated that these types of sulphurs do not result in the cracking or flaking of the deposit, whereas the inherent or intergranular sulphurs do.

5.2. **Recommendations**

With the knowledge that has been gathered from this work, the following recommendations for further studies are proposed.

Excess sulphide using the lead acetate test

Studies on the stain test, to determine presence of excess sulphide, have indicated that the degree of stain is directly proportional to the amount of sulphide present in the solution. However, this study has shown that the stain is reduced (i.e up to a nil detection) when the concentration of the sulphide was increased. This was noted when the solution was aerated in both the presence and absence of the sulphur dioxide. Further studies can determine the impact of aeration on the stain test for determination of excess sulphide.

Analysis campaign on the white solids formed in feed solution

It has been observed in the study that during the preparation of the run 12 feed solution, the solution turned milky in colour and filtration was difficult. The feed solution resulted in a white powder or paste on the surface of the metal and the metal was difficult to remove. In addition, the sulphur content of the metal produced from the run 12 solution was found to be higher at 0.45%. This study did not examine the composition of the white solids formed in the feed solution to ascertain species resulting in increased sulphurs and HKOs. Further studies can examine the composition of such solids formed when NaHS dosage is increased.

Impact of impurities on the quality and cell efficiency

Studies have shown that the presence of impurities in the feed solution has an impact on the electroplating of the manganese metal. It has been indicated in this study that a deleterious impact also occurs in the electroplating of manganese metal when the feed solution consists of excess sulphide at an average of 3.66 mmol/L. Therefore, this work can be extended to study

the optimum leaching conditions that will results in a tolerable presence of impurities prior to minimize the presence of excess sulphide in the solution.

The presence of impurities on the metal grain boundaries

This work had shown that a mixture of impurities such as Na and Mg exist for test runs that produced a metal that is nodular and flaking. It has also been observed in some cases that the impurities are present mostly at the grain boundaries in elemental form. This study did not examine the phases in which such impurities exist to ascertain grain boundaries. Further studies can examine the phases the elements exist and impact on the mechanical properties of the metal.

Buffing of cathode plates

This work had shown that the use of unbuffed cathode plates resulted in increased levels of sulphur content and lower current efficiency. Some studies identify this type of sulphurs as trapped or cavity sulphur, which can be incorporated by a solution that was trapped in the pinholes thus precipitating the sulphates. This work can be extended at Manganese Metal Company to standardize the treatment of the cathode plates and improve the availability of clean plates.

Oxidation of solution at the supertube launder

This whole study has opened a new era to the potential impact of excess sulphide in an oxidative environment. It has been shown that the design of the launder at MMC results in mass transfer of air into the solution. The presence of crystals in the launder has been considered to induce the rate in mass transfer of air. Further studies can compare the degree of oxidation at the supertube launder over a period to ascertain the change in the redox potential with crystal build-up.

REFERENCES

Agladze, M.M., Gofman, N.T., 1957. The electrolysis of manganese in the presence of impurities. Journal of Electrokhimya Margantsa 1, 25 – 51.

Artamonova, I.V., Gorichev, I.G., Godunov, E.B., 2013. Kinetics of manganese oxides dissolution in sulphuric acid solutions containing oxalic acid. Journal of Engineering 5, 714 – 719.

Bijsterveld, C.H., 1984. The precipitation of cobalt and manganese sulphides from a manganese sulphate – ammonium sulphate electrolyte (Master's thesis). Johannesburg: University of Witwatersrand.

Bryson, A.W., Bijsterveld, C.H., 1990. Kinetics of the precipitation of manganese and cobalt sulphides in the purification of the manganese sulphate electrolyte. Journal of Hydrometallurgy 37, 75 – 84.

Cheraghi, A., Yoozbashizadeh, H., Safarian, J., 2018. Chemical, microstructural and phase changes of manganese ores in calcination and pre-reduction by natural gas. The 15th International Ferro-Alloys Congress (Infacon XV), 157 – 168.

Cotton, F., Wilkinson, G., Wiley, J., 1988. Advanced Inorganic Chemistry (5th edition). Texas: Texas A&M University.

de Wet, M., 1995. Operation of laboratory size electrolytic cells (Internal report). Nelspruit: Manganese Metal Company.

Dube, V., Lewis, A.E., Pascual, M.R., 2015. Study of selective of CoS and NiS during purification of MnSO4 electrolyte (Master's thesis). Cape Town: University of Cape Town.

Docbrown, 2020. *Electrode potential charts for transition metals 3D-Block compounds complexes oxidation states (Revision Notes). Website:* http://www.docbrown.info/page07/appendixtrans11.htm. Accessed 14 June 2020.

Foxcroft, J.E., Frampton, G.L., Bryson, A.W., 1985. Temperature and pH effects in reduced manganese ore leaching (Laboratory Report). Johannesburg: University of Witwatersrand.

Glück, T., Pierterse, M.R., 1997. Laboratory test cell program databook (Internal Report). Nelspruit: Manganese Metal Company.

Gamali, I., Danilov F., Stender V., 1964. Dimensional correspondence in the electrodeposition of manganese. Journal of Applied Chemistry of the USSR 37, 349 – 353.

Hampel, C.A., 1964. The encyclopaedia of electrochemistry. New York: Reinhold Corporation.

Harris, M., Meyer, D.M., Auerswald, K., 1977. The production of electrolytic manganese in South Africa. Journal for South African Institute of Mining and Metallurgy 77, 137 – 142.

Habashi, F., 1999. A Textbook of Hydrometallurgy (second edition). Quebec City, Canada: Métallurgie Extractive Québec.

Heunisch, G.W., 1977. Stoichiometry of the reaction of sulphides with the hydrogen sulphide ion. Journal for Inorganic Chemistry 16, 1411 – 1413.

Investopedia, 2020. *What p-value tells us. Website:* http://www.investopedia .com/terms/p/p-value.asp. Accessed June 2020.

Jacobs, J.H., Hunter, J.W., Yarroll, W.H., Chruchward, P.E., Knickerbocker, R.G, 1946. Operation of electrolytic manganese pilot plant (Bulletin 463). Boulder City, Nevada: Bureau of Mines.

Kappes, M.A., 2011. Evaluation of thiosulfate as a substitute for hydrogen sulphide in sour corrosion fatigue studies (PhD Thesis). Columbus Ohio: The Ohio University.

Kleinjan, W.E., de Keizer, A., Janssen J.H., 2005. Kinetics of the chemical oxidation of polysulfide anions in aqueous solution. Journal of Water Research 39, 4093 – 4100.

Kolthoff, I.M., Moltzau, D.R., 1935. Induced Precipitations and Properties of metal sulfides. Journal for Chemical Reviews 17, 293 – 325.

Lebakeng, M., Mntambo, S., Gluck, T., 2002. Two-stage ammonium sulphide dosing effect on electrolysis (Internal report). Nelspruit: Manganese Metal Company.

Lebakeng, M., 2003. Mini plant premix reactor investigation. (Internal report). Nelspruit: Manganese Metal Company.

Lens, P.N.L., Pol, L.W., 2000. Environmental Technologies to Treat Sulfur Pollution - Principles and Engineering. London: International Water Association Publishing.

Lenthall, K.C., Bryson, A.W., 1997. Electrowinning of cobalt from sulphate solutions. The Masonry Society Annual Meeting 1997, 305 – 320.

Lewis, A.E, 2010. Review of metal sulphide precipitation. Journal of Hydrometallurgy 104, 222 – 234.

Lewis, A.E, van Hille, R, 2005. An exploration into the sulphide precipitation method and its effect on metal sulphide removal. Journal of Hydrometallurgy 81, 197 – 204.

Lewis, A.E, 2018. Process audit visit summary notes (MMC Internal report). Nelspruit: Manganese Metal Company

Lewis, W.K., Whitman, W.G., 1924. Principles of gas absorption. Journal of Industrial and Engineering Chemistry 16, 1215 – 1220.

Liu, Z.Y., Wang, X.Z., Liu, R.K., Du, C.W., Li, X.G., 2014. Electrochemical and sulphide stress corrosion cracking behaviors of tubing steels in a H_2S/CO_2 annular environment. Journal of Materials Engineering and Performance 23, 1279 – 1287.

Luther, G.W., David, T.R., Stephen, T., Anthony, O., 1996. Determination of metal (bi)sulfide stability constant of Mn^{2+}, Fe^{2+}, Co^{2+}, Ni^{2+}, Cu^{2+}, and Zn^{2+} by voltametric methods. Journal Environmental Science and Technology 30, 671 – 679.

Ma, Z., Ek, Z., 1991. Rate processes and mathematical modelling of the acid leaching of a manganese carbonate ore. Journal of Hydrometallurgy 27, 125-139.

Maciejewski, J., 2015. The effects of sulfide inclusions on mechanical properties and failures of steel components. Journal of Failure Analysis and Prevention 15, 169-178.

Merchant, H.D., 1995. Defect Structure, Morphology and Properties of Deposits (First Edition). Warrendale, Pennsylvania.

Minitab, 2020. *Designing an experiment. Website:* https://support.minitab.com/en-us/minitab/18/getting-started/designing-an-experiment/. Accessed June 2020

MMC (Manganese Metal Company)., 2009. Calcining Technical Manual Version 2 (Internal report). Nelspruit: Manganese Metal Company

Moro, K., Haubrich, F., Martin, M., 2021. Preliminary study on the reductive leaching of manganese ores using $FeSO_4$/Iron powder as reducing agents under room temperature. Journal of Engineering and Technology 6, 14 – 18.

Murray, K., Wade, PW, Jooste, M.M., 1994. Manganese metal process optimization. (Internal report). Pretoria: Council for scientific and industrial research

Murray, K., Wade, P.W., 1998. Sulphur deposition mechanisms (Internal report). Pretoria: Council for scientific and industrial research

National Association of Corrosion Engineers, 2002. Sulfide stress cracking (MR0175-2002, MR0175/ISO 15156). London, England

Ohring, M., 2002. The material science of thin films (2^{nd} Edition). London: Academic Press Limited.

Padhy, S., Patnaik, P., Tripathy, B., Ghosh, M., Bhattacharya, I., 2015. Electrodeposition of manganese metal from sulphate solutions in the presence of sodium octyl sulphate. Journal of Hydrometallurgy 165, 73-80

Perry, J.H., 1963. Chemical Engineers' Handbook. New York: McGraw-Hill Book Company.

Pereira, M.J., Lima, M.M.F., Lima, R.M.F., 2014. Calcination and characterisation studies of a Brazilian manganese. Journal of Mineral Processing 131, 26-30

Rodrigues, J.M.S., 1983. Modelling the performance of manganese electrowinning cells (Master's thesis). Johannesburg: University of Witwatersrand

Saunders, A., Ribane, W., 1986. The effect of some sulphur species on the sulphur content of manganese electrodeposits (Report No. C523M). Randburg: MINTEK

Schaekers, J.M., 1995. Oxidation of ferrous ions in aqueous solutions of manganous and ammonium sulphate (Project No: PR 95/450). Pretoria: Gencor Process Research.

Scholtz, F., 2020. Mineralogy and Analysis of Ores (Internal report). Nelspruit: Manganese Metal Company

Shea, D., Helz, G.R., 1988. The solubility of copper in sulfidic waters: Sulfide and polysulfide complexes in equilibrium with covellite. Journal of Geochimica et Cosmochimica Acta 52, 1815 – 1825

Sinnott, R., Richardson, J., Coulson, J., 2005. Coulson & Richardson's Chemical Engineering (6th edition). Oxford: Elsevier Butterworth-Heinemann.

Smialowski, M., 1962. Effect of hydrogen on iron and steel during production, fabrication and use. Pergamon Press, London

Snape, E., 1967. Sulfide stress corrosion of some medium and low alloy steels. Journal of Corrosion 23, 154-172.

Sorensen, B., Gaal, S., Tangstad, M., Ringdalen, E., Kononov, R., Ostrovski, O., 2010. Phase compositions of manganese ores and their change in the process of calcination. Journal of Mineral Processing 94, 101 – 110.

Steudel, R., Holdt, G., Nagorka, R., 1986. On the autoxidation of aqueous sodium polysulphide ions. Journal for Nature Research 12. 1519 – 1522.

Sun, Y., Tian, X., He, B.,Yang, C., Pi, Z., Wang, Y., Zhang, S., 2011. Studies of the reduction mechanism of selenium dioxide and its impact on the microstructure of manganese electrodeposit. Journal of Electrochimica Acta 56, 8305 – 8310.

Tapas, M.J., Mena, M., 2012. Electrocatalytic properties of electrodeposit black ruthenium in acidic and basic media for hydrogen production via water electrolysis. Conference proceedings of the TENCON 2012 IEEE Region 10 held in Cebu. Conducted by The Institute of Electrical and Electronics Engineers. Piscataway, New Jersey.

Todd, M., 2021. The supplier of choice for high purity Mn units to LIBS (Internal report). Conference proceedings of the Benchmark Mineral Intelligence, Africa Day. Nelspruit: Manganese Metal Company.

Walker, R., Steele, A.D., Morgan, T.D.B., 1987. The formation of pyrophoric iron sulphide from rust. Journal of Surface and Coatings Technology 31, 183 – 197

Zheng, F., Li, Y., Wang, D., Li, J., Zhu, H., 2018. The effects of Zn^{2+} and polyacrylamide (PAM) on the electrodeposition of manganese from non-selenium sulfate solutions. International Journal of electrochemical science 13, 1879-1892

APPENDIX A

A. BRIEF DESCRIPTION OF THE MMC CELLHOUSE

The cell house consists out of 96 individual cells, each comprising of 78 cathodes and 79 anodes. The cells are in the A and B bank that are divided into 6 sections, labelled from A to F. Each section has its own 1000 L header tank known as the T063, fed from upstream holding tank T061. The current enters the cellhouse at the A-cell bank and leaves at the B-bank. Within the banks there are copper busbars on the sides of the cell that distribute current to individual cathodes. The header-bars of the cathodes rest on the busbars with a point contact allowing the current to flow through in a direction illustrated by Figure A.1.

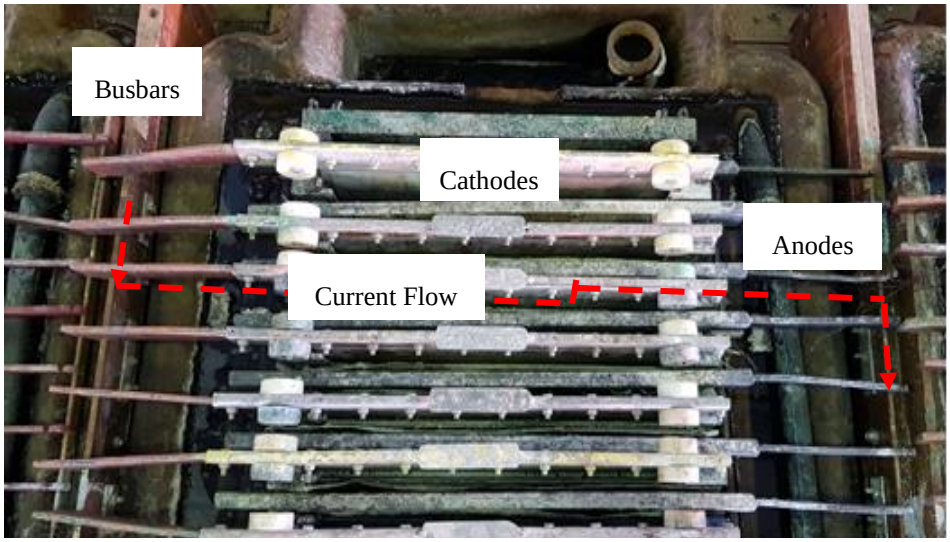


Figure A.1 Cell Design and Current Flow

The Mn deposited is removed from the cathodes by physically knocking the cathode plate with a rubber hammer, a process called knock-off. The cathode plates for Mn electrowinning are fabricated with 316 stainless steel and lead-silver anodes. These are placed in the frames made of polypropylene, and styles, separated by a polypropylene cloth, which acts as a diaphragm. The frames and styles are bolted together to form a box with plating compartments. The box is placed with a seal on a "false bottom" cell to create separate anolyte and catholyte compartments and collect MnO_2 from the anodes.

Cooling coils placed in the catholyte compartment adjacent to the plating compartments viz. internal cooling cools the cells. The recirculation flows of cool water achieve heat transfer and mixing within and between compartments. The feed solution is distributed into the catholyte compartment through a single pipe header.

This mixes with the recirculating stream from the cathode compartment and flow over the cooling pipes to enter the cathode-plating compartment by holes in the sides of the cathode frames. After passing through the diaphragms into the anolyte plating compartment, the solution then flows into the false bottom anolyte compartment and out of the cell via anolyte overflow standard pipe.

B. APPENDIX B: COMMISSIONING OF THE LABCELLS AND CHALLENGES

B.1 Dry Commissioning

The objective of the dry and cold commission was to conduct a trial check to establish the effectiveness of the components on the laboratory cells. Thus, equipment such as the rectifier was switched on to determine whether current and voltage is displayed and adjustable. The elemental heater of the water bath was switched on, temperature was adjusted accordingly, and it was found that the equipment was effective. However, a leak was detected on the water bath resulting into high water losses. The bath was thoroughly dried and silicone sealant was applied at the edge and joints inside the bath and allowed to dry overnight before it was reused. The extraction fan at the top of the cells were also tested to determine the effectiveness in extracting the ammonia gasses produced during electroplating.

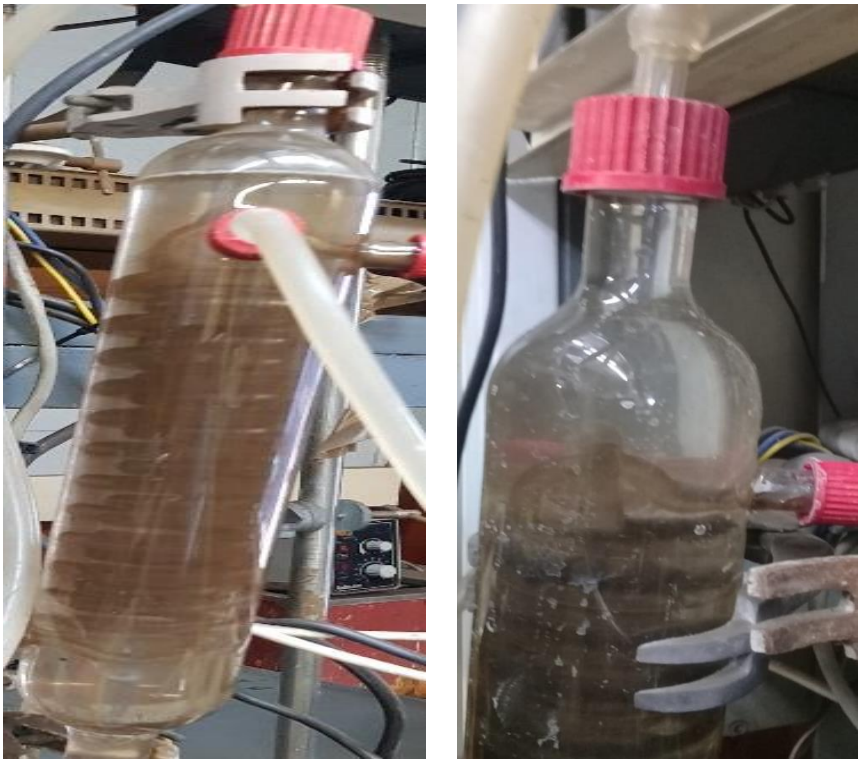
The equipment was working effectively thus ability to reduce the ammonia gas in the laboratory. The peristaltic pumps were switched on accordingly and found to be working, and adjustment of the speed was made on the pumps whereby the maximum flowrate was found to be 110 ml/min at 50 rpm. The training on the effective use of an ammeter, as illustrated by Figure B.1, was necessary to ensure that the data collected is reliable. This was after establishing that voltage reported 0 V when placed on 200 V setting and < 1 A when the current is at 600A settings. The training revealed that the setting should always be on the dotted lines, as it represents the direct current (A) and voltage (V) measured in the test programme. In addition, since the voltage and current measured are lower, the settings 20 V and 200 A were selected.



Figure B.1 Ammeter for voltage and current measurement

B.2 Cold Commissioning

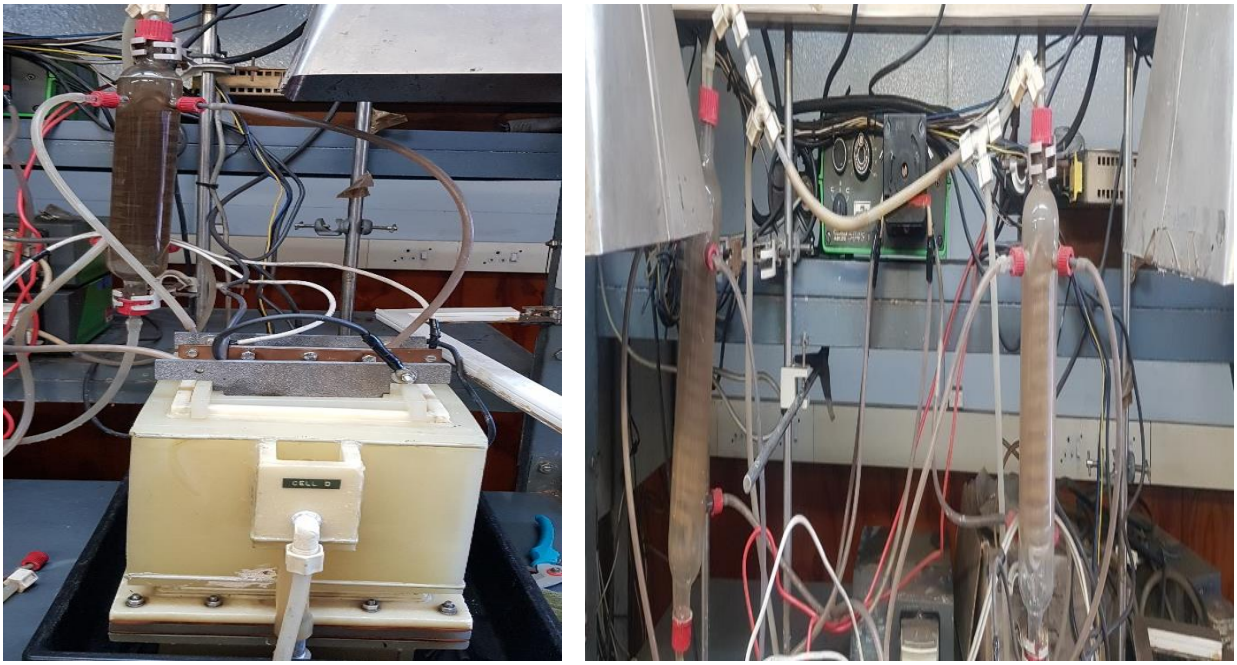
Water at ambient temperature was used as a medium to determine the movement of liquid through the circuit (i.e. supplied from the catholyte compartment for recirculation, water bath for solution heating and feed tank to supply the feed solution) in order to meet the requirements of the test programme. It was confirmed that all the pumps were able to deliver the water according to the requirements. However, the glass condenser on cell D was unable to fill-up to the top (refer to Figure B.2.a). It was necessary to ensure that the level in the glass condenser is filled to the top so that the warm water can effectively recirculate through the circuit to maintain desired temperatures in the cells. It was established that there was a pressure drop due to lose connections on the fittings. The piping and the bottle cap on the glass condenser were changed and silicone sealant was applied on the connections. The level of the warm water in the glass condenser was restored (see Figure B.2.b).



a) **b)**

Figure B.2 a) Level of water in the glass condenser b) Level of water in glass condenser restored

The cleaning solution was added in the cells and allowed to circulate through the piping for 4 hours. This was done to thoroughly remove the $Mn(OH)_2$ scale in the glass condenser and re-circulation pipes as illustrated in Figure B.3. Water was recirculated for 2 hours to rinse-off the cleaning solution. The plant solution was circulated overnight to ensure that the cleaning solution is thoroughly diluted and displaced from the labcells. The cell feed flowrate was measured and compared with the flowrate at the anolyte overflow weir. It was confirmed that both the feed rate and outlet rate are equal, measuring at 50 ml/min.

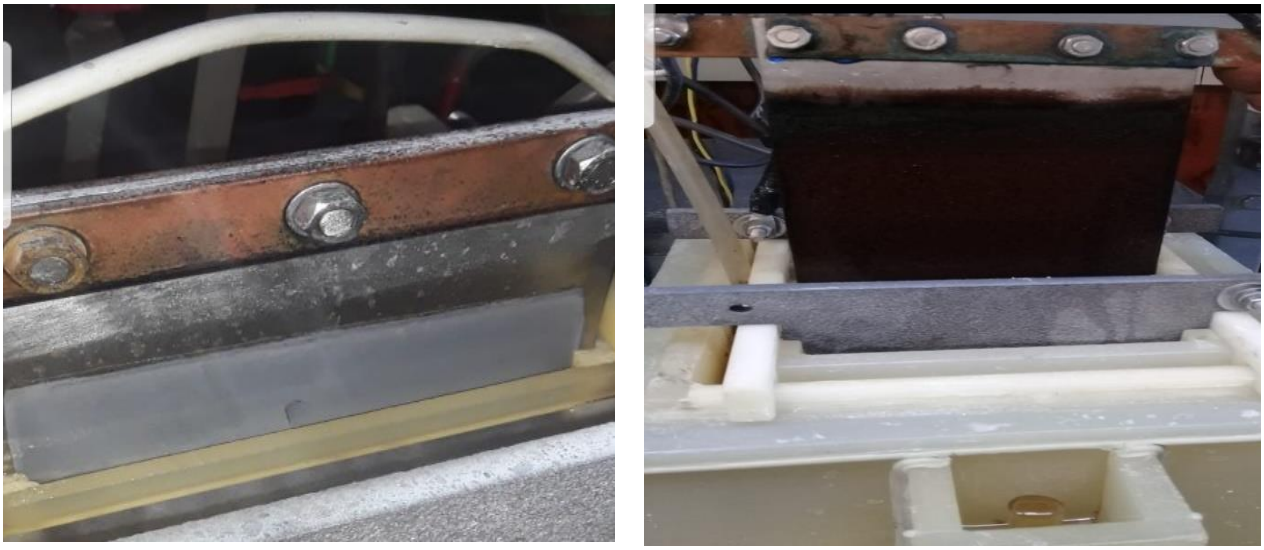


a) **b)**

Figure B.3 a) Visible residue present in the lines b) Equipment after cleaning solution

B.3 Hot Commissioning

The objective of the hot commissioning was to determine the performance of the labcells in a manner that is close to the actual test programme. The heating elements in the water bath were set at a temperature of 40 ℃ and catholyte recirculation was started. The cathode and anodes were connected accordingly with the electrical cables. Cell A was connected on the left-side and cell D was connected on the right-side of the stand as indicated on Figure 3.5. When the catholyte temperature was above 37 ℃, the rectifier and feed solution pumps were started to activate the electroplating of manganese on the cathode plates. A qualitative analysis was conducted on the cells and it was identified that after 2 hours of plating, cell A had a good plating (see Figure B.4.a) and cell D had a brown surface appearance (see Figure B.4.b).



a) **b)**

Figure B.4 a) Smooth plating on Cell A b) Brown surface of Cell D

The pH measurement was conducted on each cell and cell A measured at pH 8.34 and cell D measure at pH < 0.85. The test was stopped; the cathodes and anodes in both cells were carefully removed. Visual inspections were done on the catholyte appearance (see Figure B.5.a) where cell A was clearer and cell D was brown in colour containing solids particles. The catholyte solution in cell D was filtered and dried (the cake is illustrated on Figure B.5.b). Cell A was also stopped due to heavy metal cracking due to high manganese concentrations measured at 26.5 g/L.



a) **b)**

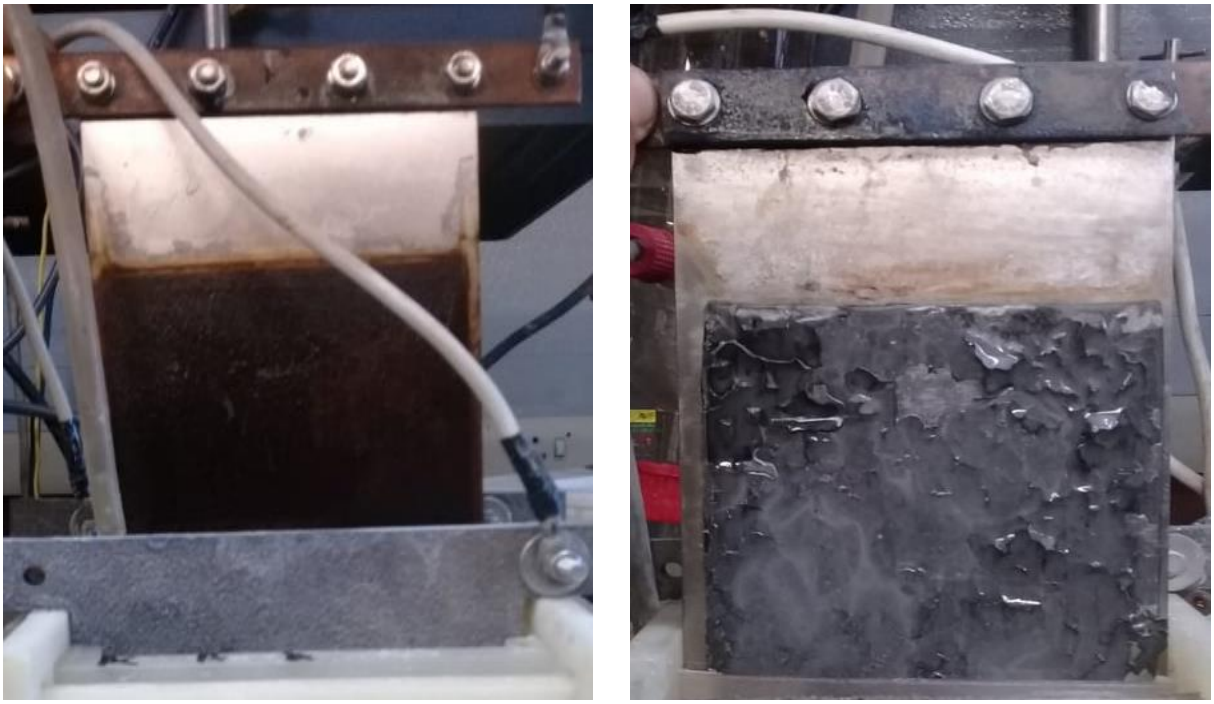
Figure B.5 a) Catholyte colour on Cell A and D b) Presence of MnO_2 in Cell D

The following were identified as likely causes for the corrosion on cell D.

1. Water inlet in the cells – leak on the glass condenser
2. Presence of cleaning solution due to improper rinsing
3. Holes on the diaphragm cloth
4. Catholyte Mn concentration
5. Electrical cable connection

To eliminate the likely causes the labcells were disconnected and preparation was done meticulously for a new run. The labcells, with the material constituent, were swopped around on the stand i.e. cell D was connected on the left-side and cell A was connected on the right-side of the stand. The solution was supplied from the same feed tank, measured at pH 7.16 and Mn concentration of 29.43 g/L. This was done to determine whether the negative impact is caused by any components in the cell D. On the start-up of the run, it was identified that cell A had the same characteristics (see Figure B.6.a) as cell D when it was connected on the right-hand side of the stand. Therefore, this ruled out the water leak due to glass condenser, holes on the diaphragm cloth, contamination due to clean solution and catholyte manganese as the likely causes.

The electrical connections were investigated, and it was established that the cathode had the same characteristics as the anodes as the electrical connections were incorrect. To attain electroplating, the electrons move from the rectifier into aqueous solution of Mn^{2+}, thus forming a metallic manganese according to Equation 2.11. However, the electrical connection was found to have been connected from cathode to cathode in between the cell A and D which hinders the electron flow due to the positive charges on both cathodes. Ideally, the opposite connection resulted in the electric field to pull the positive ions to the anodes instead of cathode, thus corroding the surface of the cathode.



a) **b)**

Figure B.6 a) Corrosion characteristics on cell A b) Cracking of deposit on the cathode plate

The other challenge noted was the heavy cracking of the metal electroplating of cells position on the left-side of the stand (see Figure B.6.b). This was associated with the Mn concentration (measured at 20.34 g/L) which were noted to have been affected by the high flows at 84 ml/min. Therefore, the data indicated the requirement to consider the flowrate as a key factor during the test programme and flowrates were reduced to 12 ml/min. It was also established that the flowrate at 12 ml/min relates to a Cellhouse flow setting of 166 m^3/hr.

APPENDIX C

C. OPTIMISATION OF THE LABCELS

The test trials were conducted to optimise and minimize any form of bias between cell A and D, immediately after the programme to commission the labcells as described in Appendix B,. The trials comprised of 4 runs, whereby, trial 1 and trial 2 compared the performance between the cells based on the Mn concentration, catholyte pH, current, voltage, temperature, and the sulphur content in the deposited metal. Trial 3 and trial 4 compared mostly the cell efficiencies, power consumption and sulphur content in the deposited manganese between the two cells.

C.1 Optimisation of the current and voltage

In the first 2 hours of starting up the labcells, the distribution of the current on the cathode plate was not equal during trial 2 as illustrated by Figure C.1. The current on the left side of the cathode plate (Ca left) measured at 0.0 A, whereas the cathode on the right side (Ca right) reported a high current at 21.4 A.

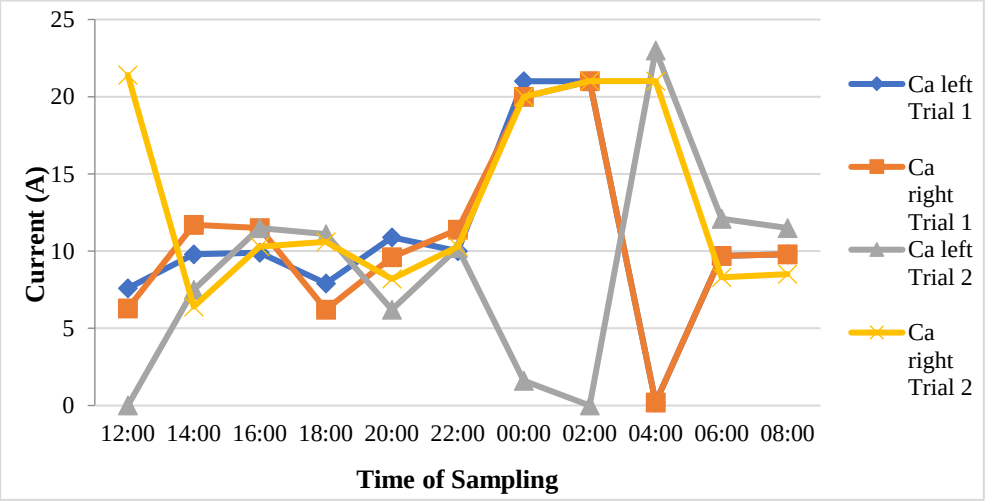


Figure C.1 Current measurement on cathode for trial 1 and trial 2

The dirt (i.e. rust in the form of cupric oxide) on the electrical contact was identified to have resulted in the non-uniform distribution of current on the cathode. The cables were swopped, and the banana sockets were cleaned with the cleaning solution. It is also noted in Figure C.1 that the variation in the current and voltage measurements increased over a period of time on both cell A and D. This is because of an error in the use of the ammeter, therefore, retraining (refer to Appendix B) was organized before the start of trial 3 and 4. This resulted into a positive

outcome as the outliers in the current and voltage measurements were minimized as shown on Figure C.2.

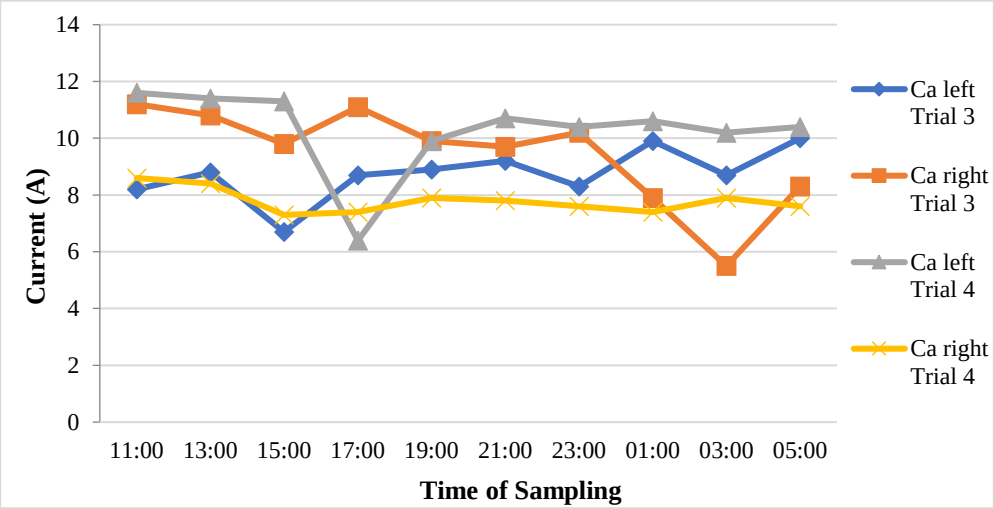


Figure C.2 The current readings on the cathode for trial 3 and 4

C.2 Optimisation of the manganese concentration

The typical Mn concentrations of the catholyte and cell feed rates are shown in Figure C.3. The sudden increase of the Mn concentration in the first few hours of trial 2 (or cell D) is because of the non-uniform distribution of current across the cathode plate. Whereby, an area of high current resulted in metal cracking, whereas an area where no current was detected was found to have no metal deposit. The deposit that cracked into the cell, re-dissolve in the catholyte thus resulting in an increase in the catholyte concentrations.

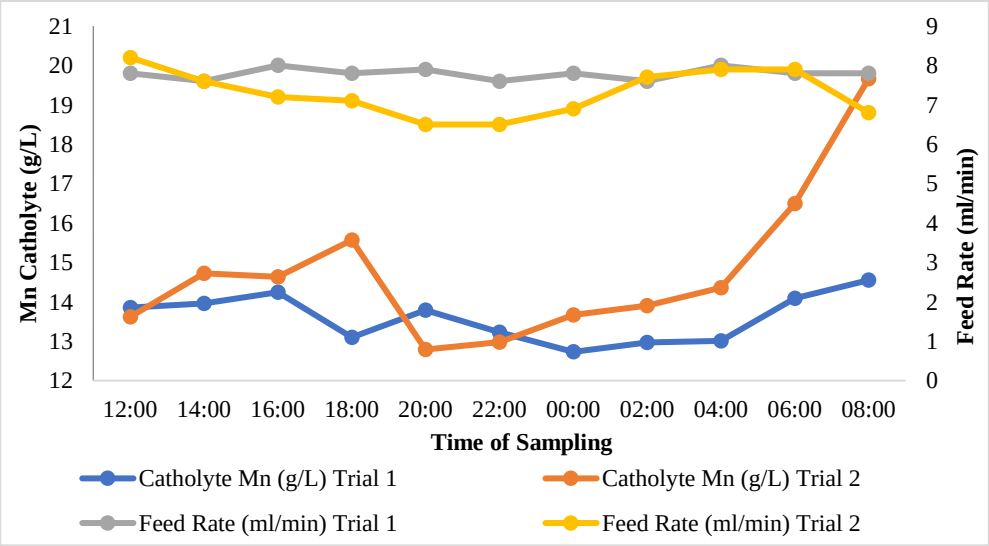


Figure C.3 Catholyte Mn concentration and flow rate

The cathode plate was stripped from the cell, and a new plate was reintroduced. Subsequently, the abrupt drop in the Mn concentration was due to the new cathode plate introduced. Gluck and Pieterse (1997) describes this phenomenon i.e. the solution close to the cathode becomes depleted in manganese ion thus causing a reduction in the concentration of the ions. The manganese ions move to the cathode surface by migration and diffusion mechanisms. Migration is the movement of ions due to an electric field, whereas diffusion is due to differences in concentration (Gluck and Pieterse, 1997). Therefore, the rate of plating is increased on the surface of a new cathode, as there is no coating which affects the electric field.

In comparison with trial 2, the deposit on trial 1 (or cell A) illustrated good adherence, smooth plating, and a light grey colour during the deposition period. The cell feed rate was also stable with minimal deviations. Furthermore, the manganese concentration was well in control with a standard deviation of 0.54 as compared to 1.95 of trial 2. Over a period, the catholyte concentration of trial 2 is increased because of the presence of sufficient ions across the face of the electrode due to solution recirculation at 100 ml/min and solution feed between 7 – 8 ml/min. However, a steep increase in the manganese concentration was observed in the last 3 hours of the experiment. It was established that the deposited metal was peeling off from the second cathode of trial 2, and flaking into the cell as shown in Figure C.4.



Figure C.4 Deposit flaking from the second cathode of trial 2

The metal flaking into the cell is attributed to an unbuffed plate that was supplied to the cell. Trial 3 and 4 were conducted to confirm the impact of the plate buffing. An unbuffed plate was introduced in trial 3 and a buffed plate in trial 4. It is noted in

Figure C.**5** that trial 3 had major cracks as compared to trial 4 comprising of smooth plating and a light grey colour. In addition, the cell efficiencies of trial 3 and trial 4 were found to be at 18.83% and 65.02% respectively. The power consumption of cell A is calculated at 27610.79 KWhr/ton as compared with cell D at 8036.21 KWhr/ton. This is because due the metal harvested from trial 3 consists of 62.4 grams compared to trial 4 at 217.2 grams. The sudden change in the performance of the cells occurred despite using the same catholyte and feed solution from trial 1 and trial 2. Therefore, the presence of unbuffed plates resulted in cracking and flaking of the metal due to an uneven deposition surface.



Figure C.5 Impact of buffed and unbuffed plated on the plating of trial 3 and trial 4

It is illustrated in Table C.1 that the use of unbuffed plates resulted in increased levels of sulphur content in the metal. Whereby, trial 1 and trial 4 comprised of a sulphur content of 0.063% and 0.0742% respectively. Whereas trial 3 consisting of an unbuffed plate on the overall runtime, had the highest sulphur content at 0.473% thus affecting the quality of the manganese metal. Glück and Pieterse (1997) identify this type of sulphurs as trapped or cavity sulphur, which is incorporated by a solution that is trapped in the pinholes thus precipitating the sulphates.

Table C.1 Sulphur content in metal from Trial run

Run	Cell Type	Metal Appearance	Sulphur Content (%)
Trial 1	A	Good adherence, smooth-grey surface	0.063
Trial 2	D (1)	Cracking, areas not fully plated. No contact	0.104
Trial 2	D (2)	No buffing, cracking, and flaking	0.084
Trial 3	A	No buffing, cracking, and flaking	0.473
Trial 4	D	Good adherence, smooth-grey surface	0.0742

C.3 Measurement of variation between equipment

The catholyte Mn samples were initially analysed at the MMC 'Solution Preparation' (Sol. Prep.) laboratory. However, it was identified that there was a 40% difference on the samples measured between the Sol Prep. and the Cellhouse as indicated in Table C.2. Therefore, the Innovex in the Cellhouse was used for analysis, as it is a close representative.

Table C.2 Comparison between the Sol. Prep and Cellhouse Innovex

Sol. Prep Innovex	Cellhouse Innovex
Calibration standard range at 26 – 36 g/L	Calibration standard ranges at 7 – 16 g/L
Cell A Mn: 15.91 g/L	Cell A Mn: 11.6 g/L
Cell D Mn: 15.09 g/L	Cell D Mn: 10.39 g/L
High Mn concentration	Low Mn concentration
Feed analysis	Catholyte analysis
Complex matrix	Simple matrix

APPENDIX D

D. EXPERIMENTAL RESULTS

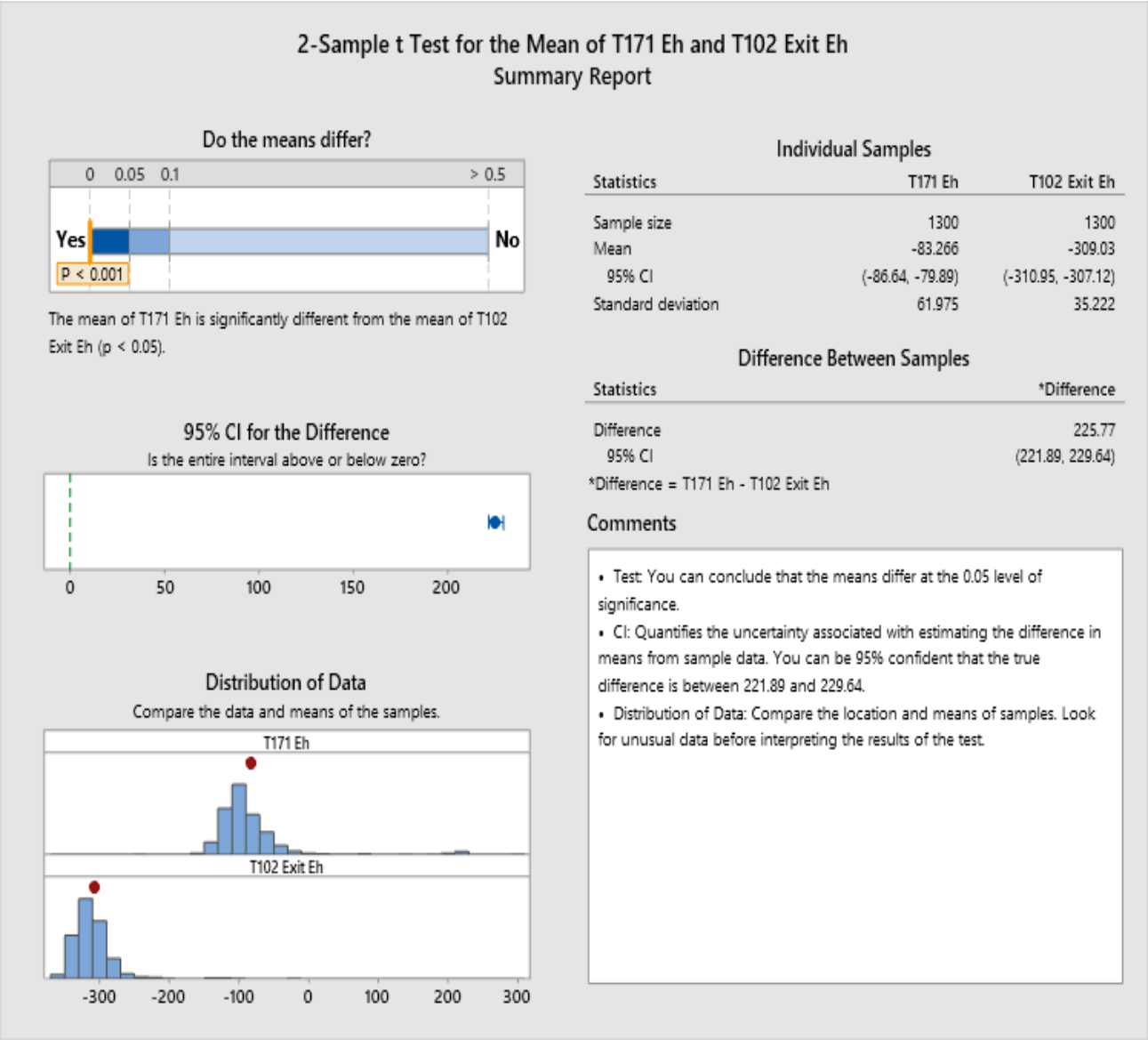


Figure D.1 Minitab summary report for T102 exit and T171 comparison

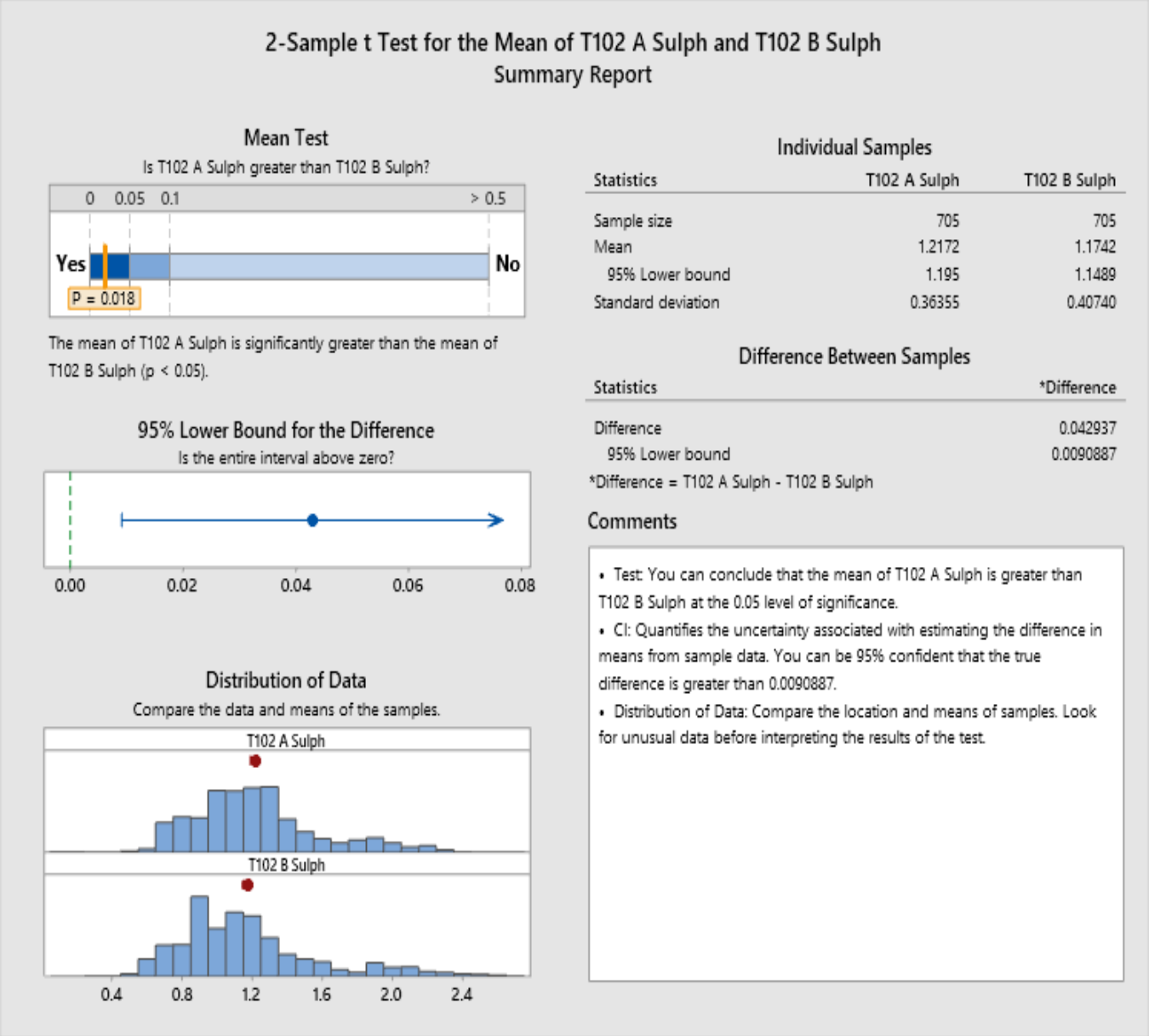


Figure D.2 The Sample t-test conducted to compare the behaviour of the sulphide dosing rates at the two lines (T102A and T120B) of the solution purification

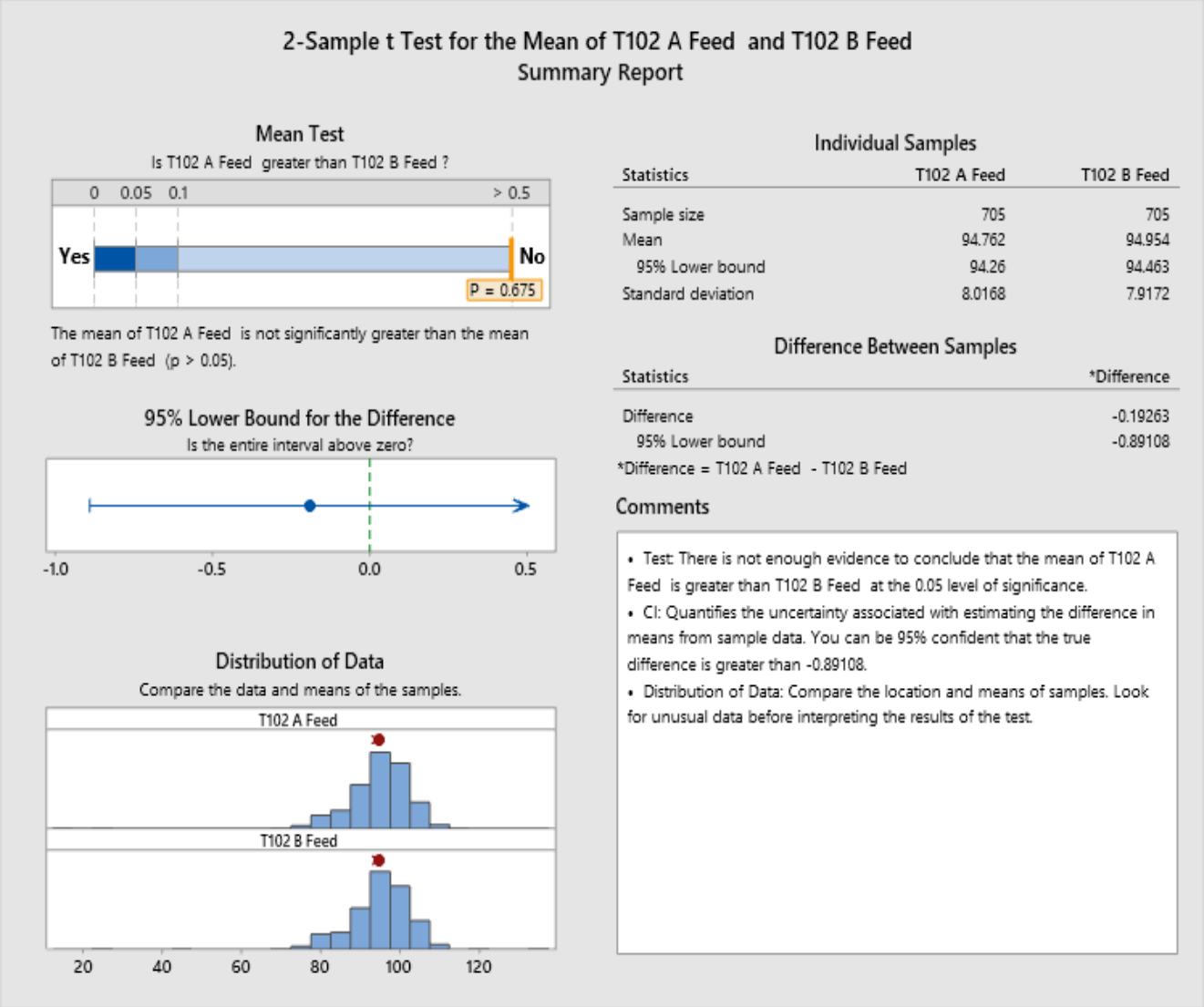


Figure D.3 The two Sample t-test conducted to compare the behaviour of the flow of solution at the two lines of the solution purification

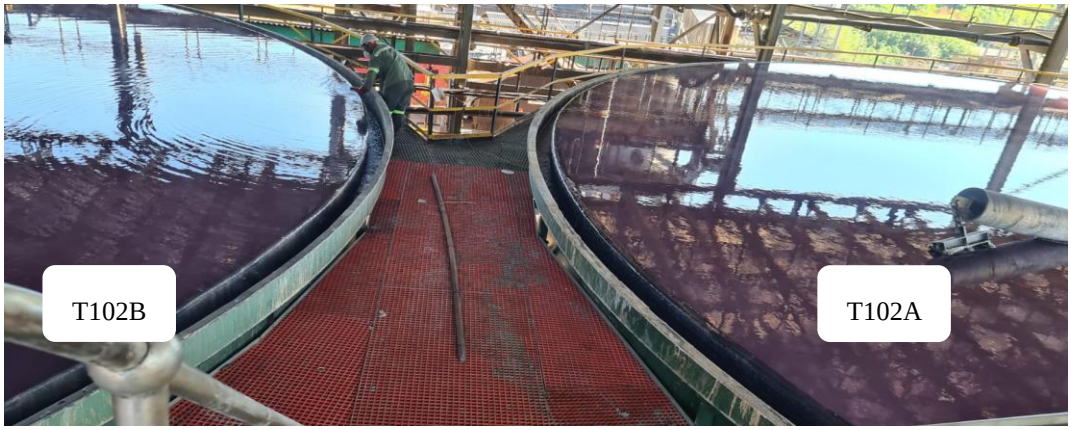


Figure D.4 Sulphide thickeners number 102-A (T102A) and 102-B (T102B) used for the purification of the solution by removal of the precipitate or solid particles

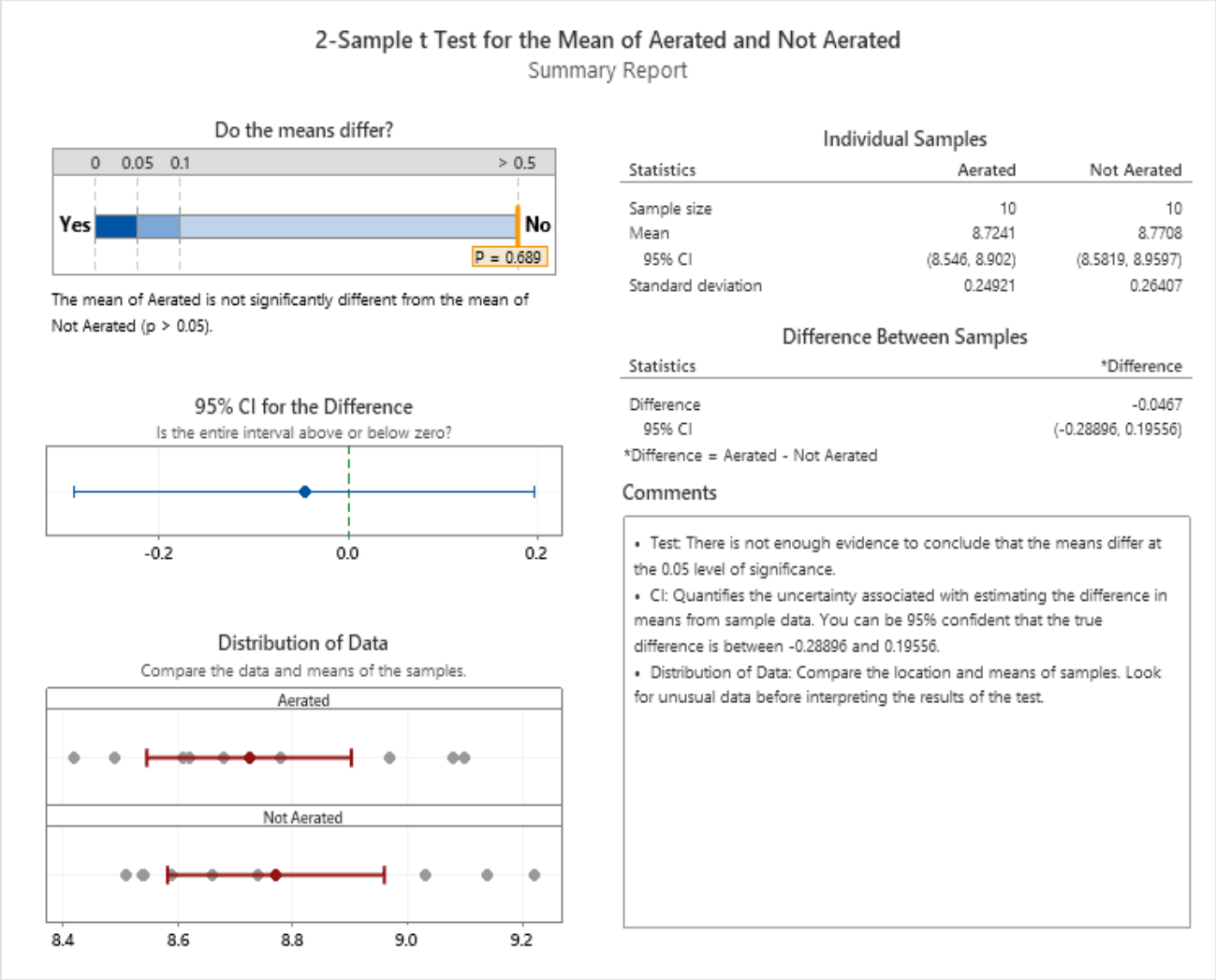


Figure D.5 The two-sample t-test conducted to compare the difference between the catholyte pH of the aerated and not aerated solution

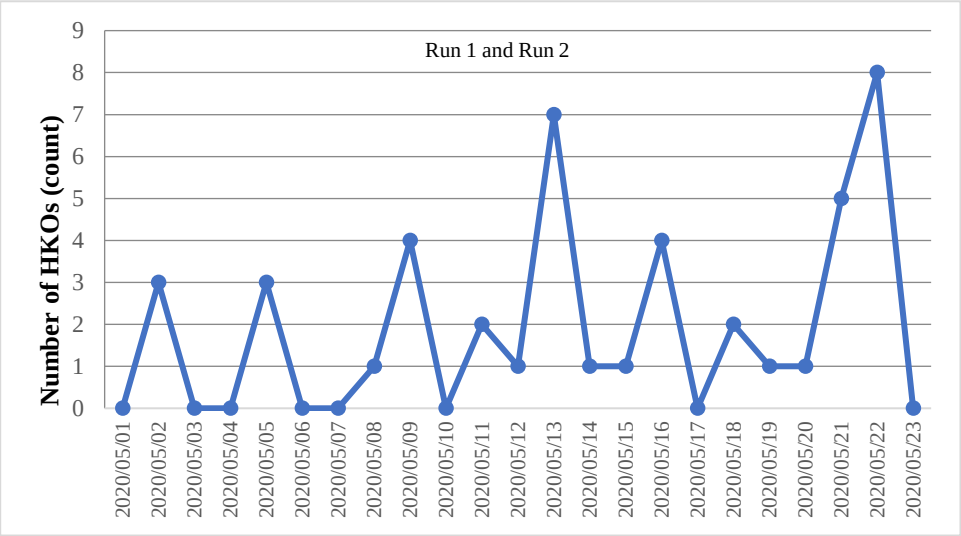


Figure D.6 The tracking of HKOs in the cellhouse plant during the test programme



Figure D.7 Anolyte blockage at the overflow weir due to the presence of $Mn(OH)_2$ in the pipeline. Mn metal flakes used to unblock the weir by metal dissolution with the anolyte



Figure D.8 Observation of cracking at the of top part of cathode plate during run 4



Figure D.9 Burning on the metal surface from the cathode plate (Run 9 – 10) due to the starting up of the cells at concentration below 9 mg/L

Table D.1 Determination of the total volume of feed solution added in the labcells for solutions consisting of 7.33 mmol/L NaHS reagent

	Volume at 10 hours	Volume at 12 hours
Flow (mL/min)	$Q = \frac{V}{t}$	$Q = \frac{V}{t}$
Volume (mL)	$V = Q \times t$	$V = Q \times t$
Volume (mL)	9.2 × 10 × 60 = 5 520	9.2 × 12 × 60 = 6 624
Volume (L)	5.520	6.624

Table D.2 Overall performance of the laboratory cells

Run No.	Temp. (℃)	Stain Test	Inlet SO_2 (g/L)	Current Density (A/m^2)	Plating hours (hr)	Volt (V)	Mass Mn (g)	% C.E.	Energy (kWhr/ton)	Sulphur (%)	In-spec
Run 1	42.10	Nil	0.32	664.17	18	9.89	154	42.16	11437.97	0.012	< 0.034
Run 2	44.30	Nil	0.32	618.54	18	10.40	117.60	32.08	15601.49	0.028	< 0.034
Run 3	40.27	Nil	0.32	1224.77	20	10.20	70.40	17.18	28955.08	0.248	< 0.034
Run 4	40.45	Faint	0.32	649.03	20	9.65	160.20	38.90	12514.66	0.139	< 0.034
Run 5 A	40.33	Nil	0.34	643.46	17	9.71	182	42.23	9070.12	0.054	< 0.034
Run 6 A	40.00	Nil	0.34	631.49	17	9.84	190	54.89	8600.12	0.065	< 0.034
Run 5 B	39.78	Nil	0.34	648.80	18	9.80	211	57.54	8310.35	0.089	< 0.034
Run 6 B	40.33	Nil	0.34	611.79	18	9.56	204.20	55.81	8426.84	0.072	< 0.034

Run 7	39.45	Nil	0.33	659.43	21	9.93	216.50	50.52	9590.07	0.014	< 0.034
Run 8	39.18	Nil	0.33	622.23	21	9.81	215	50.11	9471.1	0.017	< 0.034
Run 9	40.60	Nil	0.33	648.91	19	9.77	176.13	45.49	10478.18	0.053	< 0.034
Run 10	40.90	Medium	0.33	632.18	19	9.98	175.26	45.25	10475.4	0.089	< 0.034
Run 11	39.18	Nil	0.33	625.81	20	9.98	218.20	53.58	9087.5	0.097	< 0.034
Run 12	39.36	Nil	0.33	613.84	20	9.97	204.20	50.41	9380.1	0.450	< 0.034
Run 13	40.73	Nil	0.32	657.62	22	9.91	237.20	52.99	9126.65	0.052	< 0.034
Run 14	40.00	Nil	0.32	619.18	22	9.78	248.20	55.34	8472.09	0.073	< 0.034
Run 15	39.14	Nil	0.32	677.22	20	10.06	208.80	51.25	9577.96	0.156	< 0.034
Run 16	39.32	Dark	0.32	614.77	20	9.95	53	13.10	36520.81	0.697	< 0.034
Run 17	40.00	Faint	0.32	679.15	20	10.05	189.90	46.27	10596.8	0.089	< 0.034
Run 18	40.09	Faint	0.32	641.29	20	9.90	209.90	51.47	9116.23	0.072	< 0.034



Figure D.10 Hydrogen fire occurring in the cellhouse mostly when there is water leak in the cellhouse or during the cracking and flaking condition of the cellhouse

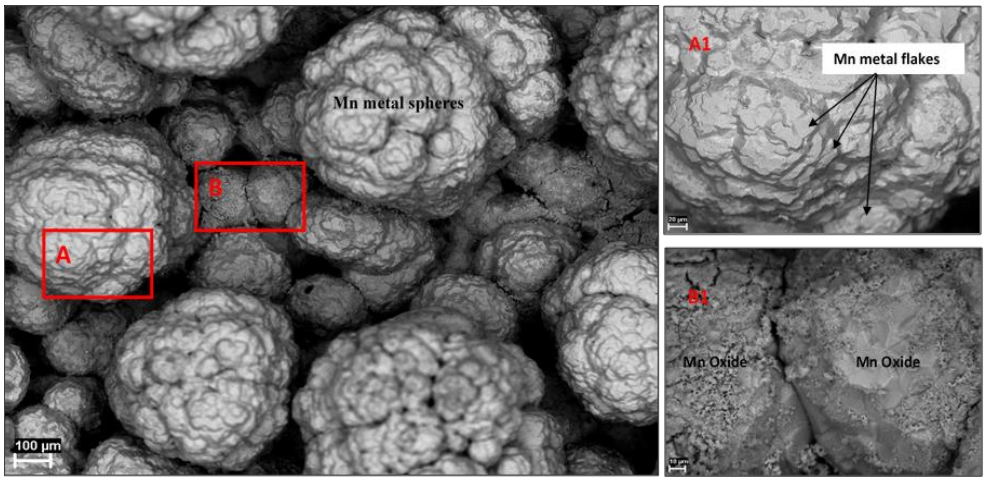


Figure D.11 BSE images of manganese metal flakes and manganese oxide in Run 7 at a resolution of 100 and 10 µm

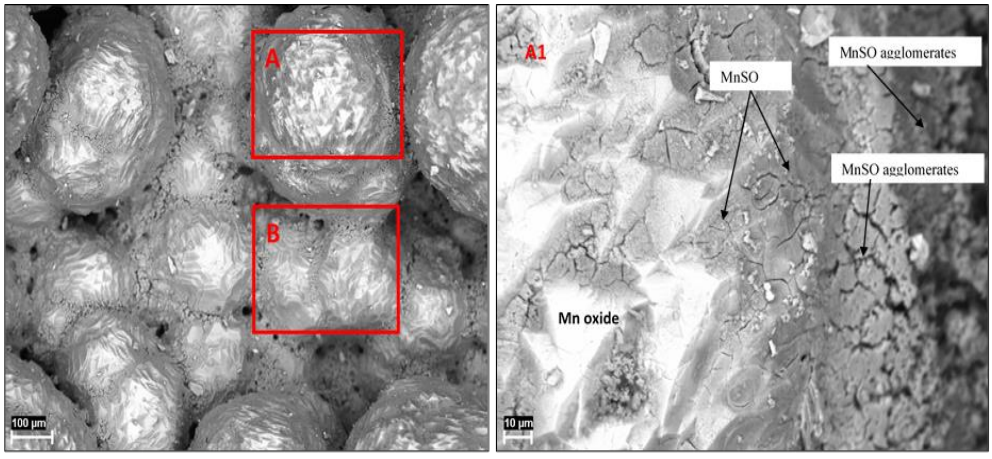


Figure D.12 BSE images of manganese oxide prisms and manganese sulphate agglomerates in Run 9 at a resolution of 100 and 10 µm

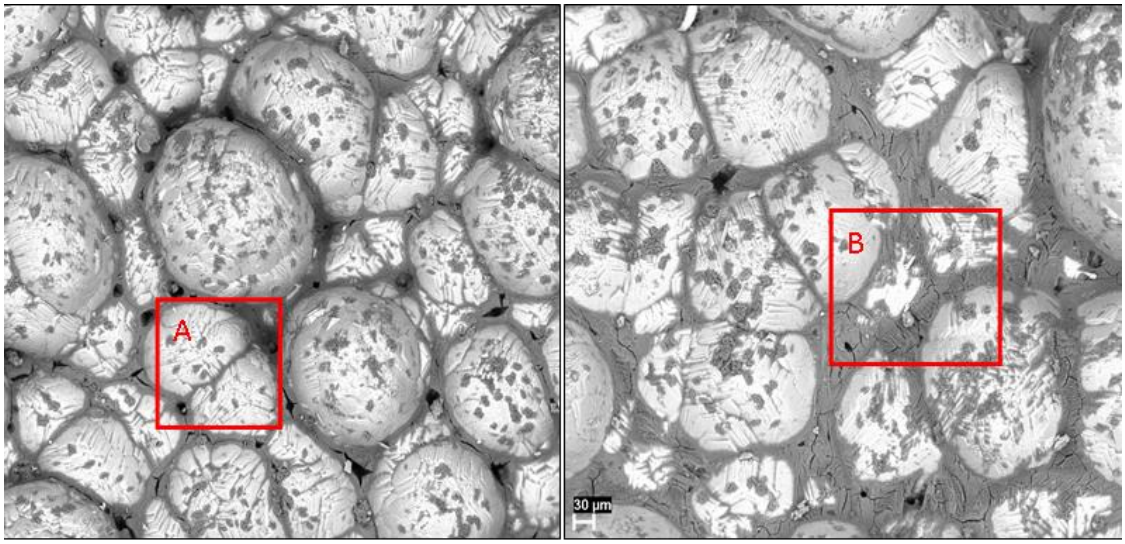


Figure D.13 Overview BSE images of well-developed manganese oxide spheres, and the cementing material in Run 12 at a resolution of 100 and 30 µm

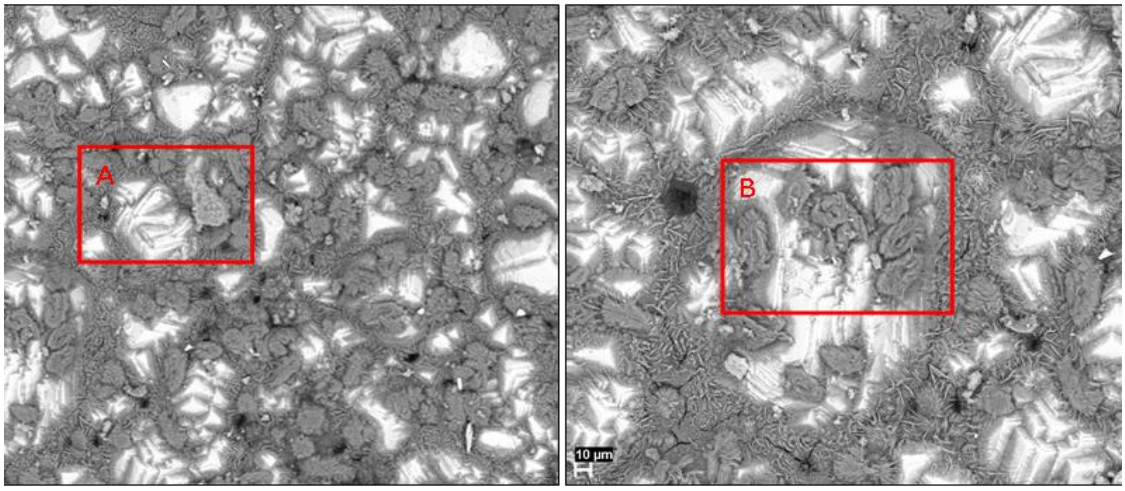


Figure D.14 Overview BSE images of well-developed manganese metal prisms with the surface coated by fibrous manganese sulphate particles in Run 16 at a resolution of 20 and 10 µm.

APPENDIX E

E. KEY OPERATION EVENTS AT MMC

MMC has conducted previous studies to assess the impact of sulphide on production output and quality. The plant performance and laboratory test work data were used, focusing mainly on the impact of sulphide on the manganese metal quality, and the outcomes are summarised below.

E.1 Recovery in the Nelspruit operations during the last quarter of FY1997 following a sustained period of low out and poor sulphur quality.

The low output from July 1995 to February 1995 was largely associated with the calcine constraint at the time. However, during first half of 1996 the quality of the metal began to deteriorate and market stresses arising from the low output and quality from MMC production became a critical issue. The recovery in April and May 1996 was brought about by a sustained reduction in sulphide dosing over a period of approximately two months. To speed up the rate of recovery a practice was followed of daily cutting the sulphide dosing altogether. Sulphide dosing was controlled by testing the solution after the sulphide thickeners using the "pink sulphide" test. The sulphide dosing remained closed until the colour of the solution sample to which an excess ammonium sulphide had been added turned purple. Whereupon sulphide dosing would recommence. This practice appeared to work well for the months of April to August 1996 and, over this period, the plant produced high levels of low sulphur manganese at reasonable current efficiencies.

E.2 Study on the sulphur in metal deportment and control prepared by Gluck et al. (1997)

There are several actual and theoretical mechanisms by which sulphur in its various chemical forms can be incorporated into a flake of manganese metal. The sulphur deportment (i.e. location and form of sulphur species in the metal) and mechanism of incorporation can thus be represented in Table E.1.

Table E.1 The details on the location and forms of sulphur species in the metal and mechanism of incorporation Gluck et al. (1997)

Types of sulphur	Incorporation mechanism	Method of control
Base layer	Hypothetical (Mechanical incorporation)	Clean uncorroded plates Choice of cathode SO_2 concentration
Inherent (Interstitial)	Electrochemical reduction	SO_2 concentration Uncombusted S Polysulphides etc. Metallic impurities
Crystal discontinuities	Hypothetical	Solution quality Growth control
Trapped (cavity)	Pinholes trap solution which precipitates sulphates	Clean plates Metallic impurities Surface tension of solution to prevent localised bubbling Suspended solids
Intragranular grain boundary	Electrochemical reduction Mechanical entrapment	Solution quality Smoothing agent Growth control
Rough, dendritic	Corrosion in valleys and precipitation of hydroxides and sulphates	Smoothing agent Plating time and conditions Electrode *"trueness"*
Flaked metal S	Cracking of metal and dissolution during plating	Metal hardness and internal stress control
Surface	Precipitation of sulphate salts from plating solution	Post stripping washing

Accompanying	Sulphate salts from above the solution line cathode mix with knocked off metal	Washing of the cathode above the solution level in the post stripping process

E.3 Petroleum and natural gas industries-Materials for use in H2S-containing environments in oil and gas production by ANSI Webstore (2020)

The NACE MR0175/ISO 15156 is a technical alignment of NACE Standard MR0175, "Metals for Sulphide Stress Cracking and Stress Corrosion Cracking Resistance in Sour Oilfield Environments," and ISO 15156, "Petroleum and natural gas industries-Materials for use in H_2S-containing environments in oil and gas production." NACE MR0175/ISO 15156 provides the necessary requirements and recommendations for the selection and qualification of carbon and low-alloy steels, corrosion-resistant alloys, and other alloys for service. Generally, this is for equipment used in oil and natural gas production or treatment plants with environment comprising of H_2S, whose failure could pose a risk to the health and safety of the public and personnel or to the environment. It can also be applied to avoid increased corrosion damage costs on the equipment. NACE MR0175/ISO 15156 consists of three standards:

1. General principles for selection of cracking-resistant materials Part
2. Cracking-resistant carbon and low alloy steels, and the use of cast irons
3. Cracking-resistant CRAs (corrosion-resistant alloys) and other alloys